Cape Peninsula
University of Technology

AN ENERGY MANAGEMENT SYSTEM FOR A HYBRID REVERSIBLE FUEL CELL/SUPERCAPACITOR IN A 100% RENEWABLE POWER SYSTEM

by

DOUDOU NANITAMO LUTA

Thesis submitted in fulfilment of the requirements for the degree

Doctor of Engineering: Electrical Engineering

in the Faculty of Engineering

at the Cape Peninsula University of Technology

Supervisor: Dr AK Raji

Bellville
July 2019

DECLARATION

I, Doudou Nanitamo Luta, declare that the contents of this thesis represent my own unaided work, and that the thesis has not previously been submitted for academic examination towards any qualification. Furthermore, it represents my own opinions and not necessarily those of the Cape Peninsula University of Technology.

Signed **Date**

ABSTRACT

Hydrogen is likely to play a significant role in the concept of low-carbon power generation in support to renewable power systems. It is abundant, eco-friendly, highly efficient and have the potential to be more cost-effective than fossil fuels provided that the engineering challenges associated with its safe infrastructure development, economical extraction and storage are solved. In the concept 100% renewable power system, a hydrogen production system may be used in conjunction with a fuel cell to form an energy storage system for power balancing and energy shifting to hinder any mismatch caused by potential variation of renewable resources. However, one of the drawbacks of a typical fuel cell is the slow response which may shorten its lifetime in case of several occurrences of sudden load variations above the fuel cell acceptable load. To avoid this issue, a complementary energy storage device with fast power response may be used to deal with sudden load fluctuations and transient regimes. In this research, a renewable power system containing a photovoltaic system and a hybrid energy storage-based fuel cell and supercapacitors is considered. The challenge when dealing with such a system is a proper energy management to coordinate the operation of the overall entity. On the other hand, a well-designed renewable power system implies a technically and economically reliable system. The aim of this research is to develop an energy management algorithm able to maintain the balance between the renewable power system and load and manage sudden load variations.

The load considered in this research consists of a three kilowatts variable DC load and a seven kilowatts non-variable AC load. Based on the solar radiation of the selected location, the results of the best possible system to satisfy such a load show a combined set of components consisting of a 29 kW photovoltaic array, a 15 kW electrolyser, a 10 kW fuel cell, a 7 kg hydrogen tank and a 7.6 kW power converter.

On the other hand, mathematical models of the components involved into the proposed renewable power system and the energy management algorithm employing rules are developed. A system integrating models of components and the energy management algorithm is simulated using Matlab/Simulink environment. Due to high computing performance requirements, the obtained Simulink model is simulated for a short duration to evaluate the effectiveness of the developed energy management algorithm. The results are presented in four scenarios demonstrating the ability of the system to maintain the balance between the supply and the demand and to manage sudden peak power occurrences.

Keywords: Energy management, energy storage, hydrogen & fuel cell, renewable energy, solar energy, supercapacitor

ACKNOWLEDGEMENTS

First and foremost, I would like to thank God for his great love and care, and for bringing hope even in the hardest time of my life.

I would also like to express my deepest gratitude to Dr Atanda Kamoru Raji, my research supervisor, for his support, encouragement, guidance and helpful critiques throughout the complexion of this research.

A word of thanks goes to all the special people in my life, for their supports and for bringing joy to my soul.

I would also like to extend my thanks to my colleagues and friends from the Cape Peninsula University of Technology for their help and encouragement throughout this research.

Lastly, I would like to acknowledge the financial assistance of the UWC HySA systems, CPUT's Centre for Postgraduate Study and University Research Fund.

DEDICATION

This thesis is dedicated to those who are dear to me, more particularly my mother Marie Nzonza. May the Good God continue always to bless her.

TABLE OF CONTENTS

TABLE OF FIGURES

TABLE OF TABLES

GLOSSARY

Al_2O_3	Aluminum Oxide
ARES	Advanced Rail Energy Storage
AFC	Alkaline Fuel Cell
CAES	Compressed Air Energy Storage
CO_2	Carbon Dioxide
Cp	Specific Heat
CHP	Combined Heat and Power
CNT	Carbon Nanotube
COE	Cost of Energy
DC	Direct Current
ES	Energy Storage
FACTS	Flexible Alternating Current Transmission System
FES	Flywheel Energy Storage
GPM	Gravity Power Module
GW	Gigawatt
HVDC	High Voltage Direct Current
HES	Hybrid Energy Storage
HESS	Hybrid Energy Storage System
H^+	Hydrogen ion
H_3PO_4	Phosphoric Acid
IEA	International Energy Agency
ICC	Ionic Charge Carriers
I_{Ph}	Photovoltaic Current
KOH	Potassium Hydroxide
K_2CO_3	Potassium Carbonate
kWp	Kilo Watt Peak Power
Li-ion:	Lithium - Ion
LHS	Latent Heat Storage
LAES	Liquid Air energy Storage
LI_2Co_3	Lithium Carbonate
LiAlO2	Lithium Aluminate
LIO	Lithiated Nickel Oxide
Li_3N	Lithiated metal nitrides
MCFCs	Molten Carbonate Fuel Cells
MnO_2	Manganese Oxide
MO_2N	Molybdenum Nitride

NiCd:	Nickel Cadmium
Na^+	Sodium-Ion
NaS	Sodium Sulfide
$NaNiCl_2$	Sodium Nickel Chloride
NASA	National Aeronautics and Space Administration
Na_2CO_3	Sodium Carbonate
NiCr	Nickel Chromium
NPC	Net Present Cost
NOCT	Nominal Operating Cell Temperature
O&M	Operating and Maintenance
Pb	Plumb
PCM	Phase Change Material
PEMFC	Proton Exchange Membrane Fuel Cell
PEM	Proton Exchange Membrane
PHS:	Pump Hydro Storage
PV	Photovoltaics
PAFC	Phosphoric Acid Fuel Cells
PBI	Polybenzimidazole
PVDF	Polyvinylidene Fluoride
PTFE	Polytetrafluoroethylene
PEMFC	Proton Exchange Membrane Fuel Cell
Q_{heat}	Quantity of Heat
RAFCs	Reversible Alkaline Fuel Cells
RTE	Round-Trip Efficiency
RFC	Reversible fuel cell
RPEFCs	Reversible proton exchange fuel cells
RuO_2	Ruthenium oxide
R_s	Series Resistance
R_{sh}	Shunt resistance
R_p	Parallel Resistance
SMES:	Superconducting Magnetic Energy Storage
SHS	Sensible heat storage
SOFCs	Solid Oxide Fuel Cells
SIC	Silicon carbide
STC	Standard Test Conditions
TES:	Thermal Energy Storage
TiN	Titanium Nitride
Vmp	Voltage at maximum power point

VOC	Open Circuit Voltage
VRES	Variable Renewable Energy Source
W_{ele}	Electrical Energy
YSZ	Yttria stabilized Zirconia
Zn- Air	Zinc- Air

CHAPTER ONE
INTRODUCTION

1.1 Background

Renewable energy technologies are expected to become major sources of energy in the planet as the population need for energy is increasing and more awareness on the effect of fossil fuels over the environment is being raised. It is predicted that renewable energy will be at the centre of the four Industrial Revolution along with the progress of information technology. To reach that point, challenges brought up by the random nature of renewable energy which impact on the power quality and competitiveness of these technologies into the market must first be overcome.

Indeed, as a result of their dependency on weather conditions, renewable generators based on solar and wind generate interrupted and unpredictable power, compromising the principal target of a power system, which is to provide reliable and continuous power. Such generators bring uncertainty in the planning and operation of a power system. An approach to manage that is to operate them connected to the grid, in this case, the connection issues have been tended to; these issues being related to the governments' policies and compliance (Sakulin et al., 2009) and some technical challenges related to the power quality and protection (Farhoodnea et al., 2012). The role of these generators into the utility grid will be to act as a help by delivering power to close-by loads and feeding back into the utility any surplus power produced. However, the problem will persist for 100 % renewable power systems as such power utilities can generate inefficient and unreliable power to the detriment of their users. In such a situation, an energy storage system can be an alternative to manage these drawbacks; it will assist to provide power as required or allow time shifting to balance the supply and the demand. Other options that can be considered to handle the intermittency and power balancing problems of renewable power systems include high-quality forecasting, advanced scheduling methodologies (Kiviluoma et al., 2012) and demand-side management (Bocklisch, 2015), however, as of now, energy storage is the best approach. Depending on the available generation, the energy can be stored for hours, days, weeks or even months.

Energy storage exists in various emerging technologies and concepts in either electric or nonelectric types influenced by the advancement of renewable energy.

A common energy storage unit has characteristics such as energy and power ratings, round trip efficiency, discharge and response times, self-discharge rates, operating temperature, lifespan, recharge time, etc. (Chatzivasileiadi et al., 2013). A literature

survey uncovers that most technologies are not technically and economically viable; from one viewpoint, taking examples of batteries, though their round-trip efficiencies is about 90%, it will still be costly to efficiently size them to satisfy the load demand in continuous power supply applications. Adding this expense to the expense of power generated by renewable sources, the system cost will be substantial (Luo et al., 2015). Furthermore, an energy storage device should have critical characteristics such as high-energy and high-power densities (Jha, 2012). However, currently, none of the existing energy storage type has provided these two features at a time (Etxeberria et al., 2010). Such a energy storage system may only be obtained by joining at least two or more energy storage units some with high-power and others with high-energy densities, to make up a hybrid energy storage system.

A high-energy density storage device can provide energy for a long time at a small power rate whereas, a high-power density storage technology may supply a very high-energy rate for only a short period (Hemmati & Saboori, 2016). Bocklisch (Bocklisch, 2015) states that the advantages of a hybrid configuration over a single energy storage system are:

- The decrease of the energy storage capital cost,
- The increase of the efficiency and storage lifetime of the overall storage unit.

Hybrid energy storage systems come in various configurations such as lithium ion – redox battery, supercapacitors – battery, compressed air – battery and flywheel – battery, battery – hydrogen combination, superconducting magnetic – battery. In 100% renewable power systems including a hybrid energy storage facility, the choice of individual energy storage units follows the two main characteristics referred to previously. The high-power storage will deal with peak power demand, fast load fluctuations and transient (Bocklisch, 2015), whereas the high-energy storage will serve to shift the availability of energy in time.

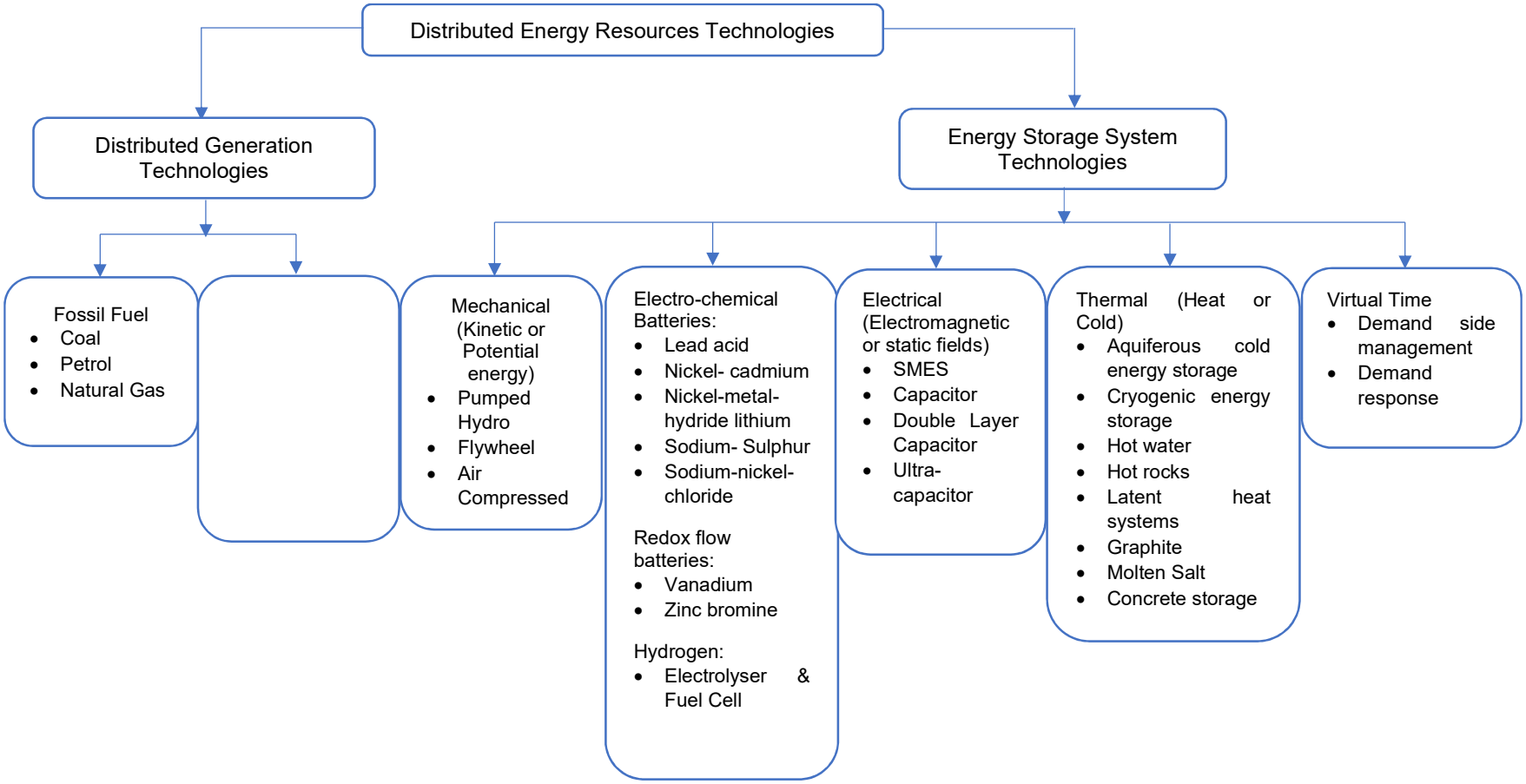

Figure 1.1: Types of Energy Storage Technologies (Torres, 2015)

In addition to the characteristics provided above, other characteristics of a hybrid energy storage are shown in the Table 1.1, while Table 1.2 and Table 1.3 give the technical features of energy storage technologies. In these tables, CAES, Li-ion, NiCd, PHS, SMES and TES are compressed air energy storage, lithium-ion batteries, nickel-cadmium batteries, pumped hydro storage, superconducting magnetic energy storage and thermal energy storage respectively.

Table 1. 1: Ideal characteristics of hybrid energy storage (Chong et al., 2016)

Characteristics	Hybrid energy storage	High-energy density storage	High-power density storage
Specific energy	High	High	Low-moderate
Specific power	High	Low-moderate	High
Response time	Fast	Moderate	Fast
Energy efficiency	High	High	High
Ease of implementation	High	High	High
Capital costs	Low	Low	Low
Durability	High	High	High

Table 1. 2: Technical characteristics of energy storage technologies (Torres, 2015)

Technologies	Power rating	Discharge time	Self-discharge per day	Suitable storage duration
PHS	100 - 5000 MW	1 - 24h +	Very small	Hours - months
CAES	5 - 300 MW	1 - 24h +	Small	Hours - months
Flywheel	0 - 250 kW	1e-3s - 15 min	100%	Seconds - minutes
Capacitor	0 - 50 kW	1e-3s - 60 min	40%	Seconds - hours
Super Capacitor	0 - 300 kW	1e-3s - 60 min	20 - 40%	Seconds - hours
SMES	0.1 - 10 MW	1e-3s - 8s	10 - 15%	Minutes – hours
Lead-acid	0 - 20 MW	Second - hours	0.1 - 0.3%	Minutes – days
NiCd	0 - 40 MW	Second - hours	0.2 - 0.6%	Minutes – days
Li-ion	0 - 100 kW	Minutes- hours	0.1 - 0.3%	Minutes – days
Flow Batteries	30 kW - 3 MW	Seconds - 10h	Small	Hours – month
Hydrogen fuel cell	0 - 50 MW	Seconds - 24h+	Almost zero	Hours – months
TES	0 - 60 MW	Seconds - 24h+	0.05 - 1.0%	Minutes – months

Table 1. 3: Energy density, power density, lifetime and cycle characteristics of energy storage technologies (Torres, 2015)

	Energy and power density				Lifetime and cycles	
Technologies	**Wh/kg**	**W/kg**	**Wh/L**	**W/L**	**Years**	**Cycles**
PHS	0.5 - 1.5	-	-	05 - 1.5	40 - 60	-
CAES	30 – 60	-	3 – 6	0.5 - 2	20 - 40	-
Capacitor	0.05 – 5	~1e5	2 – 10	1e5+	~5	5e4+
Super Capacitor	2.5 – 15	500 – 5000	2 – 10	1e5+	20+	1e6+
SMES	0.5 – 5	500 – 2000	0.2 - 2.5	1000-	20+	1e3 - 4e3
Lead-acid	30 – 50	75 – 300	50 – 80	10 - 400	5 - 15	500 – 1000
NiCd	50 – 75	150 – 300	60 – 150	-	10 - 20	2000 – 2500
Li-ion	75 – 200	150 – 315	200 – 500	-	5 - 15	1e3 - 10e3
Flow Batteries	10 – 30	-	16 – 33	-	5 - 10	12e3
Hydrogen fuel cell	800 - 10e3	500+	500 – 3000	500+	5 - 15	1000+
TES	80 – 200	-	120 – 500	-	5 - 15	-

It can be noticed from Table 1.2 and Table 1.3 that fuel cells have high-energy density, hence, having enough ability to store energy for a long-lasting term. However, their critical constraints are their slow response time and inability to handle rapid load demand variations and transient regimes. In a similar vein, supercapacitors can deliver high-power with quicker and better response to deal with transient regimes. Combining these two energy storage devices as a hybrid system can provide more flexibility in case of a power system with renewable sources and increase the energy storage lifespan, particularly in applications with peak power variations. The challenge will be on the energy management; knowing that the energy storage system consists of high-energy and high-power technologies lead to some questions such as

- How to optimally use the total storage system?
- How to share the power stored in each of them?
- How to deal with the transient and sudden changes that can appear?
- How to prevent the supercapacitor from deep discharging, etc.?

For that cause, various control approaches for energy management systems have been proposed; the common ones are referred to as classical methods and are based on algorithms using rules and filtration-based methods (Chong et al., 2016). Other methods such as fuzzy logic, artificial neural network, neu-fuzzy, model predictive control may be used, etc.

1.2 Statement of the research problem

Energy storage can increase the reliability of a renewable power system by reducing power fluctuations, enhancing the system flexibility, enabling the conservation of the electricity generated and enlarging the overall storage lifetime. In the context of hybrid energy storage containing both high-energy density and high-power density storage units, one of the challenges is to manage the stored energy. The problem in this research is, therefore, the energy management for a hybrid reversible fuel cell - supercapacitor in a renewable power system.

1.3 Research aim and objectives

The aim of this research is to develop an energy management algorithm to maintain the balance between the 100% renewable power system and load and manage sudden load variations.

The specific objectives are:

- to design a cost-effective and reliable renewable power system;
- to develop mathematical models of the components;
- to make use of developed models to conduct system studies of a hybrid reversible fuel cell - supercapacitor in a 100% renewable power system;
- to develop the control scheme of the different power electronics devices used;
- to develop an energy management algorithm;
- to conduct simulation studies of the system.

1.4 Significance of the research

A 100% renewable power systems are more suitable for isolated areas with no access to electricity. In Africa, for instance such places are subjected to severe poverty and little development activities. The implementation of such power systems in these areas present potential benefits ranging from:

- improving community services such as water delivery and public health as none of these services runs without electricity,
- preventing exposure to harmful pollutants associated with use of fuel wood, cow dung, kerosene for cooking and lighting,

- creating jobs and other economic benefits and,
- allowing community empowerment.

1.5 Outline of the thesis

Besides the introduction, the rest of the thesis is organised as follows:

Chapter two presents a literature survey on the concept of 100 % renewable power systems, different types of energy storage technologies including their characteristics, types of fuel cell systems and electrolysers by considering their characteristics and operating principles, etc. and an assessment of supercapacitors.

Chapter three focuses on the design of an optimal 100 % renewable power system based on a photovoltaic system and using a hybrid reversible fuel cell supercapacitor for the storage of electrical energy.

Chapter four is centred around the mathematical modelling of components involved in the system namely photovoltaic array, electrolyser, fuel cell, hydrogen tank, power electronics converters and supercapacitors.

In this chapter, the models of the components are integrated and implemented using Matlab/Simulink. Thereafter, the energy management algorithm is developed and implemented based on a set of rules and using power balancing equations. A simulation study is carried to evaluate the performance of the developed energy management algorithm.

Chapter five concludes the thesis and identifies topics for further research.

1.6 Publications

The publications below have evolved from the doctoral research:

Luta, Doudou N. & Raji, A.K. 2017a. A SysML based hybrib photovoltaic-wind power system model. *Journal of Energy Technology Research*, 1(2): 1–12.

Luta, Doudou N & Raji, A.K. 2018a. Comparing fuzzy rule-based MPPT techniques for fuel cell stack applications. *Energy Procedia*, (September): 19–21.

Luta, Doudou N. & Raji, A.K. 2018. Decision-making between a grid extension and a rural renewable off-grid system with hydrogen generation. *International Journal of Hydrogen Energy*, 43(20): 1–14. https://doi.org/10.1016/j.ijhydene.2018.04.032.

Luta, Doudou N. & Raji, A.K. 2019a. Energy management system for a hybrid hydrogen

fuel cell-supercapacitor in an islanded microgrid. *Proceedings - 2019 Southern African Universities Power Engineering Conference/Robotics and Mechatronics/Pattern Recognition Association of South Africa, SAUPEC/RobMech/PRASA 2019*: 611–615.

Luta, D.N. & Raji, A.K. 2016. Energy Management System for a Renewable. *2019 International Conference on the Domestic Use of Energy (DUE)*: 20–24.

Luta, Doudou N & Raji, A.K. 2018b. Fuel cell micro-CHP for energy access in rural areas. In *2018 IEEE PES/IAS PowerAfrica, PowerAfrica 2018*. Cape Town: IEEE.

Luta, Doudou N. & Raji, A.K. 2019b. Fuzzy rule-based and particle swarm optimisation MPPT techniques for a fuel cell stack. *Energies*, 12(5).

Luta, Doudou N & Raji, A.K. 2017. Maximum Power Point Tracking Simulation for a Low Temperature Fuel Cell. *International Journal of Emerging Technology and Advanced Engineering*, 7(12): 290–301.

Luta, D.N. & Raji, A.K. 2019. Optimal sizing of hybrid fuel cell-supercapacitor storage system for off-grid renewable applications. *Energy*.

Luta, Doudou Nanitamo & Raji, A.K. 2019. Performance and Cost Analysis of Lithium-Ion Battery for Powering Off-Grid Telecoms Base Stations in Africa. *International Journal of Engineering Research in Africa*, 43: 101–111. https://www.scientific.net/JERA.43.101 18 August 2019.

Luta, Doudou N. & Raji, A.K. 2017b. Potential benefits of renewable fuel cell systems for rural communities' power supply. In *2nd EAI International Conference for Research, Innovation and Development for Africa*. Victorai Falls: European Alliance for Innovation. http://eudl.eu/doi/10.4108/eai.20-6-2017.2270897.

Luta, Doudou N. & Raji, A.K. 2019c. Renewable Hydrogen-Based Energy System for Supplying Power to Telecoms Base Station. *International Journal of Engineering Research in Africa*, 43: 112–126. https://www.scientific.net/JERA.43.112 17 August 2019.

Raji, A.K. & Luta, D.N. 2018. Modeling and Optimization of a Community Microgrid Components. , 00(September): 19–21.

CHAPTER TWO
REVIEWS OF LITERATURE

2.1 Introduction

This chapter presents a literature survey on the concept of 100 % renewable power systems, different types of energy storage technologies including their characteristics, types of fuel cell systems and electrolysers by considering their characteristics and operating principles, etc. and an assessment of supercapacitors.

Regarding the concept of 100 % renewable power systems, key drivers that need to be considered in the expansions of 100 % renewable power systems are presented. These key drivers include elements such as demand side management, expansion and liberalisation of markets, grid support services from renewable energy, diversifying renewable resources, bulk energy storage, transmission network efficiency and flexibility, role of smart grids, power system stability with non-synchronous generators and effective utilisation of excess generations.

On the other hand, various forms of energy storage technologies such as mechanical, electrochemical, electrical, thermochemical, chemical and thermal are discussed about. Their characteristics and applications are as well considered.

Similarly, types of fuel cell systems and electrolysers considering their characteristics and operating principles, etc. are reviewed.

A section dedicated to supercapacitor is also considered in this chapter, it presents the types of supercapacitors, their main characteristics and part involved in supercapacitors.

The last section is dedicated to the brief review of photovoltaic systems; starting from its history, evolution, operating principle, technology classification, etc.

2.2 Concept of 100% renewable power system

Countries around the world came to the point of realising that the sustainability for better future on earth is linked to the reform in the energy sector, a shift from the use of traditional energy sources such as fossil fuels and nuclear which are always reported as causing negative impact to the environment to more clean and replenished sources need to be accomplished. Theoretically speaking, potentials offered by the latter type of energy mentioned above exceed largely any other type. Consequently, renewable energy technologies are gaining interest and all around the world, their use is becoming more significant.

Among these renewable technologies, both photovoltaic and wind power generations are the most emerging, alongside with others such as high thermal solar power, wave energy, small hydro power, biomass, etc. Apart from the fact that these sources are suitable in dealing with environmental conservation, they can as well offer more opportunities ranging from socioeconomic development to energy access and energy security; as most renewable energy technologies are decentralised, they offer more opportunities in terms of job creations, especially in rural communities in developing countries and knowing that clean and reliable energy contributes in reducing poverty, allowing access to better education and better health, on the other hand, there is a correlation between the economic growth and the energy access level into a country, the more the economy grows, the energy demand also increases and renewable energy technologies allow electricity access to areas far from the utility grid where the construction of power lines are economically unfeasible, using for instance photovoltaic, wind, hydropower, biomass standalone technologies, etc., these areas can have access to electricity in a clean and cheap way.

Lastly, regarding energy security, it is to mention that renewable energy resources are available and evenly distributed on the earth; hence, as an illustration, considering sun and wind, as long as the sun will shine and the wind will blow, the power generated from renewable technologies will always be available and supplied without disruption whereas fossil fuels have a major problem in price fluctuation which usually depends on geopolitical consideration, besides not being evenly distributed on the earth, other countries are fully depending on the importation of this commodity, in the event of import crisis, a secured supply of energy might be compromised. Another aspect to consider regarding energy security is the depletion of fossil fuels; it is expected that sometime in the future, the reserves of fossil fuels on the earth will be exhausted; this will have an enormous effect on the energy supply security knowing that the present world energy supply is dominated by this commodity.

Despite these opportunities, renewable energy sources still have some drawbacks which are hindering their development; it is difficult to generate much energy from renewable sources as it is the case for fossil fuels generators, in this case, there might be a need of whether reducing the energy used or building more power plants, or again balancing different types of renewable technologies. The reliability of supply is as well one of the drawbacks; renewable sources such as those based on solar, wind or hydro are weather dependent, thus, the power generated from these sources are therefore unpredictable, their operations are influenced on whether or not the sky is clear enough to collect sunlight to generate electricity from photovoltaic panels or to collect heat and produce electricity, or if there is enough wind blowing to turn the blades of a wind turbine or again if there is enough water to fill the dam and drive a turbine. Another drawback to mention is the initial capital cost; considering that renewable sources are new technologies, their current cost are still high exceeding considerably fossil fuel generators.

In current years, photovoltaics (PV) and wind generators have encountered radical cost decreases. PV technologies have experienced the highest reduction in cost (Trancik & Cross-Call, 2013) because of improved efficiencies, material costs, economies of scale and research and development (Breyer et al., 2013; Hansen et al., 2019). The PV cost decrease patterns are expected to decrease further in the future (Comello et al., 2018) and comparative patterns can be found for wind power industry (IRENA, 2018). Various researchers reported that presently, wind and PV are cost-competitive with fossil fuel-based power generators (IEA-PVPS, 2018).

Presently, the idea of 100 % renewable energy is gaining popularity among different stakeholders. (Hansen et al., 2019) reports that, in Europe, countries like Sweden and Denmark are targeting to accomplish zero net greenhouse gas emissions by 2045 and 2050 respectively (Child et al., 2019; Mathiesen et al., 2011; Pursiheimo et al., 2017). Moreover, various Asian and African countries including Bangladesh, Barbados, Cambodia, Colombia, Ethiopia, Ghana, Mongolia, Vietnam, Hawaii and California are aiming to the same target (Mathiesen et al., 2011).

As of now, a couple of countries such as Norway and Costa Rica supply practically all power from for hydropower. A nation like Uruguay has been the first to accomplish the objective of 100 % renewable power systems in a blend of renewable sources. Also, a few urban communities have focused on 100% renewable power source by 2050 for the energy use. These urban areas are Copenhagen (Denmark), Frankfurt and Hamburg (Germany), Malmo and Vaxjo (Sweden), Oxford Country (Australia), Vancouver (Canada) and The Hague (Netherlands) (REN21, 2018). A comparative pattern exists among bigger organisations, such as IKEA, BMW and Walmart (RE100,

2019) and innovation organisations incorporating Google, Apple, Sony, eBay and Facebook among numerous others (Moodie, 2016), and even the main organisation from the internal centre of the fossil fuel business, Wartsila, that has focused on 100% renewable power.

Depending essentially on energy from renewable resources like wind and solar will require a change in the manner power systems are arranged and operated. Some significant advances should be made to create power systems with the flexibility expected in maintaining the stability and reliability while depending principally on variable energy resources. These advances include policies, technical changes and institutional systems.

(Papaefthymiou & Dragoon, 2016) states that nine elements should be considered as the key drivers for the change that are likely normal to all power systems. The significance of these features will differ from system to system considering local conditions, yet every one of them is significant towards creating systems able to operate efficiently and dependably on renewable resources. There key drivers are shown Figure 2.1 and include demand side management, expansion and liberalisation of markets, grid support services from renewable energy, diversifying renewable resources, bulk energy storage, transmission network efficiency and flexibility, role of smart grids, power system stability with non-synchronous generators and effective utilisation of the excess generation.

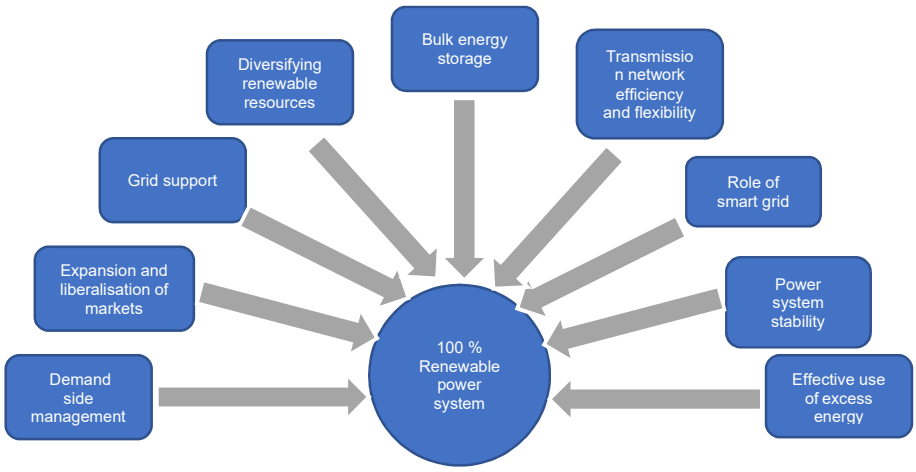

Figure 2.1: Key drives for 100 % renewable power systems. (Papaefthymiou & Dragoon, 2016)

2.2.1 Demand side management

Traditional power systems depend on controlling supply for adjusting purposes, however, controlling demand plays a major role at higher penetration of renewable sources as it relatively reduces the cost source of power system flexibility (Milligan & Kirby, 2010). Demand side management gives the most reduced cost of renewable energy support (López-Peña et al., 2012). In future, demand side management is expected to mobilise abroad clusters of end users allowing the increase and decrease of the demand all the time, grow demand flexibility by including energy storage and facilitate dynamic demand management with energy efficiency opportunities (Perlstein et al., 2012).

2.2.2 Expansion and liberalisation of markets

Capacity markets might be important to guarantee reliability by supporting required flexible resources that will not be competitive on energy basis (Klessmann et al., 2008). Guaranteeing low-cost service will require markets to allow as many participants as possible, including conventional generating resources, variable resources, distribution system-level generation, demand resources, and energy storage. Moreover, the market will operate in close real time and in brief time increments to enable constant adjustment to fluctuations. Markets should go beyond national borders to permit participation from a more extensive scope of potential flexible sources, but also to average variability over more different variable resources (Cochran et al., 2012). Getting over the current lim2itations will require institutional modifications and consolidating isolated power markets.

2.2.3 Grid support services from renewable energy

In numerous markets, motivating forces intended to promote renewable energy production expect that traditional generations keep on providing required grid support including frequency control, contingency reserve, voltage control, and adjusting services. As systems depend on renewable sources, those grid services will progressively need to originate from renewable resources as well. This implies important changes in the task of renewable sources (Papaefthymiou & Dragoon, 2016).

2.2.4 Diversifying renewable resources

The main parameter to consider for the implementation of renewable technologies is the cost of the energy generated without focusing on the quality and the variability of renewable resources. For instance, wind power generators tend to be implemented in places where the wind resource and transmission access are available. As a result,

resources will be bunched together, and the output of the generator tends to increase and decrease depending upon the renewable resources. This prompts a higher aggregated fluctuation, expanding the flexibility burden on the power system (Budischak et al., 2013). Few regions have chosen to take up renewable power source improvement zones to give motivating forces to spread resource developments under various weather conditions that might be less firmly correlated with each other. Another probability is to explicitly recognize the extent to which new resources are related with existing resources, giving financial motivations to areas that are less emphatically associated with the output of resources. The benefits of expanding geographic diversity should be balanced against the expense of new transmission infrastructure (Papaefthymiou & Dragoon, 2016).

2.2.5 Bulk energy storage

Energy storage is reported as the backbone of a power system with high penetration level of renewable generators (Akinyele & Rayudu, 2014; Ould Amrouche et al., 2016). The storage of energy can occur at any or all the three parts of a power system namely the primary energy input level which may be water in hydro reservoirs, coal piles, etc., at the grid level for instance batteries, pumped storage, and so on, and toward the end client level that is hot water tanks, electric vehicles, ice storage, and so forth. Today balancing supply and demand is practised to a great extent at the primary energy input level, by changing the supply of power from controllable generators to coordinate demand for power.

As renewable generators become prevailing in the power generation, the role of traditional power plants on balancing is decreased and alternative arrangements are expected to connect times of limited supply for periods of weeks or even a long time at any moment. Such longer-term energy storage is named bulk energy storage to recognize it from energy storage giving shorter-term framework adaptability needs (Ogland-Hand et al., 2019). The focal challenge of high penetration levels of renewable generators is discovering bulk energy storage choices that are not prohibitively costly.

2.2.6 Transmission network efficiency and flexibility

The development of large-scale transmission systems is needed in numerous 100 % renewable power system situations. An integral approach is required for the advancement of large-scale transmission, including favourable public reception of these improvements, usage of compensation strategies for the inhabitants affected by the implementation of new projects and creating mechanisms for financing of cross-border transmission system projects. Another option to consider is the utilisation of

power networks in more efficient ways by allowing dynamic evaluation of transmission capacity and more control of power flows. (Migliavacca, 2013). Improving the control of transmission and measurement technology can allow better usage of the available capacity of the transmission network. Another viewpoint to effective utilisation of transmission is geographic specificity of market costs; uniform market costs over extensive territories infer a "copper plate" zone where the transmission network qualities are not unmistakeable to advertise members. This regularly prompts blockage, that is settled by re-dispatching generation systems (Neuhoff et al., 2013).

2.2.7 Role of smart grids

Ordinary power systems are operated by controlling a modest number of grid components which include generators and control devices such as switches, transformer taps, reactors, and so forth. Depending on a network of smaller renewable distributed generations, small-scale energy storage devices and controllable demand introduce complexity in the power system, creating the need to implement two-way communication. This two-way communication and control infrastructure are achieved through the concept of smart grid. A key challenge is streamlining the task of distributed generations as per the general agreement of numerous partners, including end clients, circulation framework administrators, and the bigger power system (Brown, 2014).

2.2.8 Power system stability with non-synchronous generators

Traditional power generation systems are largely dominated by synchronous generators responsible of providing auxiliary services to maintain the stability. Operating a power system without a large fraction of these types of generator is a concern as the system might be subjected to instability. To achieve high penetration of renewable generators, specific actions need to be taken to guarantee the system stability. Key techniques for handling this challenge is to enable power converters. In case of wind and solar power plants, they ordinarily inject power into the utility grid through power inverters which can be controlled.

2.2.9 Effective utilisation of excess generation

Providing most or all energy demand from renewable generators suggests an excess of energy over numerous hours of the year. For instance, in systems with high penetration of wind generators, there are times when the wholesale market costs drop to zero, or even become negative. As renewable generators are included, these occasions will turn out to be frequent and include more energy. The two most challenging characteristics of high penetration levels will be seasons of prolonged low

efficiency and times of excess. Although much consideration has been paid to the seasons of prolonged low efficiency, excess will be a similarly significant component to oversee. Answers for this is either bulk energy storage.

2.3 Electrical energy storage technologies pour renewable energy applications

2.3.1 Introduction

One of the drawbacks of renewable generators, particularly those based on solar and wind is their intermittency, making their output power unreliable for continuous power supply. Through energy storage, these renewable sources may gain reliability and flexibility by storing any surplus energy generated whenever the resources are available and re-use it during low power generation period. In such a context, energy storage can decrease power fluctuations from renewable power sources, improve their flexibility and allow the dispatching of electricity generated while contributing as well to the security of energy supply.

In power systems, energy storage presents several benefits, which include

- reducing the energy wastage from renewable generators and increase energy usage;
- assisting in energy management;
- helping in the reduction of the quantity of primary energy used (fossil fuels) when generating electricity or heat, which in turn not only decrease the emission of CO_2 and other greenhouse gases but also assist in the conservation of fossil fuels to reduce its depletion;
- allowing the deployment of renewable, clean and intermittent energy resources into the grid and help in the load shifting;
- helping in the planning, operation, and frequency regulation of power systems;
- matching the demand with the supply, maintaining stability and improving the power quality of power systems.

Energy storage refers to the techniques used to convert one form of energy (mainly electrical energy) to another form; then the stored energy can be converted back to electrical form in case of need. Generally, an energy storage system consists of a medium storage, a power conversion system and a balance of the system.

Energy storage technologies are often classified according to their functions, response times, and suitable storage durations. The most used criterion is based on the form of

energy stored. As shown in Figure 2.2, energy can be stored in various forms such as mechanical, electrochemical, electrical, thermochemical, chemical and thermal.

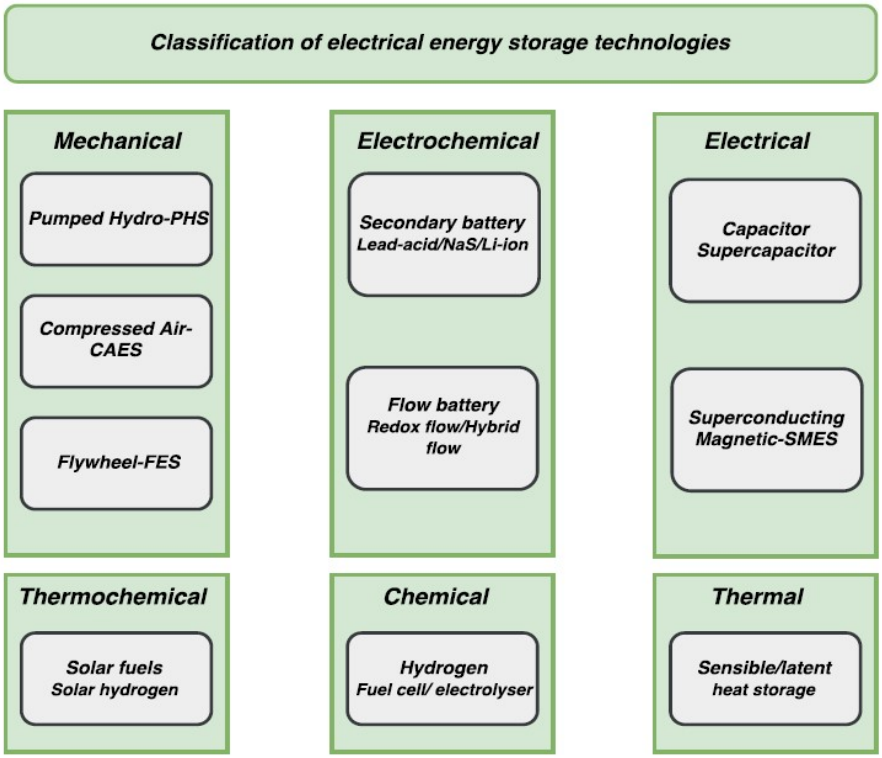

Figure 2. 2: Classification of energy storage technologies. (Luo et al., 2015)

2.3.2 Energy storage efficiency

A common energy storage technology is subjected to losses as shown in Figure 2.3, these losses depend usually on the storage time.

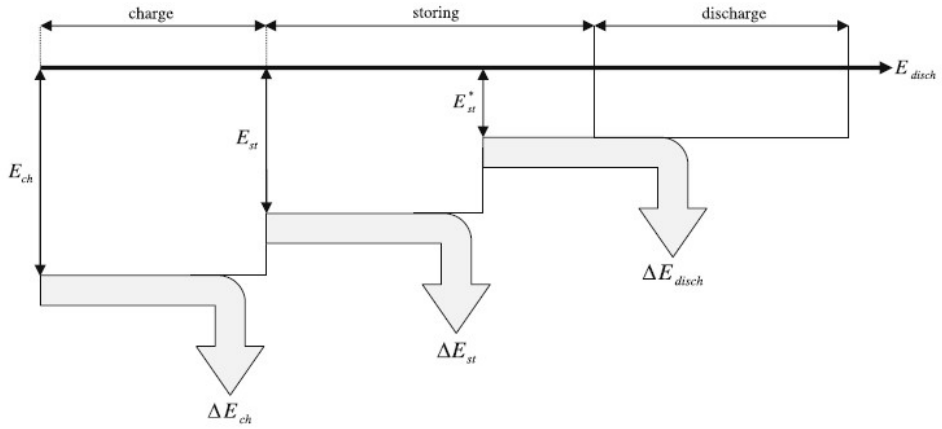

Figure 2.3: Equilibrium of energy in an energy storage system (Palizban & Kauhaniemi, 2016)

The energy delivered by the energy storage device to a load is expressed in Equation 2.1 as:

$$E_{Delivered} = E_{Generate} - \Delta E_{Loss} \quad (2.1)$$

where $E_{Generate}$ and ΔE_{Loss} are the generated energy and energy loss respectively.

Whereby the energy loss is given as (Palizban & Kauhaniemi, 2016):

$$\Delta E_{Loss} = \Delta E_{ch} + \Delta E_{st} + \Delta E_{disch} \quad (2.2)$$

where ΔE_{Loss}, ΔE_{ch}, ΔE_{st} and ΔE_{disch} are the energy losses, energy losses during the storage, and energy losses during charge and discharge respectively.

An important parameter of an energy storage system is the efficiency of each energy flow step, the efficiency of a charge step is defined as:

$$\eta_{ch} = \frac{E_{st}}{E_{ch}} \quad (2.3)$$

where E_{st} and E_{ch} are the stored energy and energy during charging respectively.

The storage period in an energy storage is defined as:

$$\eta_{st}(t) = \frac{E_{st}^{*}}{E_{st}} \quad (2.4)$$

where E_{st}^{*} and E_{st} are the existing stored energy and stored energy respectively.

The efficiency of discharging is given in Equation 2.5 as (Palizban & Kauhaniemi, 2016):

$$\eta_{disch} = \frac{E_{st}^{*}}{E_{disch}} \quad (2.5)$$

where E_{disch} is the discharging energy.

The energy storage efficiency is expressed as (Palizban & Kauhaniemi, 2016):

$$\eta_{st} = \frac{E_{out}}{E_{Generate}} = \eta_{st}.\eta_{st}(t).\eta_{disch} \quad (2.6)$$

where E_{out} and η_{st} are the output energy and the storage efficiency respectively.

2.3.3 Electrical energy storage technologies and characteristics

2.3.3.1 Mechanical energy storage

Mechanical energy storage technologies are electromechanical systems that convert electrical energy into forms that can be easy stored. The most common storage technologies in this category include Pumped Hydroelectric Storage (PHS), Compressed Air Energy Storage (CAES) and Flywheel Energy Storage (FES).

2.3.3.1.1 Pumped Hydroelectric Storage (PHS)

A typical Pumped Hydroelectric Storage (PHS) is presented in Figure 2.4. It is the oldest and largest of all the energy storage technologies available into the market and is based on the gravitational principle. PHS consists of two large water reservoirs arranged in such a way that the elevation of one is higher than that of the other. Its operation consists of water being pumped from the lower to the upper reservoir during off-peak demand periods. The stored water is then released back to the lower reservoir while drive a generator for electricity generation when needed.

The energy stored in a PHS is equivalent to the product of the volume of water and the height difference between the upper and lower reservoirs as expressed in Equation 2.7

$$E_{stored} = \alpha V\left(H_{upper} - H_{lower}\right) \tag{2.7}$$

where α is the product of the density of water and the gravity acceleration, V is the volume of water, and H_{upper} and H_{lower} are the upper and lower heights respectively.

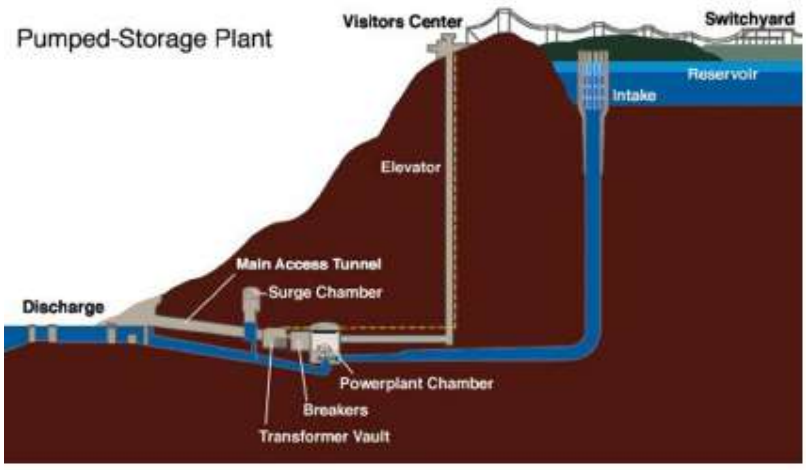

Figure 2. 4: Schematic diagram of a PHS (Akinyele & Rayudu, 2014)

PHS is a widely used option for large-scale storage applications representing 3% of the world's total installed power capacity (Luo et al., 2015) and 97% of the total storage capacity and a power rating in the range of 100 MW to 3000 MW (Akinyele & Rayudu, 2014). This power rating is the highest of all the available storage technologies, therefore, it is predominantly used for energy management, frequency regulation and provision of reserve. The round-trip efficiency (RTE) of this technology is in the range of 70 to 80%, but generally 75% depending upon the technical characteristics of the equipment. Its expected lifespan is between 40 and 60 years (Akinyele & Rayudu, 2014).

The RTE is also referred to as an AC/AC efficiency and always below 1 due to losses. This RTE is given by Equation 2.8 as:

$$RTE = \frac{E_{out}}{E_{in}} \tag{2.8}$$

where E_{out} and E_{in} are the energy output and input respectively.

PHS is seen as an attractive storage technology as its autonomy depends on the volume of water stored and can start up within few minutes, however, the main drawbacks of PHS are their high capital cost, need for appropriate implementation site, long construction period and environmental concerns.

2.3.3.1.2 Compressed air energy storage (CAES)

Besides PHS, compressed air energy storage (CAES) (see Figure 2.5) is another mature and commercially available energy storage technology with large power storage capability. The power rating of a single CAES is in the range of 50 MW to 300 MW. A typical CAES consists of the main components namely (Kousksou et al., 2014a; Akinyele & Rayudu, 2014):

- A motor/generator that uses clutches to alternate between the compressor for the air storage and the turbine train for electricity generation.
- A two or more stages air compressor with intercoolers and after-coolers to accomplish economy of compression and reduce the moisture content of the compressed air.
- A turbine train consisting of both low- and high-pressure turbines.
- An underground cavern or above ground vessels for compressed air storage.
- Equipment controls and auxiliaries (fuel storage and heat exchanger units).

The operation of a CAES is based on the conventional gas turbine generation. During low power demand periods, the excess electricity drives a motor/generator which in turn runs a chain of compressors to inject air into a storage vessel at pressure around 4 MPa to 8 MPa. The stored air is in the form of high-pressure air. When the power generation cannot meet the load demand, the stored compressed air is released and heated by a heat source. The heat source can be from the combustion of fossil fuel or the heat recaptured from the compression process. The compressed air is then used to drive the turbines.

CAES technologies have an estimate efficiency of about 70% with an expected lifespan of 40 years.

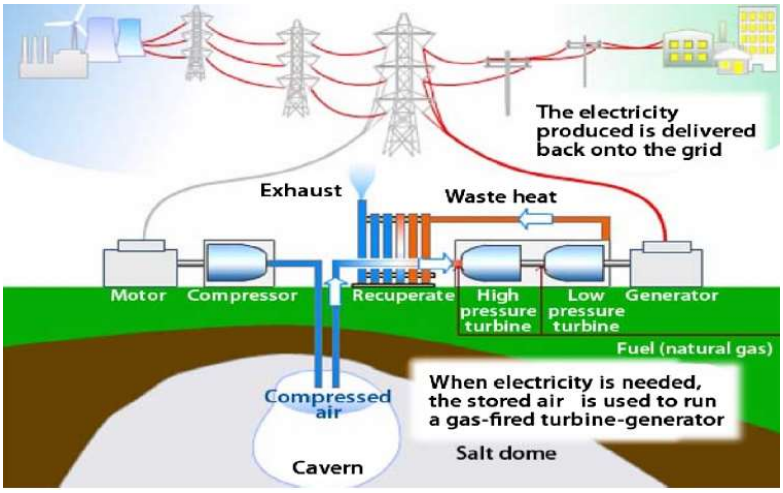

Figure 2. 5: Schematic diagram of a CAES. (Aneke & Wang, 2016)

2.3.3.1.3 Flywheel energy storage (FES)

A flywheel energy storage (FES) consists of a flywheel, a group of bearings, a reversible electrical motor/generator, a power electronic system and a vacuum chamber (see Figure 2.6). It stores energy by the means of the rotor acceleration at a high-speed rate, and then this energy is conserved in the system as kinetic energy. The kinetic energy is released by reversing the process through the motor/generator. As the stored energy is released, the flywheel rotor slows until it is completely discharged. A typical FES has the potential of charging and discharging fast and is not influenced by the variation of their operating temperature. The power rating of FES technologies is between 150 kW and 1 MW (Mousavi G et al., 2017; Bolund et al., 2007).

Some of the benefits of FES include

- require little space;
- have lower maintenance requirements as compared to batteries and their lifetime is not influenced by their deep discharge contrary to batteries;
- have long lifetime.

However, FES technologies have a drawback of no tolerating idling losses during the time when the flywheel is on standby which can lead to a self-discharge of around 20% of the stored capacity per hour.

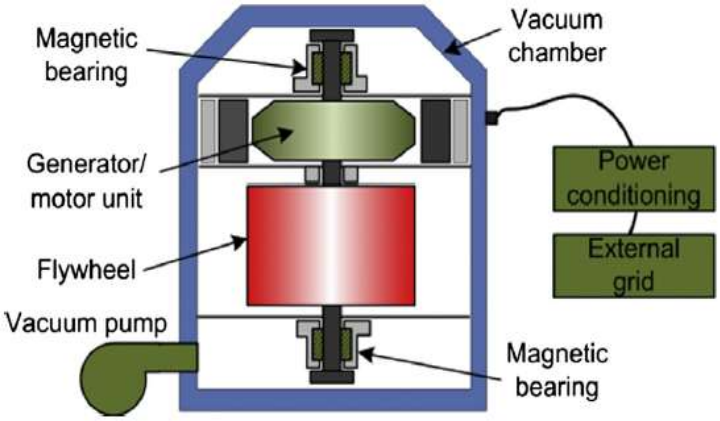

Figure 2. 6: Schematic diagram of a FES. (Luo et al., 2015)

2.3.3.2 Electrochemical energy storage

Electrochemical energy storage technologies are closed systems capable of converting reversibly chemical energy into electrical. Depending on their operating conditions, their efficiency can reach values around 80 to 90%. The available types of electrochemical energy storage differ from each other depending upon the nature of the chemical reaction, structural features, and design. They are classified in four categories based on to their principle of operation, there categories include primary battery, secondary battery, reverse cell, and fuel cell.

2.3.3.2.1 Primary batteries

Primary batteries are no rechargeable. They use either aqueous and non-aqueous electrolytes contained within an absorbent material or a separator. Batteries based on aqueous electrolyte comprise Leclanche Zinc-Carbon and Zinc Chloride, Alkaline Zinc–

Manganese Dioxide, Zinc-Air, Zinc–Silver Oxide, and Zinc–Mercuric Oxide, while non-aqueous electrolyte batteries are Lithium–Thionyl Chloride, Lithium–Sulfuryl Chloride and Lithium–Sulphur Dioxide, Lithium–Manganese Dioxide, Lithium–Carbon Monofluoride, Lithium–Iron Disulphide, Lithium-Iodine, Lithium–Silver Vanadium Oxide, Lithium–Copper Oxide.

2.3.3.2.2 Secondary batteries

Also known as rechargeable batteries, secondary batteries are the oldest and classical technique for storing electrical energy in an electrochemical form. They include one or more electrochemical cells and an individual cell consists of a liquid, paste or solid electrolyte along with a positive electrode (anode) and a negative (cathode). The reactions occurring in those batteries are reversible, grating them the ability to recharge once a voltage is applied across the electrodes. Their sizes range from less than 100 W to large megawatts (see Table 2.1).

The major drawbacks of batteries are their high capital cost, materiel availability, loss of charge when idle, and loss of capacity over time (see Table 2.2). They are extensively used in the automotive industry, aerospace operations, marine and submarine missions, electronics devices and power systems. In the power system context, they are used for different purposes such as power quality improvement, energy management and ride-through. Commercially available batteries include lead-acid battery, lithium-ion battery, sodium-sulphur battery, nickel-cadmium battery, sodium-nickel chloride battery, iron-chromium battery, bronze bromine battery, zinc-air battery, vanadium-redox battery, etc.

Table 2. 1: Comparison of battery energy technologies (Zhang et al., 2018)

Battery technology	Rated power (MW)	Energy density (Wh/kg)	Discharge duration (h)	Energy efficiency (%)	Lifetime/cycles	Storage costs (US $/kWh)
Lead-acid battery	<36	<50	<8	75 – 85	3 – 12 years/500 – 1200	300 - 600
Lithium-ion battery	<102	<200	<6	90-94	5-15 years/1000-10,000	1200-4000
Vanadium based flow battery	<28	<30	<10	70-85	5-15 years/12,000-18,000	600-1500
Sodium-sulphur battery	<50	<240	<8	75-86	5-10 years/2500-4000	1000-3000
Aluminium-ion battery	N/A	<60	<6	90-94	5-15 years/1000-10,000	300-600

Table 2. 2: Advantages and disadvantages of battery energy storage technologies (Zhang et al., 2018)

Battery technology	Advantages	Disadvantages	Applications
Lead-acid battery	Low capital cost	Limited life cycle, long charging time, high self-discharge and environmental	Frequency control, load adjustment and hot spare
Lithium-ion battery	High energy densities, high efficiency and long life cycle	High production cost requires special charging circuit	Frequency control, load shifting and power quality
Vanadium flow battery	High power, long life cycle, fast charge and discharge	High production cost, large area	Load shifting, emergency standby and power quality
Sodium-sulphur battery	High power and energy densities, high efficiency	Production cost and safety concerns	Load adjustment and standby power
Aluminium-ion battery	Low capital cost, fast charge and discharge, high efficiency	Under development, low energy density	N/A

2.3.3.2.2.1 Lead-acid batteries

Lead acid batteries are the most mature and cheapest of rechargeable batteries. They consist of cells containing a positive electrode of lead dioxide ($Pb0_2$) forming the cathode and an anode of lead (Pb). Both electrodes are submerged into a sulphuric acid acting as an electrolyte. Two types of lead-acid batteries can be distinguished namely flooded batteries which are the most available technology, and valve-regulated batteries still under research and development. (Kousksou et al., 2014a) The cost of a typical lead-acid battery ranges between US $300 to US $600. It is characterised by a high reliability and an efficiency of about 70 to 90%. Some of the drawbacks of these batteries include a relatively poor performance at low and high temperature, a short lifespan (3 – 4 years), a low depth of discharge (<20%), the need for periodic water maintenance, a low specific energy and power and the inability of providing frequent power cycling in partial state of charge which may lead to a premature failure because of sulfation (Ould Amrouche et al., 2016; Nair & Garimella, 2010; Bhuiyan & Yazdani, 2012). Despite all the drawbacks, lead-acid batteries have been utilised in power systems due to their low costs.

2.3.3.2.2.2 Lithium-ion (Li-ion) batteries

Li-ion batteries are mostly used in mobile phones, portable electronics and medical devices; however, this type of battery is attracting much interest in other applications such as electric vehicles and stationary energy storage as they are smaller, lighter and

more powerful than other batteries. The energy and power density of a Li-ion battery is in the ranges of 90 Wh/kg to 190 Wh/kg and 500 W/kg to 2000 W/kg, while its efficiency is high (over 95%) and self-discharge rate low (5% per month) (Doudou Nanitamo Luta & Raji, 2019).

The anode of Li-ion batteries consists of lithiated metal dioxide, the cathode is made from graphite and the electrolyte is a lithium salt dissolved in organic graphite. The operation of Li-ion batteries is such that there is a transfer of lithium ions from the anode during charging and reversibly during discharging. Equation 2.9 and Equation 2.10 show the chemical reactions during the charging and discharging at the anode and the cathode (Akinyele & Rayudu, 2014). Li-ion batteries have a cell voltage of 3.6 V, which is higher than that of lead-acid batteries which are 2 V. (Li, 2008)

Anode: $C + xLi^+ + xe^- \leftrightarrow Li_xC$ (2.9)

Cathode: $LiMO_2 \leftrightarrow Li_{1-x}MO_2 + xLi^+ + xe^-$ (2.10)

2.3.3.2.2.3 Vanadium flow battery

Vanadium flow battery is the most mature battery of a category referred to as redox (reduction oxidation) flow batteries. Redox flow batteries are one of the most recent and highly promising technologies for stationary energy storage applications (Ponce de Leon et al., 2006; Alotto et al., 2014). They use redox processes species in fluid solution stored in external tanks and inserted into the redox flow battery whenever wanted. The operation of this group of batteries is such that several electrochemical reduction and oxidation reactions occur in two liquid electrolytes consisting of metal ions. The reduction from one of the electrodes extracts electrons and ions electrolytes, while the oxidation at the other electrode reassembles them into the other electrolyte (see Figure 2.7). Ions move from the anode to the cathode through an electrolyte that hinders electrons to pass, hence driving them in an external circuit in the form of electricity.

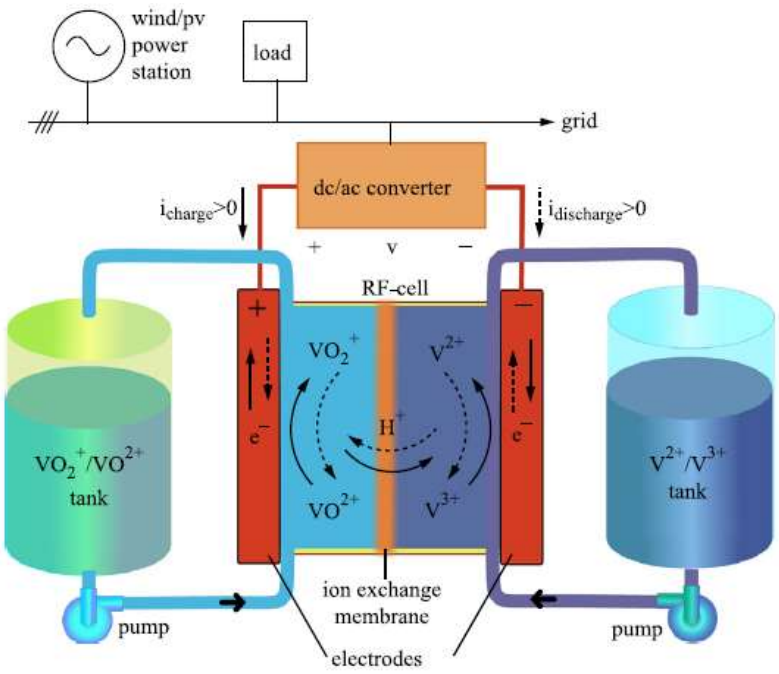

Figure 2. 7: Diagram of a redox flow battery (Alotto et al., 2014)

Vanadium flow batteries use various ionic vanadium materials to transfer electrons. As shown in Equation 2.11 and Equation 2.12, throughout the charging time at the anode, V^{3+} (vanadium +3) is converter to V^{2+} (vanadium +2) by gaining an electron, while during discharge, V^{2+} is converter back to V^{3+} by losing an electron. In the similar manner, the process of electron transfer takes place between ions V^{2+} (vanadium +4) and VO_2^+ (vanadium +5) at the cathode (Akinyele & Rayudu, 2014; Choi et al., 2017).

Anode: $V^{3+} + e^- \leftrightarrow V^{2+} \qquad E_o = -0.25V$ (2.11)

Cathode: $VO^{2+} + 2H^+ + e^- \leftrightarrow VO_2^+ + H_2O \quad E_o = 1V$ (2.12)

The net reaction of a vanadium redox battery cell is expressed as (Choi et al., 2017):

Net: $VO^{2+} + HO_2 + V^{3+} \leftrightarrow VO_2^+ + 2H^+ + V^{2+} \qquad E_o = 1.25V$ (2.13)

2.3.3.2.2.4 Sodium-sulphur battery

Sodium-sulphur battery is a good candidate for energy storage applications in renewable power systems. It consists of sodium anode, sulphur cathode and electrolytes based on beta-Al_2O_3 ceramic. The beta-Al_2O_3 electrolyte also serves as a separator to hinder contact between the anode and the cathode.

A sodium-sulphur battery operates based on the electrochemical reactions occurring between sodium and sulphur and the creation of sodium polysulfides. These reactions are expressed in Equation 2.14 and Equation 2.15 as (Wen et al., 2008):

Anode: $2Na = 2Na^{+} + 2e^{-}$ (2.14)

Cathode: $xS + 2e^{-} = S_x^{2-}$ (2.15)

Net: $2Na + xS = Na_2S_x$ (2.16)

During discharge, the sodium is oxidised to form Na^{+} as shown in Equation 2.14 thereafter, moves across the beta-Al_2O_3 electrolyte and combines with the sulphur reduced at the cathode as expressed in Equation 2.15 to generate sodium pentasulfide. The overall cell reaction is given by Equation 2.16. During the charging process, the reactions are reversed, and the sodium polysulfide is decomposed to sodium and sulphur and migrate to the anode and cathode respectively (Bito, 2005). The open-circuit voltage of a sodium-sulphur battery cell is about 2.075 V (Wen et al., 2008), which is higher as compared to other common batteries.

2.3.3.3 Thermochemical energy storage

Thermal energy storage systems are utilised to address the mismatch resulting from the discontinuity of energy systems based on solar energy to maintain continuous electricity supply (Gil et al., 2010) . They include a minimum of three stages which are heated charging, storage and discharging. Three methods of storing thermal energy can be distinguished namely sensible heat storage, latent heat storage and thermochemical storage. Table 2.3 provides details of the comparison between the three types of thermal energy storage. This section is dedicated to thermochemical energy storage, whereas the next section will focus on thermal energy storage.

A simplified representation of a thermochemical energy storage is presented on Figure 2.8. The reactions occurring in this energy storage system are reversible as expressed in Equation 2.17 (Pardo et al., 2014):

$A + \Delta H_r \Leftrightarrow B + C$ (2.17)

Heat is kept during the endothermic reaction stage and discharged during the exothermic stage. The storage of thermochemical heat is related to the reaction enthalpy. During the charging stage (endothermic reaction), thermal energy is utilised to separate a chemical reactant (A), into composites (B) and (C), while during the

discharging stage, the composites (B) and (C) are combined to react and form the initial reactant (A) by releasing heat.

In general, the thermal energy stored in thermochemical system is expressed by Equation 2.18 as:

$$Q = nA\Delta H_r \tag{2.18}$$

where $\boldsymbol{n}$ is the number of moles of the reactant $\boldsymbol{A}$ and $\Delta \boldsymbol{H_r}$ is the reaction enthalpy.

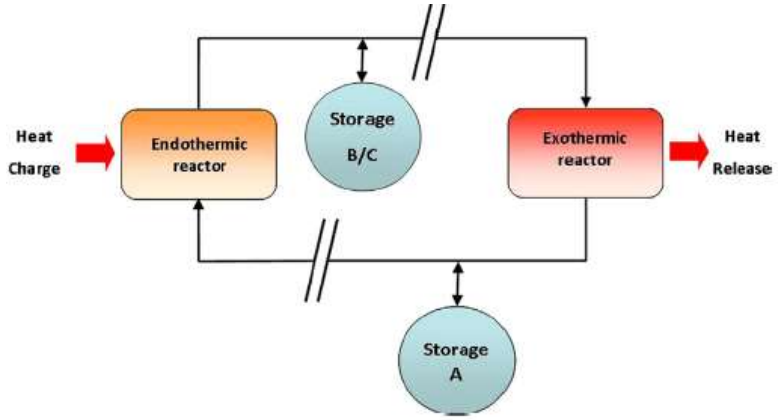

Figure 2. 8: Layout of a thermochemical energy storage (Pardo et al., 2014)

2.3.3.4 Thermal energy storage

Two methods are used to store thermal energy namely sensible heat storage and latent heat storage. Sensible heat storage method is further subdivided into liquids and solids storage methods, whereas latent heat storage method can be grouped in solid-liquid, solid-gaseous and solid-solid storage methods as depicted in Figure 2.9 (Sharma et al., 2009).

Sensible heat storage (SHS) operation is such that thermal energy is stored by increasing the temperature of a solid or liquid material based on its heat capacity and change in temperature during the charging and discharging processes. The quantity of the stored heat is related to the specific heat of the medium, the change of temperature and the quantity of storage material (Alva et al., 2018).

The quantity of heat that can be stored in sensible heat storage method is given by Equation 2.19:

$$Q = \int_{T_i}^{T_f} mC_p\, dT = mC_p(T_f - T_i) \tag{2.19}$$

where Q is the quantity of heat m is the mass of the material C_p is the specific heat of the material, T_f and T_i are the final and initial temperature of the material respectively.

Table 2.3 shows the sensible heat storage capacity of some solid-liquid materials. Water happens to be the best SHS liquid available as it is most cost-effective and has a high specific heat. However, for temperature high than 100^o C, oils, molten salts and liquid metals, etc. are preferred (Sharma et al., 2009).

On the other hand, latent heat storage (LHS) considers the heat absorption or release when a storage material passes through a phase change from solid to liquid or liquid to gas or vice versa. Equation 2.20 and Equation 2.21 give the storage capacity of the LHS system with a PCM medium (Sharma et al., 2009).

$$Q = \int_{T_i}^{T_m} mC_p\, dT + ma_m \Delta h_m + \int_{T_i}^{T_m} mC_p\, dT \tag{2.20}$$

$$Q = m[C_{sp}(T_m - T_i) + a_m \Delta h_m + C_{lp}(T_f - T_i)] \tag{2.21}$$

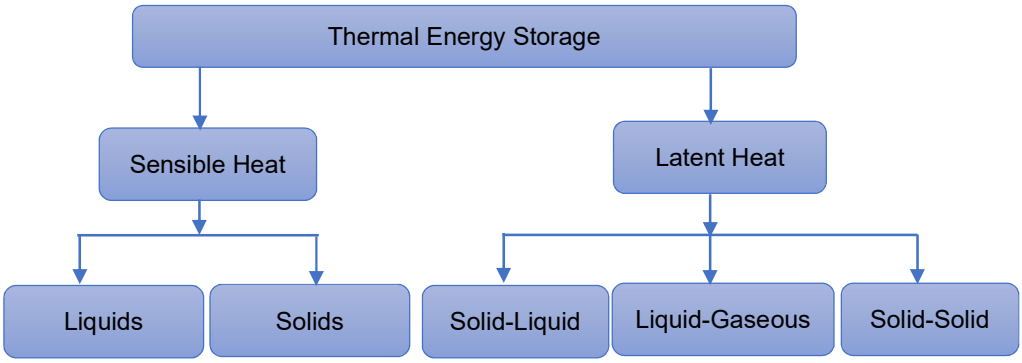

Figure 2. 9: Thermal energy storage technologies, developed from (Alva et al., 2017)

Table 2. 3: Characteristics of thermal energy storage systems (Pardo et al., 2014)

	Sensible heat storage system	Latent heat storage system	Thermochemical storage system
Energy density Volumetric density Gravimetric density Storage temperature Storage period Transport Maturity Technology	• Small ~ 50 kWh m3 of material • Small ~ 0.02 - 0.03 kWh kg of material charging step temperature • Limited (Thermal losses) • Small distance • Industrial scale • Simple	Medium ~ 500 kWh m3 of material Medium ~ 0.05 - 0.1 kWh kg of material Changing step temperature Limited (Thermal Losses) Small distance Pilot scale Medium	High ~ 500 kWh m3 of reactance High ~ 0.5-1 kWh kg of reactant Ambient temperature Theoretically unlimited Distance theoretically unlimited Laboratory scale complex

Table 2. 4: Comparison of thermal energy storage technologies (Pardo et al., 2014)

Performance parameter	Type of thermal energy storage		
	Sensible TES	Latent TES	Chemical
Temperature range	Up to: • 110 °C (water tanks) • 50 °C (aquifers and ground storage) • 400 °C (concrete)	20 - 40 °C (paraffins) 30 – 80 °C (salt hydrates)	20 - 200 °C
Storage density	Low (with high temperature interval) 0.2 GJ/m^3 (for typical water tanks)	Moderate (with low temperature interval) 0.3 – 0.5 GJ/m^3	Normally high 0.4 – 3 GJ/m^3
Lifetime	Long	Often limited due to storage material cycling	Depends on reactant degradation and side reactions
Technology status	Available commercially	Available commercially for some temperatures and materials	Generally, not available, but undergoing research and pilot project tests
Advantages	• Low cost • Reliable • Simple application with available materials	• Medium storage density • Small volumes • Short distance transport possibility	• High storage density • Low heat losses • Long storage period • Long-distance transport possibility • Highly compact energy storage
Disadvantages	• Significant heat loss over time (depending on the level of insulation) • Large volume needed	• Low heat conductivity • Corrosively of materials • Significant heat losses (depending on the level of insulation)	• High capital cost • Technically complex

The comparison of thermal energy storage systems is dependent on six parameters namely the energy density, the storage temperature, the storage period, and the material transportation possibility, the maturity of the system and the complexity of

related technologies. Table 2.3 shows the characteristics of each storage technology, whereas Table 2.4 gives the comparison of thermal energy storage technologies based on the six parameters mentioned above.

2.3.3.5 Characteristics and comparison of electrical energy storage

A typical energy storage technology is characterised based parameters such as energy density, power density, lifetime, capital and operating cost, storage capacity and duration, etc., some of the characteristics ar4e presented in below sections.

2.3.3.5.1 Energy density and power density

Power density refers to the ratio of the rated power output of an energy storage device over its volume (Chen et al., 2009; Kousksou et al., 2014b). It differs from energy density, as the latter is defined as the ratio of the actual energy storage over the volume of the storage device which is regarded as the total volume of the energy storage device including the storing element, accessories, supporting structures and inverters systems (Chen et al., 2009; Kousksou et al., 2014b).

Energy storage devices with high-power density are suitable for application requiring high power quality demand through large discharge currents and fast response time. This category includes energy storage devices such as flywheels, supercapacitors and SMES and conventional batteries. Flow batteries are lower in power density as compared to conventional batteries. Among batteries, Li-ion, NaS and $NaNiCl_2$ have higher energy density than others. On the other hand, CAES, PHES have high-energy density.

2.3.3.5.2 Lifetime

The lifetime of any given energy storage device plays a key role in choosing whether the technology is adequate for a specific application. From investment perspective, energy storage technologies with long lifespans are preferred over those with short lifespan (Aneke & Wang, 2016). Generally, energy storage devices such as PHES, CAES and flywheel have long lifespans. On the contrary, batteries have a short lifespan due to chemical deteriorations during their operations.

2.3.3.5.3 Capital and operating costs

The cost of an energy storage technology is an important factor for it commercialisation. This cost includes the purchase, operating cost, maintenance, disposal and replacement costs. Auxiliary components used in some energy storage technologies may increase the total cost of the device, making the technology to be economically viable only above a minimum energy content and energy production (Kousksou et al.,

2014b; Aneke & Wang, 2016). Energy storage technologies such as PHES, CAES and Zn-Air are relatively low-cost systems. CAES may have lower capital cost per kWh as compared to PHES, however, it suffers from lower return efficiency. Technologies such as flywheel, SMES, supercapacitors have the highest cost of capital per kWh, however, their capital cost per kWh per cycle is low, making them suitable for high-power applications for short duration (Aneke & Wang, 2016).

2.3.3.5.4 Storage capacity and duration

Storage capacity refers to the total amount of energy available in the storage device. Large scale energy storage devices have also large storage capacity. Because of self-discharge, the storage duration is considered as an important parameter when choosing an energy storage system. Storage technologies with low self-discharging ratios are appropriate for long energy storage use. In general, energy storage systems such as PHES and CAES have large storage capacity, hence, they are commonly used for grid scale energy storage application (Aneke & Wang, 2016).

2.3.4 Hybrid energy storage topologies

The basic way of connecting two energy storage technologies as a hybrid system is through a direct DC coupling (Figure 2.10a). The benefit of this approach is its simplicity and cost effectiveness, in addition to only small variations in the DC-bus voltage. However, direct DC coupling does not present the possibilities for power flow control and energy management and as a result, there is ineffective use of the energy storage devices.

The second energy storage coupling architecture in a hybrid energy storage topology is via a bidirectional DC-to-DC-converter (Figure 2.10b). The converter can either permit the connection of a “high-power” or a “high-energy” storage system. In the latter case the “high-energy” storage device can be protected against peak power and fast load fluctuations. The DC-to-DC-converter then operates in current-controlled mode. A drawback of this solution is the fluctuation of the DC-bus voltage, which is identical to the voltage of the “high-power” storage.

The two last topologies are the most common and promising coupling architectures (Figure 2.10c and Figure 2.10d) and are referred to as the parallel converter topologies. The DC-to-DC-converter associated with the “high-power” storage plays the role of regulating the voltage of the DC bus and operating the high-power storage system in a broader voltage band. In addition to these parallel converter topologies, a serial cascade-type of converter topology is also feasible, however, it is generally expensive and difficult to be controlled (Esmaili et al., 2013).

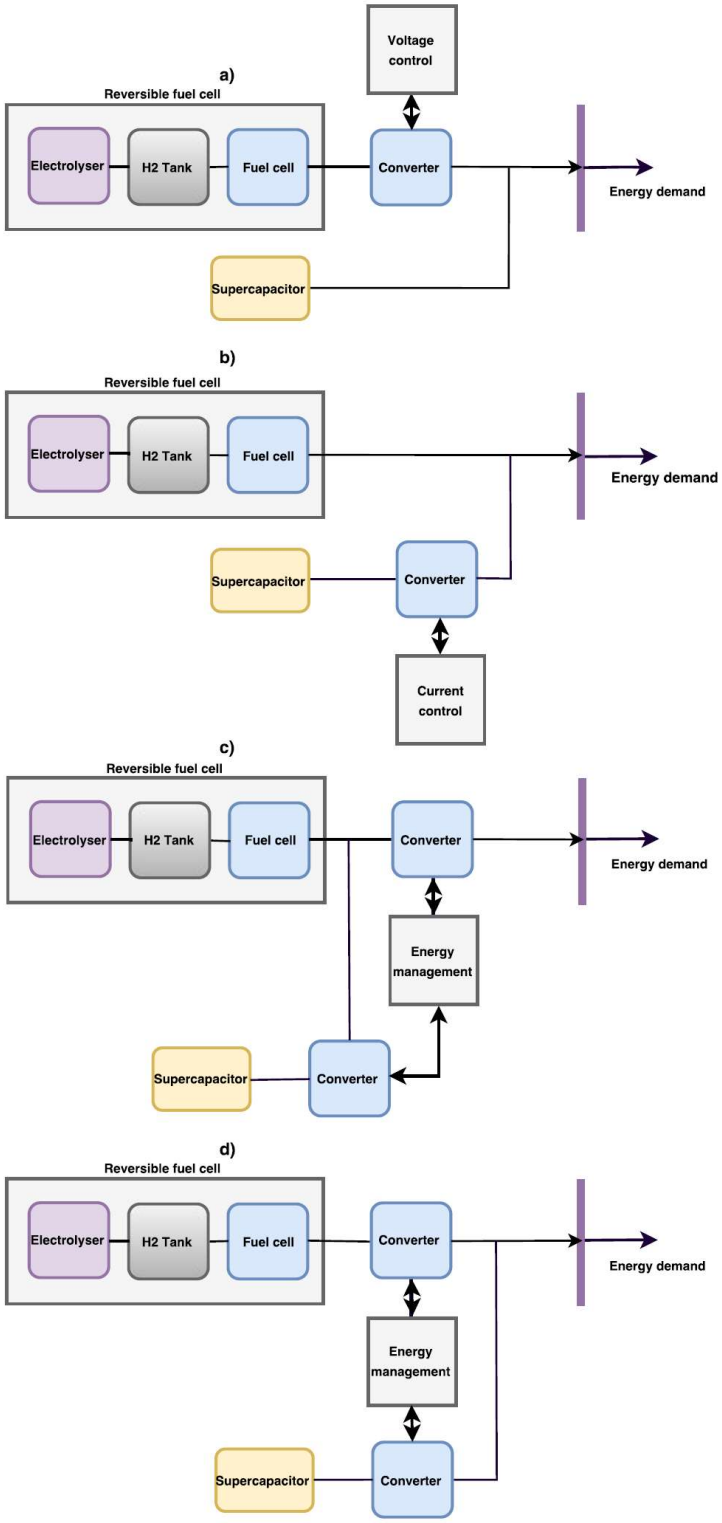

Figure 2.10: Hybrid energy storage topologies

2.4 Fuel cells

2.4.1 Introduction

Fuel cells are one of most emerging technologies for power generation. There are electrochemical devices that convert chemical energy from electrolytic reactions directly into electricity by rejecting heat and water. In general, fuel cells are efficient and clean platforms for energy conversion, moreover, they are suitable to be used with renewable sources and energy carriers such as hydrogen for energy security and sustainable growth. Consequently, they are considered as power generation devices of the future. Since fuel cells are independent of any moving part, no noise or vibration is associated with their operations. They can also be stacked in modular form to meet any load requirement in a wide range of applications including in transportation, portable and stationary power generation. Furthermore, fuel cells show great capabilities for use in microgrids (Caisheng et al., 2005), and unlike other green energy technologies (wind and solar power systems), they can operate at any site without geographic limitations to provide optimal services (Nehrir et al., 2006).

Fuel cells are classified according to the type of electrolytes used and their operating temperature, however, proton exchange membrane also known as polymer electrolyte membrane, fuel cells (PEMFC) are one of the most promising types already in the early commercialisation stage (Luta & Raji, 2018; Luta & Raji, 2017). Research is still ongoing to optimise and improve their performance, minimise their costs and increase their durability.

This section is dedicated to review fuel cell fundamentals, technologies, advantages and drawbacks, characteristics and features, thermodynamic and electrochemical principles.

2.4.2 Fuel cell fundamentals

Fuel cells consist of a negatively charged electrode (anode), a positively charge electrode (cathode) and an electrolyte membrane between them. These electrodes are made up of porous materials covered with a layer of catalysts, often in platinum for PEMFCs. The basic operation of a PEMFC is shown in Figure 2.11 Molecular hydrogen (H_2) migrates from a gas-flow stream to the anode for the electrochemical reaction.

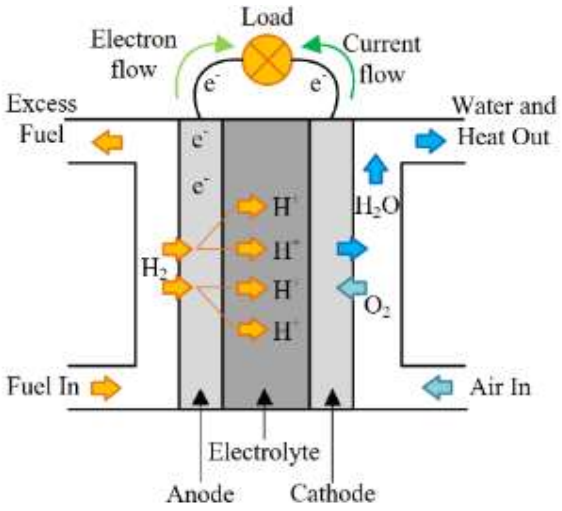

Figure 2.11: **Internal schematic of a proton exchange membrane fuel cell** (Vagus, 2012)

The hydrogen is oxidised to create hydrogen ions and electrons based on the Equation 2.22:

$$H_2 \rightarrow 2H^+ + 2e^- \tag{2.22}$$

The hydrogen ions migrate to the acidic electrolyte, whereas the electrons head toward an outside circuit to go to the negative electrode. At the cathode, water is formed through the reaction between electrons and hydrogen with the oxygen supplied from an external gas-flow stream as expressed in Equation 2.23:

$$\frac{1}{2}O_2 + 2H^+ + 2e^- \rightarrow H_2O \tag{2.23}$$

The overall reaction in a fuel cell producing water, heat (Q_{heat}) and electricity (W_{ele}) follows Equation 2.26 below:

$$H_2 + \frac{1}{2}O_{2^-} \rightarrow H_2O + W_{ele} + Q_{heat} \tag{2.24}$$

The water by-products and heat are removed endlessly to maintain appropriated conditions for power generation.

In general, fuel cells present many benefits in comparison with conventional power sources such as internal combustion engines and renewable generators. These benefits are (Das et al., 2017):

- ❖ Higher power efficiency;
- ❖ Noise-free operation;
- ❖ Less maintenance requirement;

- ❖ Economical, as it does not need any fossil fuel for its operation.

However, they also have critical limitations such as poor voltage profile against current density, slower dynamics and the presence of higher current ripples.

2.4.3 Type of fuel cells

In a fuel cell, hydrogen is the principal reactant while oxygen is the oxidant, however, various other sorts of reactants such as ethanol or some fuels derived from biomass are also being used depending upon the type of fuel cell technology; these technologies can be grouped according to the electrolytes used, operating temperatures, power outputs, electrical efficiencies, and applications. PEMFCs have the most substantial variety of applications because of their flexibility. A report of production revealed that in 2010, 97% of fuel cells in markets were PEMFCs (Doudou N. Luta & Raji, 2019d; Lucia, 2014a). They are the most promising contender for transport applications because of their high-power density, fast start-up time, high efficiency, low operating temperature, and simple and safe handling. However, PEMFCs are still too costly to be economically feasible or competitive. Alkaline Fuel Cells (AFCs) have the best performance while operating on pure hydrogen and oxygen, yet their narrow tolerance to impurities (especially carbon oxides) and short lifetimes block their job for terrestrial applications; they are prevalently utilised for extraterrestrial purposes.

Phosphoric Acid Fuel Cells (PAFCs) are perhaps the most commercially developed devices operating at intermediate temperatures. PAFCs are utilised for combined-heat-and-power (CHP) applications with high efficiencies. Molten Carbonate Fuel Cells (MCFCs) and Solid Oxide Fuel Cells (SOFCs) are high-temperature power devices fitting for cogeneration and combined cycle systems. MCFCs have the highest efficiencies that can be obtained from methane-to-power transformation in the size scope of 250 kW to 20 MW, while SOFCs are most appropriate for base-load utility applications. Working on coal-based gases condenses the primary contrasts between the most widely recognised fuel cell types accessible in the market or still under development. Table 2.5 gives the most available fuel cells, however, this section focuses on the best-known types which include alkaline fuel cell, phosphoric acid fuel cell, molten carbonate fuel cell and solid oxide fuel cell.

2.4.3.1 Alkaline Fuel Cell

Alkaline Fuel Cell is one of the prior fuel cell units utilised for NASA's space missions. Previously, it was called as Bacon fuel cells after its British designer. It works at low temperature of around 100^{o}C like PEMFC and has the capacity to achieve 60 to 70% of efficiency. It utilises a fluid solution of the potassium hydroxide (KOH) as an

electrolyte. It carries negative charged particles from the anode to cathode and discharges water as its by-product. This type of fuel cell has a quick start, which is one of its favourable benefits. Its significant drawback is its sensitivity to CO_2 since it requires more time to respond and consumes the alkaline in the electrolyte, thus decreasing the concentration of hydroxide particles during reactions (Kirubakaran et al., 2009). It needs a separate platform to expel the CO_2 from the air. The utilisation of a destructive electrolyte is additionally a drawback since it has shorter life expectancy. AFCs are utilised in transportations, for instance in fleet vehicles and boats, and space shuttles.

2.4.3.2 Phosphoric Acid Fuel Cell

Phosphoric Acid Fuel Cell works at around 175 to 200ºC. This working temperature is practically double when contrasted with that of PEMFC. It uses a fluid phosphoric acid as an electrode. Compared to PEMFC and AFC, Phosphoric Acid Fuel cell is exceptionally tolerant to impurities in the changed of hydrocarbon fuels. The chemical reaction engaged with this power module is the same as PEMFC where pure hydrogen is utilised as fuel (Farooque & Maru, 2001). The cogeneration is additionally possible because of its high-working temperature and the potential is accessible for boiling water supply just as electricity based on the heat and power load profile. The downside of PAFC is same as PEMFC, its cost rises because of utilisation of platinum as a catalyst. Size available in the market are 100 kW, 200 kW and 500 kW plants for stationery and heat applications.

$$H_2 = 2H^+ + 2e^- \quad \text{Anode} \tag{2.25}$$

$$\frac{1}{2}O_2 + 2H^+ + 2e^- \rightarrow H_2O \quad \text{Cathode} \tag{2.26}$$

$$H_2 + \frac{1}{2}O_2 \rightarrow H_2O \quad \text{Overall} \tag{2.27}$$

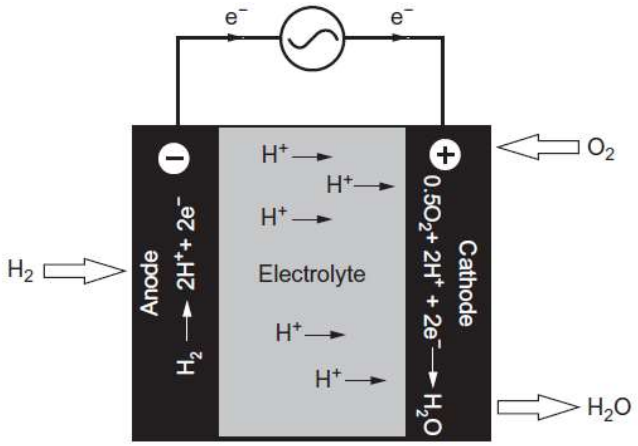

Figure 2.12: Phosphoric Acid Fuel Cell (Barbir et al., 2016)

2.4.3.3 Molten Carbonate Fuel Cell

Molten Carbonate Fuel Cell works at high temperature, which is about 600 to 700 °C. It comprises two permeable electrodes with great conductivity in contact with a molten carbonate cell. Because of its interior reforming capacity, it isolates the hydrogen from carbon monoxide fuel and the disintegration of hydrogen is taken through the water shift reaction to deliver hydrogen. At that point, the result of reaction is accepted as the same as PEMFC to generate electricity. The benefits of MCFC are (Farooque & Maru, 2001):

- higher efficiency of about 50 to 60%,
- no need of metal catalysts and separate reformers because of its high-working temperature.

Similarly, the drawbacks of this type of fuel cell are

- no tolerance to sulphur,
- moderate start up is one of its disadvantages. It is essentially utilised for medium and huge power applications.

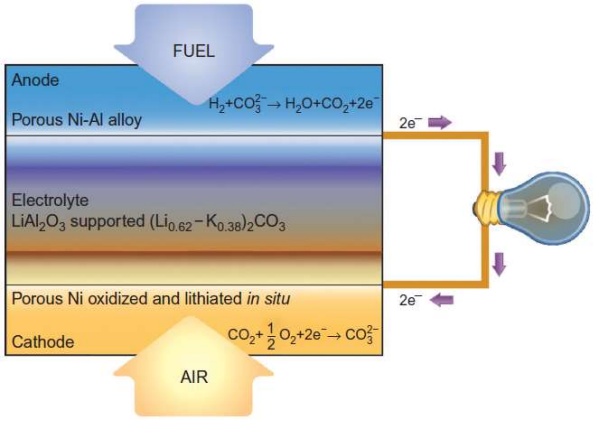

Figure 2.13: Molten Carbonate Fuel Cell (Barbir et al., 2016)

2.4.3.4 Solid Oxide Fuel Cell

Solid Oxide Fuel Cells (SOFC) are fundamentally high operating temperature energy devices. They utilise as electrolytes a thick yttria stabilised zirconia, which is a strong ceramic material. Oxygen $O^{=}$ consolidates with hydrogen H^{+} to generate water and heat. The power is produced at a high-working temperature of around 1000 ^{o}C. The primary benefit of a typical SOFC is its high efficiency of about 50 to 60 % and a different reformer is not required to extract hydrogen from the fuel because of its inner reforming capacity. Through cogeneration, waste and heat can be reused to make extra power (Swider-Lyons et al., 2003; Farooque & Maru, 2001). However, the moderate start up, high cost and non-tolerance to sulphur substance in the fuel cell are some of its disadvantages. This type of fuel cell is not appropriate for bigger load demand fluctuations. Thus, SOFCs are fundamentally utilised for medium and high-power applications.

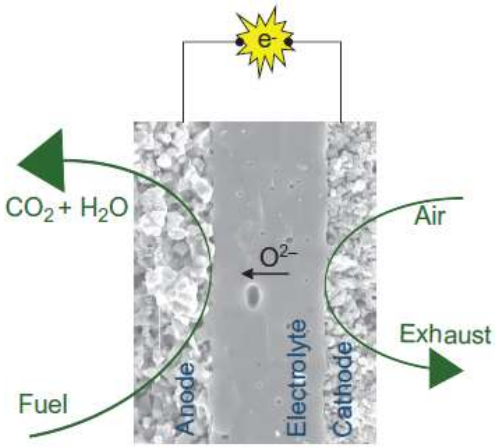

Figure 2.14: Solid Oxide Fuel Cell (Barbir et al., 2016)

Table 2. 5: Common fuel cells technologies, characteristics, advantages and disadvantages (Edition & Virginia, 2004; Lucia, 2014b; Lucia, 2014a; L.O.Vasquez, 2007; Larminie & Dicks, 2003; Peppley, 2013)

Fuel cell type	Typical Electrolyte	Typical anode/ and cathode catalysts	Interconnect material	Typical fuel	Charge Carrier	Operating Temperature (^{0}C)	Advantages	Disadvantages	Electrical efficiency (%)
Low-temperature proton exchange membrane	Solid Nafion	Anode: platinum supported on carbon Cathode: platinum supported on carbon	Graphite	Hydrogen	H^+	60 - 80	• High-power density • Compact structure • Rapid start-up • Due to low temperature operation • Highly modular for most applications • Excellent dynamic response	• Expensive catalyst • Complex water and thermal management • Low-grade heat	40 – 60
High-temperature Proton exchange membrane	Solid composite Nefion Polybenzimidazole (PBI) doped in phosphoric acid	Anode: Platinum Ruthenium supported on carbon Cathode platinum ruthenium Supplied on carbon	Graphite	Hydrogen	H^+	110 - 180	• Simple water thermal management • High-grade heat • Accelerated reaction kinetic	• Expensive catalyst • Humidification issues • Accelerated stuck degradation	50 – 60
Solid oxide	Solid Yttria stabilised Zirconia (YSZ)	Anode: Nickel YSZ Composite Cathode: Strontium doped lanthanum (LSM)	Ceramics	Methane	O^{2-}	800 - 1000	• Inexpensive catalyst • High electrical efficiencies • Possibility of internal reforming • Fuel flexibility • High-grade heat	• Durability issues • Slow start-up • Low power density • High thermal stresses • High manufacturing cost	55 – 65
Molten Carbonate	Liquid alkali carbonate (LI_2Co_3, Na_2CO_3, K_2CO_3) in lithium aluminate ($LiAlO_2$)	Anode: Nickel Chromium (NiCr) Cathode: lithiated nickel oxide (LIO)	Stainless steel	Methane	CO_3^{2-}	600 - 700	• Possibility of internal reforming • Less strict material requirements • Inexpensive catalyst • Fuel flexibility • High electrical efficiencies • High-grade heat	• Low power density • Slow star-up • Electrolyte corrosion and evaporative losses • Corrosion of metallic parts • Air crossover • Catalyst dissolution in electrolyte	55 – 65

Fuel cell type	Typical Electrolyte	Typical anode/ and cathode catalysts	Interconnect material	Typical fuel	Charge Carrier	Operating Temperature (^{0}C)	Advantages	Disadvantages	Electrical efficiency (%)
Phosphoric acid	Concentrated liquid phosphoric acid (H_3PO_4) in Silicon carbide (SIC)	Anode: platinum supported on carbon Cathode: platinum supported on carbon	Graphite	Hydrogen	H^+	160 - 220	• Simple water management • High-grade heat • Technologically mature reliable	• Low power density • Relatively slow start-up • Expensive auxiliary system • Expensive catalyst • Low electrical efficiency • High cost • Relatively large system size • Low electrical efficiency • Electrolyte acid loss	36 - 45
Alkaline	• Potassium hydroxide (KOH) water solution • Anion exchange membrane (AEM)	Anode: Nickel Cathode: silver supported carbon	Metallic wire	Hydrogen	OH^-	Below 0 - 220	• Relatively low cost • Catalyst inexpensive • High electrical efficiency • Wide range of operating temperature	• Complex and expensive electrolyte management • Low power density • Highly corrosive electrolyte	60 – 70
Direct methanol	Solid Nefion	Anode: platinum ruthenium supported on Carbon Cathode: platinum supported on carbon	Graphite	Liquid methanol – water solution	H^+	Ambient - 110	• Compact size • Ease fuel storage and delivery • Simple thermal management • High fuel volumetric energy density	• High cost • Fuel toxicity • Low power density • Low cell voltage efficiency • Complex water management • Fuel and water crossover	35 - 60
Direct ethanol	• Solid Nefion • Alkaline media • Alkaline acid media	Anode platinum ruthenium supported on Carbon Cathode: platinum supported on carbon	Graphite	Liquid Ethanol water solution	H^+	Ambient - 120	• High fuel volumetric energy density • Compact size • Relatively low fuel toxicity • Simple thermal management • Easy fuel storage and delivery	• Low power density • Slow star-up • Low cell voltage and efficiency • High cost • Fuel and water crossover	20 – 40

2.4.4 Reversible fuel cells

2.4.4.1 Introduction

Producing cost effective, efficient and environmentally friendly energy to meet the world energy demand is the main challenge for the current and future societies. The growth of renewable power generators has been very significant lately, similarly fuel cell technologies have shown their capability to efficiently convert hydrogen or other type of fuels into electricity with near zero emission. Hydrogen technologies can therefore contribute in the power generation sector, especially in combination with renewable generators (Winter, 2009; Ursua et al., 2012).

The power generated from renewable generators such as those based on solar and wind is intermittent as they are weather dependent. Reversible fuel cells (RFC) can play a vital role in support to these technologies as any excess electricity generated can be used to produce hydrogen and then the produced hydrogen can later be used to generate back electricity. Thus, reversible fuel cell represents a promising form of energy storage technology for renewable applications.

A reversible fuel cell or regenerative fuel cell is a fuel cell technology that can operate in power generation mode and in a hydrogen production mode (Paul & Andrews, 2017; D.N. Luta & Raji, 2019). As shown in Figure 2.15, this sort of fuel cell comes into two types namely discrete reversible and unitised reversible fuel cells (Doddathimmaiah, 2008). A discrete reversible fuel cell is such that the electrolyser and the fuel cell are separated while integrated within a same system. In contrast, unitised reversible fuel cell is a single unit with dual ability to either function as an electrolyser or as a fuel cell (Doddathimmaiah, 2008). The hydrogen production stage is referred to as the charging phase, whereas the power generation period is referred to as the discharging cycle.

Recently, significant advancement in regenerative fuel cells has been reported as results of the development of protons exchange membrane fuel cells and water electrolysers. Consequently, the most typical reversible fuel cell technologies use proton exchange membrane technology, while other types may be based on technologies such as hydroxyl anion exchange membrane and high temperature solid state oxygen anions conducting membrane (Soloveichik, 2014). Some of the applications of reversible fuel cells are space vehicles, satellites, aircraft, distributed energy generation, energy storage for central grids and off-grid systems supplied by renewable energy (NASA, 2005).

(a)

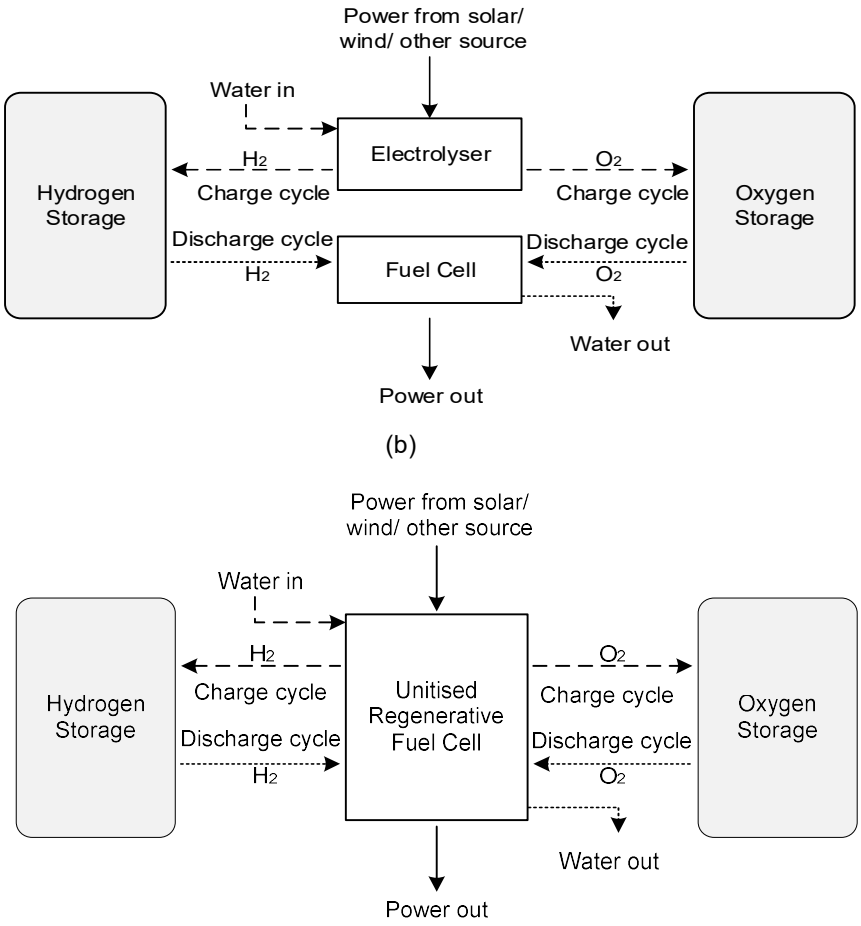

Figure 2. 15: (a) Discrete reversible fuel cell (b) Unitised reversible fuel cell (D.N. Luta & Raji, 2019)

Generally, the design of reversible fuel cell stack is identical as the design of conventional fuel cell stacks, thus, the electricity generation process is as well the same as for fuel cells. This section is only dedicated to the hydrogen production using the electrolyser.

2.4.4.2 Electrolyser

One of the cleanest and encouraging methods for producing hydrogen is through water electrolysis using electricity from renewable sources.

The process consists of utilising power from these renewable generators to split water into hydrogen and oxygen. This chemical reaction is performed by the means of a device known as electrolyser.

The key procedure of electrolysis is the exchange of atoms and ions by the expulsion or expansion of electrons from the outside circuit. The general equation of water electrolysis is expressed as:

$$H_2O + electric\ energy + heat \rightarrow \frac{1}{2}O_2 + H_2 \quad (2.28)$$

Various types of electrolyser can be distinguished according to the electrolyte used. The most common ones are alkaline electrolyser, proton exchange membrane electrolyser and solid oxide electrolyser. By combining these types of electrolyser with their corresponding fuel cell stacks, we obtain the three most common reversible fuel cells which are reversible alkaline electrolyser, reversible proton exchange membrane fuel cells and reversible solid oxide fuel cells.

2.4.4.3 Reversible alkaline fuel cells

Reversible alkaline fuel cells (RAFCs) typically utilise as the electrolyte, an aqueous solution of potassium hydroxide (KOH), they work in fuel cell mode in the scope of 60 to 120°C and can yield the most astounding voltage at comparable current densities while ran with pure hydrogen and oxygen. A typical schematic of a reversible alkaline fuel is shown in Figure 2.16.

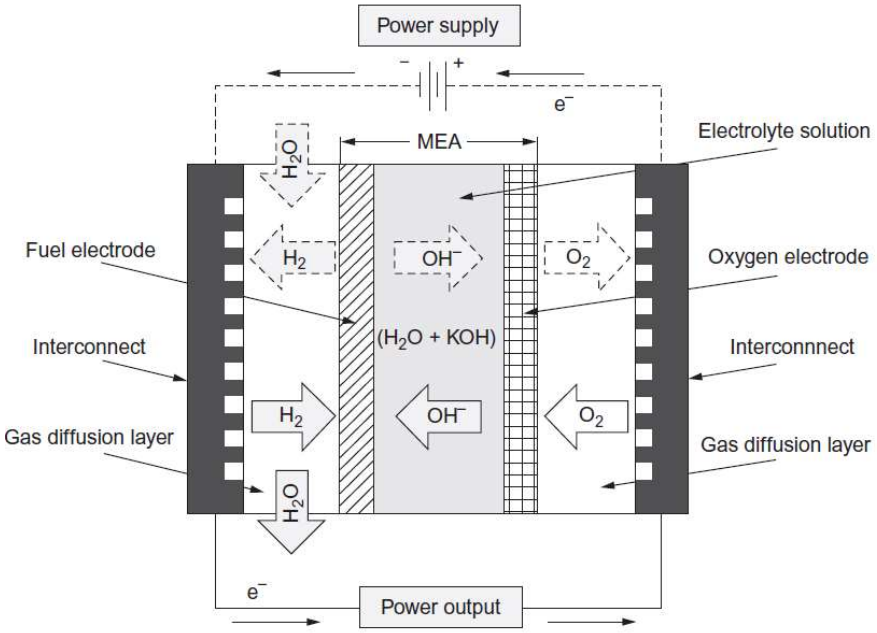

Figure 2.16: Reversible Alkaline Fuel Cells (Barbir et al., 2016)

In the electrolyser mode, the hydrogen electrode is the cathode and the oxygen electrode is the anode, whereas in the fuel cell mode, the hydrogen electrode is the anode and the oxygen electrode is the cathode. The half reactions and ionic charge carriers (ICC) in a reversible alkaline fuel cell are shown in Table 2.6.

Table 2.6: Reactions and ionic carriers in a reversible alkaline fuel cell (Barbir et al., 2016)

Process	Fuel Electrode	ICC	Oxygen electrode
Electrolysis mode	$2H_2O + 2e^- \rightarrow H_2 + 2OH^-$	OH^-	$2OH^- \rightarrow \frac{1}{2}O_2 + H_2O + 2e^-$
Fuel cell mode	$H_2 + 2OH^- \rightarrow 2H_2O + 2e^-$	OH^-	$\frac{1}{2}O_2 + H_2O + 2e^- \rightarrow 2OH^-$

2.4.4.4 Reversible proton exchange membrane fuel cells

Reversible proton exchange or polymer electrolyte membrane fuel cells (RPEFCs) are recent sort of energy devices that utilise hydrogen. They comprise two porous electrodes, that are isolated by a polymer electrolyte membrane and can operate in fuel cell as well as in electrolyser mode. In electrolyser mode, the hydrogen electrode is the cathode and the oxygen electrode is the anode, while in fuel cell mode, the cathode is the oxygen electrode and the anode the hydrogen. A typical schematic of a reversible proton exchange membrane fuel cell is shown in Figure 2.17.

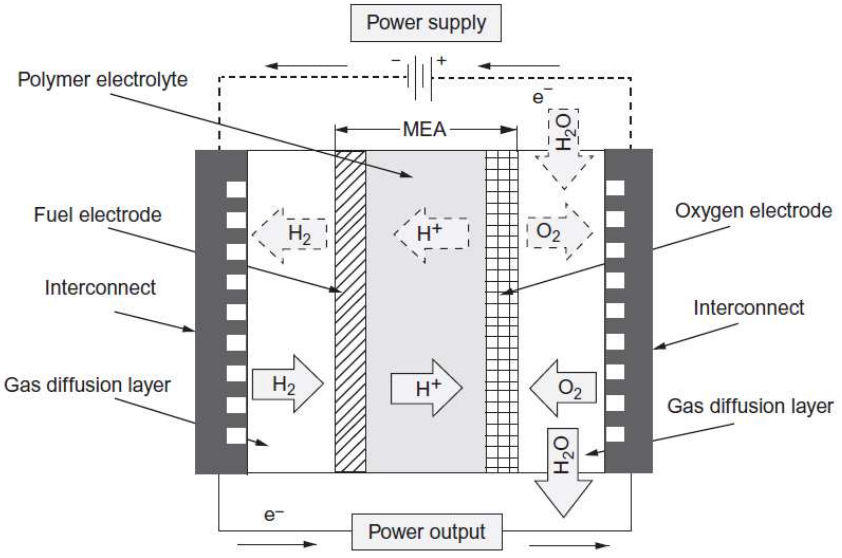

Figure 2. 17: Reversible proton exchange membrane fuel cells (Barbir et al., 2016)

The half reactions and ionic charge carriers (ICC) in a reversible alkaline fuel cell are shown in Table 2.7.

Table 2. 7: Half-cell reactions and ionic charge carriers in the $H_2 - O_2$ (Barbir et al., 2016)

Process	Fuel Electrode	ICC	Oxygen electrode
Electrolysis mode	$2H^+2e^- \rightarrow H_2$	H^+	$H_2O \rightarrow \frac{1}{2}O_2 + 2H^+ + 2e^-$
Fuel cell mode	$H_2 \rightarrow 2H^+ + 2e^-$	H^+	$\frac{1}{2}O_2 + 2H^+ + 2e^- \rightarrow H_2OH^-$

2.4.4.5 Reversible solid oxide fuel cells

In the previous couple of years, the solid oxide electrolysis field has pulled in many research entities and the outcomes recommend that this technology can be substantially more efficient than low-temperature electrolysers. Reversible solid oxide fuel cells consist of two porous electrodes isolated from each other by a dense oxide ion-conducting electrolyte (Figure 2.18). The half reactions and ionic charge carriers (ICC) in this type of fuel cell are shown in Table 2.7.

.

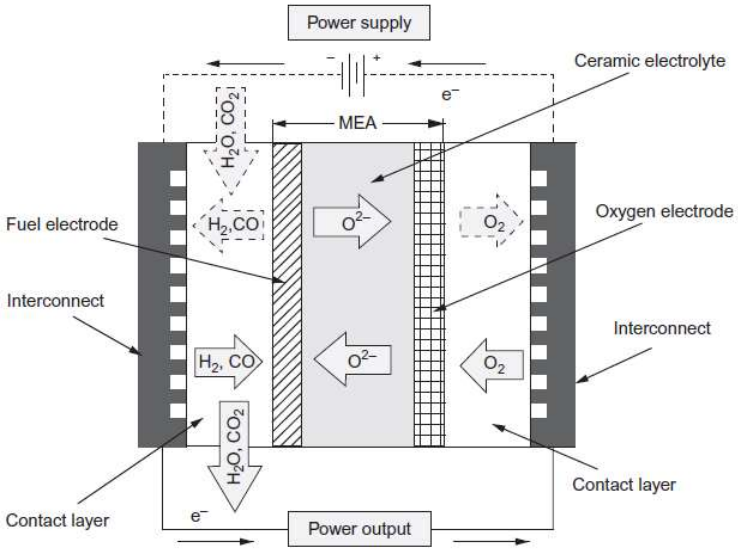

Figure 2.18: Reversible solid oxide fuel cells (Barbir et al., 2016)

2.5 Supercapacitors

2.5.1 Introduction

Supercapacitors are electrochemical energy storage devices, well known for their extremely high-power density, very low internal resistance, high cycle lifetime and cycling efficiency. They store energy by physically separating positive and negative charges. These charges are stored on two parallel plates divided by an insulator. Supercapacitors are also known as electric double-layer capacitors, electrochemical double layer capacitors or ultra-capacitors (Ould Amrouche et al., 2016). They use polarised liquid layers between conducting ionic electrolytes and conducting electrode to increase the capacitance. They allow a much higher energy density, with a high-power density, but the voltage varies with the energy stored and they have a higher dielectric absorption. The most important parameter is the relatively low, State of Charge dependent maximum voltage of 2.5 V and a great efficiency which is in the range of 95% (Ould Amrouche et al., 2016). The output power of a typical supercapacitor is lower than that of electrolytic capacitors, however, can reach around 10 kW/kg. Then again, their specific energy is higher than the one of capacitors (Raza et al., 2018).

Supercapacitors are interesting technologies as they fill the hole between aluminium electrolytic capacitors and batteries, which can store huge amount of energy, yet do not offer high power densities because of their storage mechanism. Table 2.8 compares the characteristics of a supercapacitor against the battery and the capacitor; supercapacitors cannot be discharged in merely seconds, yet in addition be charged in such a brief timeframe period.

Table 2. 8: Comparison between supercapacitor and battery capacitors (Raza et al., 2018)

Characteristics	Capacitor	Supercapacitor	Battery
Specific energy (Wh/kg)	< 0.1	Up to 1091	Up to 1606
Specific power (W/kg)	> 10,000	Up to 19,6000	< 1000
Discharge time (s)	10^{-6} – 10^{-3}	s to min	0.03 – 3 h
Charge time (s)	10^{-6} – 10^{-3}	s to min	1 – 5h
Coulombic efficiency (%)	About 100	Up to 99	70 – 85
Cycle life	Almost infinite	> 500,000	About 1000

Supercapacitors can be utilised alone or combined with another energy storage technology (batteries) to improve power efficiency and enhance cycle life (Mutarraf et al., 2018). In 100 % renewable power systems, they can be used to eliminate fast power fluctuations from generators such as wind turbines and are usually in a hybrid form with batteries (Torres, 2015).

2.5.2 Elements of supercapacitor

A supercapacitor consists of elements such as electrode material, electrolyte material, current collectors, Binder and Separators as displayed in Figure 2.19. The electrode and electrolyte material are viewed as the dynamic part and others are the passive elements of the supercapacitor. Typically, a supercapacitor comprises two current collectors/active electrode materials that are isolated by a layer of electrolytes or separator.

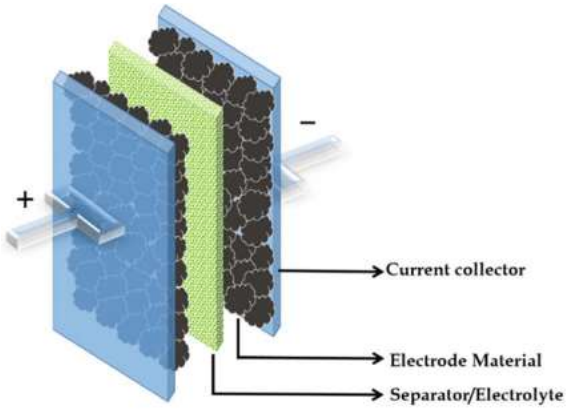

Figure 2.19: Internal Layout of supercapacitor (Samantara & Ratha, 2018)

2.5.2.1 Electrode materials

The electrode materials contribute significantly towards the supercapacitor storage performance. In view of the electrode materials, the supercapacitors can be grouped into three types shown in Figure 2.20; electrochemical double layered capacitors, pseudo-capacitors and hybrid capacitors (Hadjipaschalis et al., 2009). The carbon materials such as activated carbon, carbon aerogels, carbon nanotubes (CNTs), graphene and so on demonstrate the behaviour of electrochemical double-layered capacitors. In opposition, the exceptional redox active transmission metal oxides are under the pseudocapacitive class, where the charge storage happens as a result of the physicochemical adsorption (redox response) on the electrode surface.

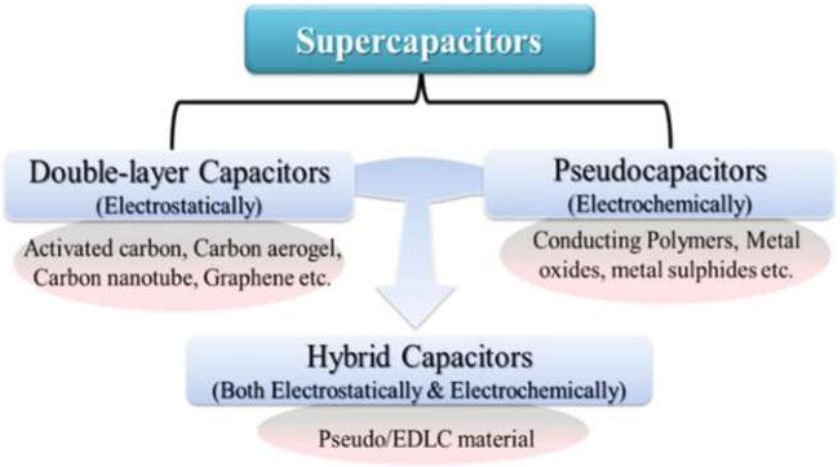

Figure 2. 20: Different types of supercapacitor (Hadjipaschalis et al., 2009)

2.5.2.1.1 Electrode materials based on carbon

Due to their chemical stability, outstanding electrical conductivity, vast theoretical surface area, low assembling and handling cost, high temperature tolerance, environmental friendliness; carbonaceous materials have increased full focus as the electrode material to produce electrochemical double layered capacitor type supercapacitors (Zhang et al., 2009; Maletin et al., 2013)The charge storage happens just by the physical gathering of charged particles at the electrode/electrolyte interface of the electrode material instead of in the bulk material. Therefore, the capacitance performance firmly relies upon the specific surface area and surface morphology of the cathode materials. The high surface region carbon materials principally incorporate the carbon nanotubes, carbon nano fibers, carbon aerogels, template mediated permeable carbon materials and so on (Kock et al., 1996; Lee et al., 2006).

2.5.2.1.2 Conducting polymers

The modest price, great conductivity (in doped state), insignificant environmental effect, wide operational potential windows (up to 3.1 V in non-aqueous electrolyte) and tuneable redox activity (by changing the chemical composition) made the conducting polymers as the appropriate material for supercapacitor development (Fan & Maier, 2006; Prasad et al., 2004). The charge storage component in conducting polymer-based supercapacitors includes the oxidation and reduction of both the surface and bulk of the polymeric backbone of electrode material (Clemente et al., 1996; Kalaji et al., 1999). Based upon the charge created on conducting polymers when the oxidation or reduction reactions occur, conducting polymers are grouped into three sorts which are p-doped (polyaniline, polypyrrol and so forth.), n-doped (polythiophene

subsidiaries) and n-p doped (polythiophene, poly (3-fluorophenyl) thiophene). Similarly, depending upon the arrangement of conducting polymer materials, supercapacitors are categorised as Type-I (the two electrodes are same p-type conducting polymers), Type-II (two diverse p-type conducting polymers) and Type-III (having both n-and p-doped conducting polymers as electrodes) supercapacitors (Villers et al., 2003). The determination of a reasonable potential window is particularly basic for smooth operation of conducting polymers-based supercapacitor.

2.5.2.1.3 Metal oxides

The use of metal oxides in supercapacitors display better energy storage efficacy as opposed to the conventional carbon materials and exceptional long cycle performance contrasted with the conducting polymers-based electrode materials. Hence, efforts have been made to create higher cost-effective conductive metal oxides with variable valence states (Barranco et al., 2009; Kim et al., 2005). Among various transition metal oxides, any semblance of RuO_2, MnO_2, cobalt oxides, nickel oxides and so forth have been very much reported. These oxides-based electrode materials store the electrical charge by both physical collection and surface redox responses in the specified working potential window (Samantara & Ratha, 2018).

2.5.2.1.4 Metal nitrides

Enhanced conductivity has been reported in the case of metal nitrides which are developing as elite pseudocapacitive materials for asymmetric supercapacitors. Because of the high electrical conductivity in contrast with metal oxides, metal nitrides are believed to have improved power density (Bouhtiyya et al., 2012; Kim & Popov, 2002; Balogun et al., 2015). Lithiated metal nitrides (Li_3N), transition metal nitrides (Mo_2N, VN, TiN) have demonstrated electrochemical properties (Balogun et al., 2015). Although the utilisation of these metal nitrides is similarly restricted in supercapacitors, their robust chemical properties and excellent lithiation/delithiation property could effectively actualise for both asymmetric and hybrid supercapacitor technologies. In contrast with pseudocapacitive metal oxides, they are fit of generating high power density. Among the referenced nitrides, titanium nitride (TiN) has been the most broadly studied anode because of its high electrical conductivity and mechanical stability (Samantara & Ratha, 2018).

2.5.2.1.5 Composite materials

Among other carbon-based electrode materials, graphene has nearly higher theoretical specific capacitance and surface area (Raccichini et al., 2015). However, it is too

difficult to accomplish such high values practically speaking (Stankovich et al., 2006). Thus, composite materials of graphene with the carbon nanomaterials, metal oxides and directing polymers have been created. These added substances anticipate the restacking procedure in the reduced graphene oxide producing accessibility of progressively available surface area to the electrolyte in electrochemical supercapacitors, in this manner expanding the specific capacitance values. However, the unpredictable method and prerequisite of specific instrumental set ups for the synthesis of these composites require intense research and optimisation so as to make more open doors for the improvement of efficient and superior electrode materials (Samantara & Ratha, 2018).

2.5.2.2 Electrolyte materials

The major challenge in the supercapacitor improvement is to increase the energy density, which can be acquired by either expanding the capacitance of electrode material or by augmenting the operating potential of the device. Preferably, widening of potential windows will be favourable for expanding the energy density of the device and, furthermore, in decreasing the stacking numbers to achieve higher potential differences. An increase in the cell voltage is consequently compelling contrasted with expanding the capacitance of electrode materials for energy density improvement.

Various types of electrolytes have been implemented and utilised in supercapacitors with variable potential windows; aqueous electrolyte-based supercapacitors (1.0 V to 1.3 V), organic electrolytes-based supercapacitors (2.5 V to 2.7 V), ionic fluid supercapacitors (3.5 V to 4.0 V) and so forth (Zhong et al., 2015).

2.5.2.3 Current collector

The current collector is a passive element of the supercapacitor; however, it has an important role to play towards the durability and cell potential improvement (Zhong et al., 2015). The choice of a current collector relies upon the sort of electrolyte taken and electrode material with which the supercapacitor has been manufactured. For strong acid-based electrolytes, corrosion resistive metal foil current collectors are utilised. Besides, to limit the cost of supercapacitors, materials like indium tin oxide and carbon-based materials have been developed (Ryu et al., 2014; Cho et al., 2012). For alkaline electrolyte-based supercapacitors, the low-cost nickel-based materials are picked as suitable current collectors. Nickel foam has gained notoriety as excellent current collector having higher surface area than standard metal foils and fit for using the electrochemical activity of the active electrode material (Gong et al., 2014). For non-

aqueous electrolyte (organic and ionic liquids) based supercapacitors, the aluminium current collectors are broadly utilised (Brandt et al., 2013; Lewandowski et al., 2012).

2.5.2.4 Binders

The performance of supercapacitors is strongly influenced by the content and kind of binder utilised. Binders have for some time been utilised by mixing with the powdered active electrode material that not just keeps up the structural integrity of the electrode material film but help as well in accomplishing better adhesion between the active material and current collector. In general, fluorinated polymeric materials like, poly vinylidene fluoride, Polytetrafluoroethylene, Nafion, natural cellulose, polyvinyl pyrrolidone, polyacrylic corrosive and conductive polymers (polypyrrol, polyaniline and so forth) have been utilised as the binder for the manufacture of supercapacitors (Aslan et al., 2014; Varzi et al., 2014; Kang et al., 2014).

2.5.2.5 Separator

Like current collectors and binders, separators are a passive element of electrochemical capacitors. Even though it has no contribution to the capacitive performance, yet it plays a critical role by hindering any physical contact between the electrodes and encouraging electron exchange between them. The properties of the separator like electrical insulators, ion exchange capacity, chemical/electrochemical inertness, high mechanical strength, optimal thickness, porosity and surface morphology and so forth impacts on the performance and durability of a supercapacitor (Zhong et al., 2015).There are wide range materials from which different separators can be manufactured, for example, polypropylene, PVDF, PTFE, cellulose polymer layers (cellulose nitrate, 3.3 Current Collectors 29 cellulose acetic acid derivation layers and so on.), glass fibre, Celgard, Nafion 115, graphene oxide films, eggshell layers and so forth (Yu et al., 2012; Tõnurist et al., 2012; Shulga et al., 2014).

2.6 Photovoltaic systems

2.6.1 Introduction

The photoelectric effect discovered by Edmund Becquerel in the year 1839 (Chua, 2016) has led to the establishment of the photovoltaics industry. The discoveries by Max Planck and Albert Einstein (Díaz-González et al., 2015) in the mid-1900s prompted the first silicon solar cell made by Daryl Chapin, Calvin Fuller, and Gerald Pearson in 1954 (Papiewski John et al., 1996) years later, this same solar cell led to more than 40 GW of installed photovoltaic power systems in the world.

Figure 2.21 illustrates the yearly development of photovoltaic generation (Bahar, 2019); photovoltaic demonstrated a growth of 40% for power generation in 2017 and is well on track to meet its sustainable development scenario (SDS) target, which requires normal yearly growth of 17% between 2017 and 2030.

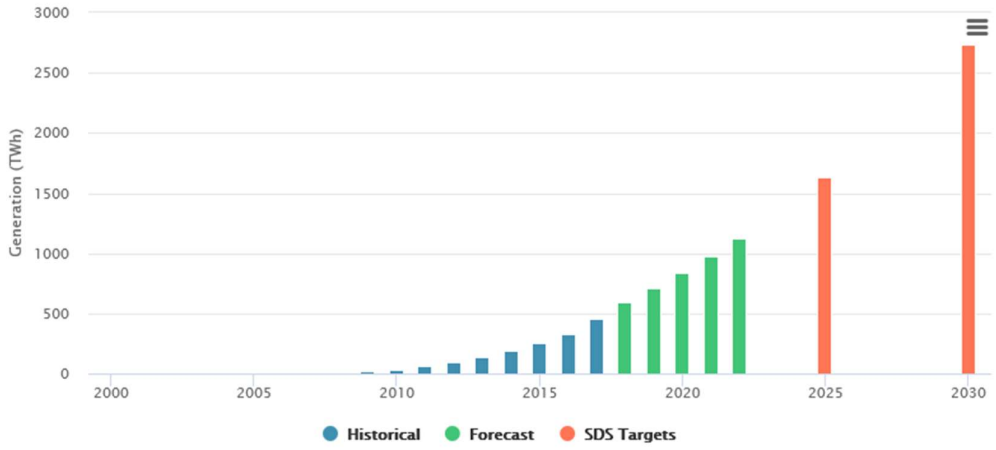

Figure 2. 21: Yearly development of photovoltaic generation (Bahar, 2019)

Photovoltaic power industry drove the development in renewable power in 2017, as deployment expanded in China and costs kept on falling. Since 2010, costs have fallen by 70% for new photovoltaic large power utilities. It is estimated that the power generation from photovoltaic systems has grown by over a third in 2017, up to 460 TWh, which is nearly 2% of the total electricity generation worldwide.

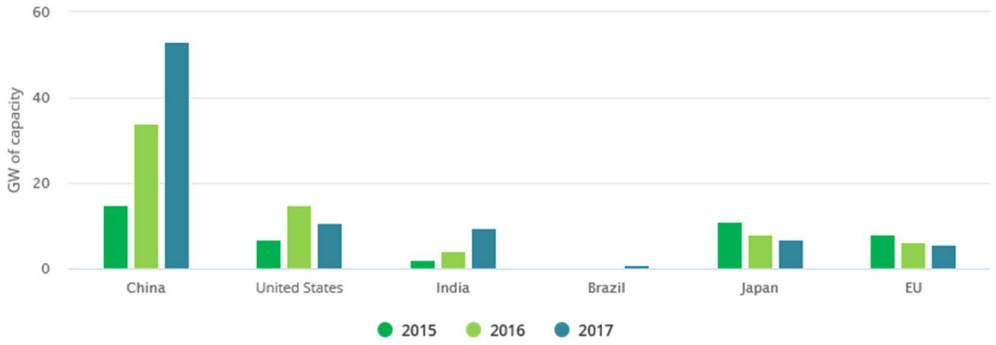

Figure 2. 22: Net photovoltaic capacity additions from 2016 to 2018 (Bahar, 2019)

Figure 2.22 shows the photovoltaic deployment from 2015 to 2017, a record of 98 GW in 2017 was driven by China with a total capacity of 53 GW. The average photovoltaic costs are expected to keep on declining in the coming years due to the increase in the competition and manufacturing capacity development in China and South East Asia. After China, the United States remains the second-biggest photovoltaic market. However, capacity increases declined by practically 30% to 10.6 GW in 2017. India's yearly photovoltaic capacity increase augmented dramatically with 9.6 GW. In Japan, photovoltaic capacity development decreased by 12% to 7 GW. In the European Union, yearly photovoltaic augmentations were steady at just below 6 GW. Because of these developments, photovoltaic investment achieved its most elevated amount ever, at over US$ 145 billion. Photovoltaic industry is well on track to reach the Sustainable Development Scenario target (SDS target), which requires a photovoltaic power generation to develop from 460 TWh in 2017 to more than 2700 TWh in 2030.

2.6.2 Photovoltaic operating principle

A photovoltaic system is designed around solar cells which are elements comprising semiconductor materials capable of absorbing sunlight to generate electron-hole pairs. These electron-hole pairs are then separated and migrate to the negative terminal for the electron (n-type) and positive terminal for the hole (p-type) to produce electricity. Figure 2.23 shows the operation of a solar cell.

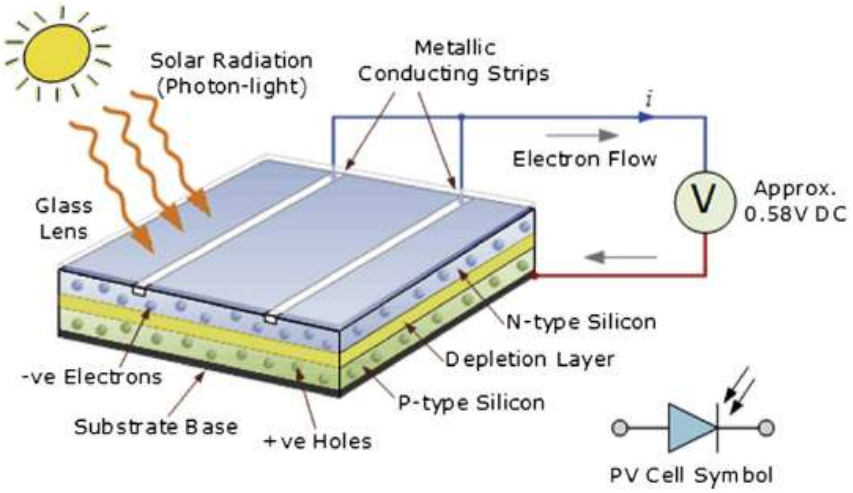

Figure 2. 23: Operation of a solar cell (Amin et al., 2017)

2.6.3 Classification of photovoltaic technologies

There are numerous approaches to classify photovoltaic technologies such as classification based on material (either inorganic or natural), device configurations, etc. Figure 2.24 shows the classification of photovoltaic technologies based on their generations.

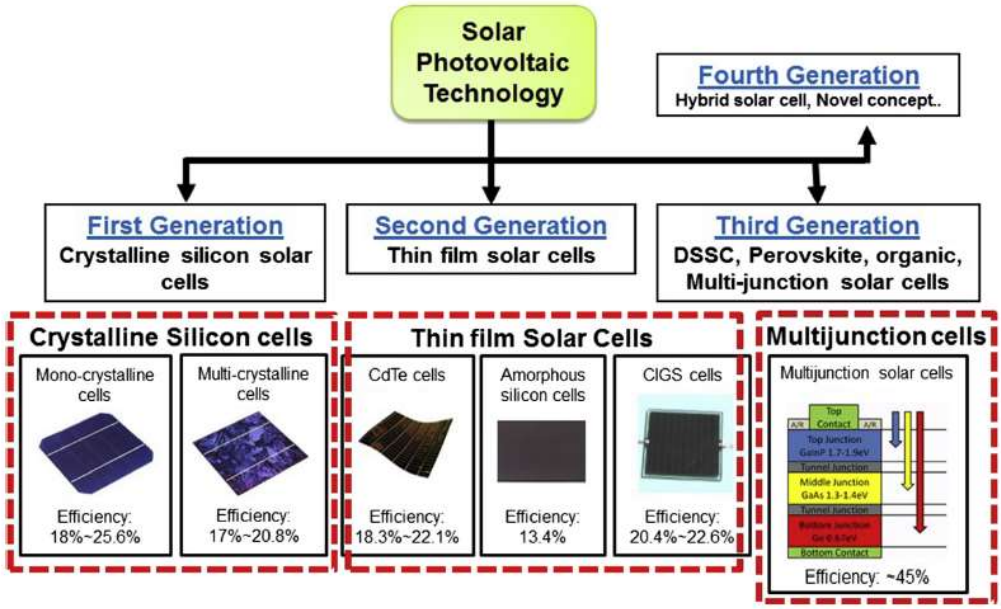

Figure 2. 24: Solar cell technology (Amin et al., 2017)

2.6.3.1 First-generation photovoltaic technology

The first-generation photovoltaic technologies are made from semiconductors p–n junctions comprising of silicon. Silicon cells have a very high efficiency which is close to 20%, however, very pure silicon is required, and the cost is high as compared to their power output. Silicon cells are produced from pure silicon, and they are very efficient as their efficiency are around 33%. First-generation photovoltaic technologies represented 89.6% of the photovoltaic market production in 2007. However, the piece of the overall industry of these cells are declining. The fabrication processes of these cells are costly; thus, it may take 5 to 6 years to pay back for the buying costs of these cells.

2.6.3.2 Second-generation photovoltaic technology

The second-generation photovoltaic technologies aimed on decreasing the price of first-generation technologies by utilising thin-film materials. Consequently, thin-film technologies have been viewed as the potential low-priced system, high-efficiency solar cell which can supplant silicon cells in the photovoltaic industry. The benefit of thin-film cells over the silicon ones is their low-temperature-preparing techniques, low material use, variety of deposition process, and their similarity with low-cost substrates. Joining all the mentioned benefits, low-priced photovoltaic cells are reachable and suit the criteria for large-scale applications. The various types of thin-film solar cells are cadmium telluride, copper–indium–gallium–diselenide, copper–zinc–in–sulfide, and amorphous silicon cells.

2.6.3.3 Third-generation photovoltaic technology

The third-generation photovoltaic technologies are created to improve electrical performance of second-generation cells while keeping up low fabrication costs. The efficiency of cells is around 30% to 60%. The third-generation photovoltaic technologies include multijunction photovoltaic cells, tandem cells, nanostructured cells to get better incident light and to convert the excess of thermal energy thus improving voltages or carrier collection.

2.6.3.4 Photovoltaic module

A typical solar cell generates less than three watts at around 0.5 V DC. To acquire enough power and voltage rating for high-power applications, cells are associated in series and parallel designs forming a module. A module can have a rated power running from a couple of watts to hundreds. By adding equivalent modules in series, the voltage rises relatively to the quantity of modules in series, while the current

remains the same. On the other hand, by adding or same modules in parallel, the voltage in the branch remains unchanged while the current increases relatively to the quantity of modules in arrangement in parallel.

2.6.3.5 Photovoltaic module characteristics

The characteristics of a photovoltaic module include the open-circuit voltage, short-circuit current, maximum power point, fill factor and efficiency.

2.6.3.5.1 Open circuit voltage

The open-circuit voltage expresses the voltage at the terminals of the photovoltaic module when no load is connected to it.

2.6.3.5.2 Short circuit current

The short-circuit current corresponds to the current that can flow from the photovoltaic module when its terminals are short-circuited.

2.6.3.5.3 Maximum power point

A maximum power point represents the point at which the photovoltaic module supplies the highest power. The voltage and the current corresponding that point are referred to as maximum power voltage and maximum power current respectively.

2.6.3.5.4 Efficiency

The photovoltaic module efficiency is defined as the ratio of electrical energy produced by the module over and the solar energy striking the module. This efficiency depends not only on available solar energy but also on the conversion rate.

2.6.4 Off grid and grid connected photovoltaic systems

Generally, a photovoltaic power system can operate in off-grid or grid connected mode. Off-grid photovoltaic systems comprise one or several photovoltaic modules, a battery for electrical capacity, cabling, mounting structure, and a charge controller. As the output power of the PV panel changes with the solar radiation and temperature, the charge controller is expected to condition the DC output power and convey it to the batteries. Off-grid systems are typically intended to meet specific loads, for instance in solar home systems; a couple of modules give power to charge a battery through the day, and some lighting devices and radio or TV can be supplied at night. Other

applications include rural or remote areas with no access to the electricity from the main utility grid.

On the other hand, grid-connected photovoltaic systems comprise at least 1 PV modules, one or a few inverters to convert direct current photovoltaic into alternating current, cabling, and a mounting structure and are grid-connected through the inverter. Their sizes run from around 50Wp through small-scale (0.5 to 4 kW) for private property holders, to medium scale (4 kW to 100 kW), to large scale (0.1 MW to 100 MW), while very large-scale photovoltaic systems may go above 1 GW.

2.7 Summary

This chapter was dedicated to a literature survey on the concept of 100 % renewable power systems, different types of energy storage technologies including their characteristics, types of fuel cell systems and electrolysers by considering their characteristics and operating principles, etc. and an assessment of supercapacitors; key drivers that need to be considered in the expansions of 100 % renewable power systems were presented.

The key drivers for the development of 100 % renewable power systems include elements such as demand side management, expansion and liberalisation of markets, grid support services from renewable energy, diversifying renewable resources, bulk energy storage, transmission network efficiency and flexibility, role of smart grids, power system stability with non-synchronous generators and effective utilisation of excess generations. In addition, various forms of energy storage technologies such as mechanical, electrochemical, electrical, thermochemical, chemical and thermal was discussed about. Their characteristics and specific applications were as well considered. Furthermore, a section focusing on supercapacitors was also considered. It presented the different types of supercapacitors, their main characteristics and part involved. Lastly, a brief review of photovoltaic systems; starting from their history, evolution, operating principle, technology classification and characteristics were presented.

CHAPTER THREE
OPTIMAL DESIGN OF THE RENEWABLE POWER SYSTEM

3.1 Introduction

This chapter deals with the optimal design of the proposed renewable power system, this design is based on the algorithm presented in Figure 3.2. Due to the intermittency of renewable energy sources, 100% renewable power systems may not meet the hourly energy demand. In such a case, the use of energy storage devices can decrease the impact of this uncertainty to the load. Moreover, the optimal design of renewable energy systems makes the overall system cost to be effective and reliable.

As the complexity of renewable power systems increase, conventional optimisation methods are not adapted to deal with the complicated optimisation problems whereby the efficiency of the method needs to be demonstrated.

To optimise a system, an explicit mathematical formulation expressing the system is required. For complex optimisation problems, it is complicated to use a mathematical formulation as the system has a high-dimensional space or non-linear nature. In the same vein, simulation tools can be used to estimate the performance of systems, despite that, a simulation might not provide an optimal solution of the optimisation problems. Therefore, simulation models need to be combined with an optimisation method to obtain optimal or nearly optimal results.

A literature review reveals that optimisation methods used for renewable systems focus on various objectives such as minimising emission, maximising reliability, minimising cost, etc. The adopted optimisation method focuses on minimising the net present cost of the system.

3.1.1 System description and operation

The system includes components such as photovoltaic panels (PV), an electrolyser, fuel cell stack, hydrogen tank, supercapacitor, power converter and loads as shown in Figure 3.1. The PV operates as the principal source of power to meet the load demand, whereas the electrolyser-fuel cell and supercapacitor are used as an energy storage system to compensate power variations. The system runs such that PV generate as much power as available depending on the available renewable resources to meet the load demand. Any excess of power is used to produce the hydrogen through the electrolyser and charge the supercapacitor. Inside the electrolyser, water is decomposed into hydrogen and oxygen. The decomposed hydrogen is accumulated

and used when required to generate electricity. On the other hand, the supercapacitor store energy using any excess power generated.

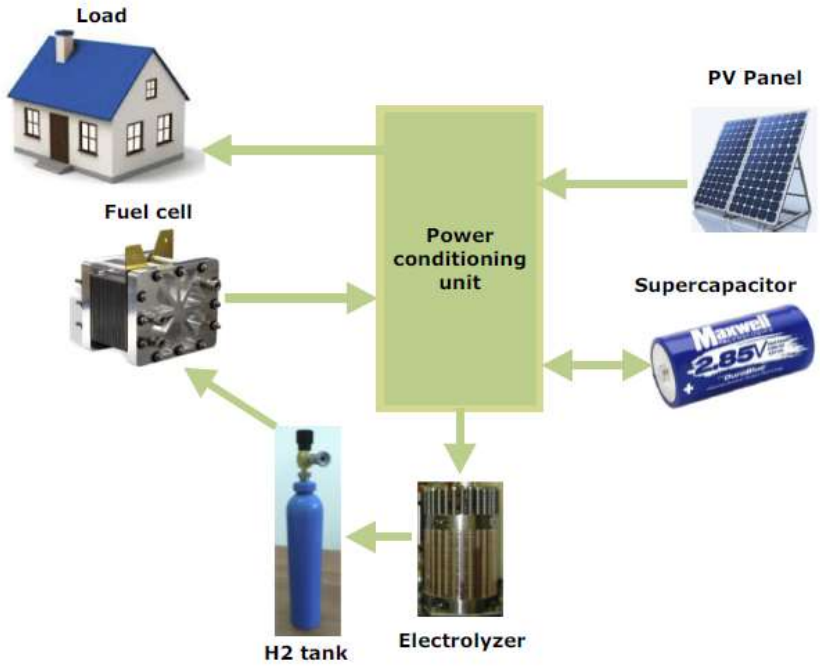

Figure 3.1: System architecture

3.1.2 Optimisation methodology

The optimisation procedure consists on balancing the produced and consumed energies at each time step of the year. This involves deciding on system configurations that might be technically feasible with respect to the system constraints. It also evaluates the installation and operation costs of the feasible system over the project lifetime. Input data such as solar resources of the selected site, load profile, and economic and technical data of the components are needed to obtain the optimal system configuration. Figure 3.2 shows the flowchart of the optimisation approach. The suitable configuration is chosen based on the Net Present Cost and the cost of energy and the reliability of the system configuration to meet the load demand.

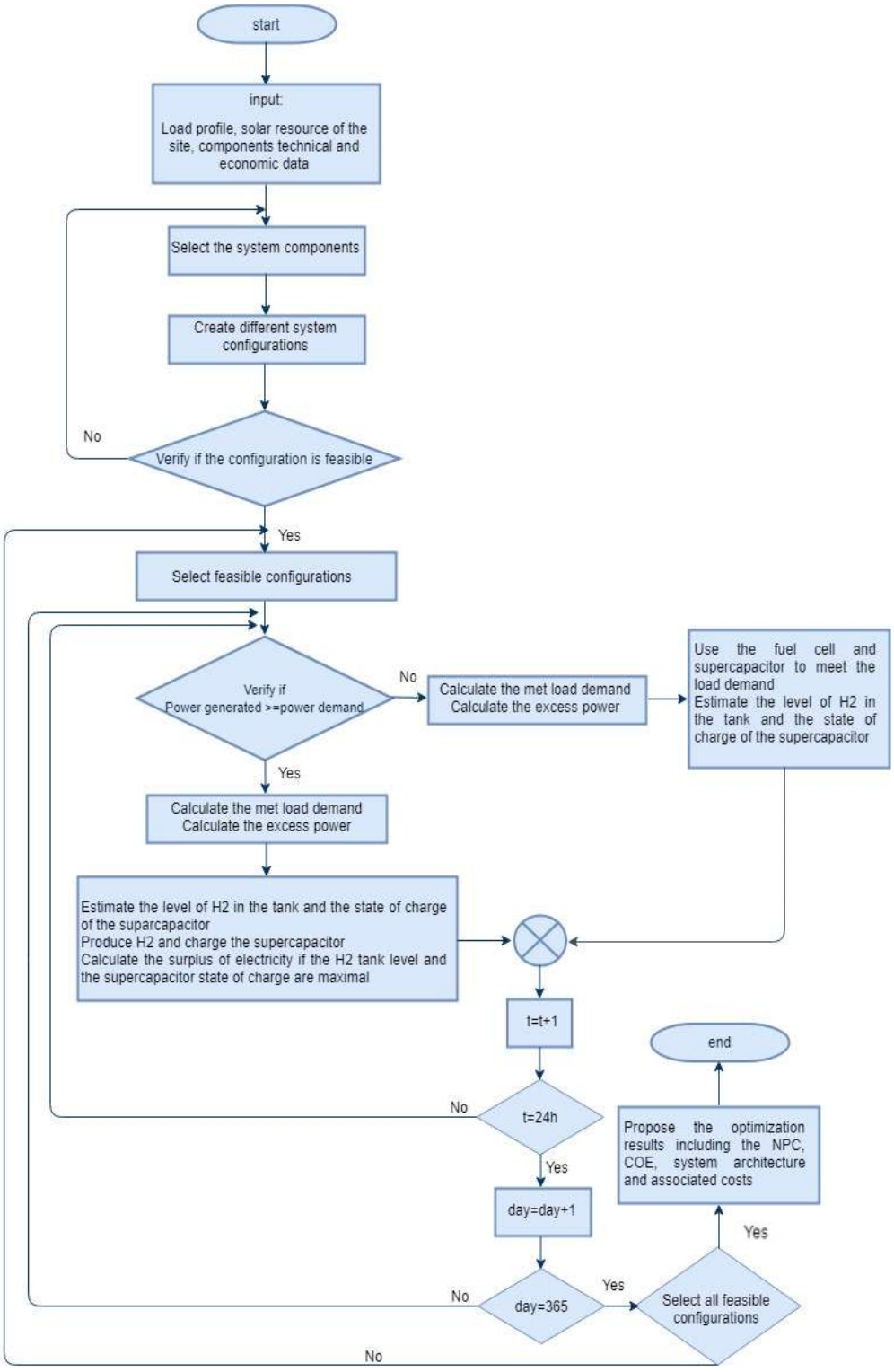

Figure 3.2: Optimisation algorithm

3.1.2.1 Net Present Cost

The NPC is defined as the sum of all the necessary costs in the project lifetime. These costs include the capital, operating and maintenance (O&M), replacement, and fuel costs minus the salvage cost representing the estimated value of the system at the end of the project lifetime. The NPC can be expressed using Equation 3.1 as follows (Kalinci et al., 2015):

$$NPC = \sum_{N=1}^{N=t} f_{d,N} \left(C_{cap} + C_{rep} + C_{main} - C_s\right) \quad (3.1)$$

where C_{cap}, C_{main}, C_{rep}, and C_s are the capital, O&M, replacement, and salvage costs respectively, t is the project lifetime and $f_{d,N}$ is given by Equation 3.2 as (Kalinci et al., 2015):

$$f_{d,N} = \frac{1}{(1+i)^N} \quad (3.2)$$

where i and N are the annual interest rate and the year respectively.

3.1.2.2 Cost of Energy

The system COE is given by Equation 3.3 as follows (Kalinci et al., 2015):

$$COE = \frac{AC_T}{E_{served}} \quad (3.3)$$

where E_{served} is the system primary load and AC_T is the total cost of the component "a" at each year of the project lifetime and provided by Equation 3.4 as (Kalinci et al., 2015):

$$AC_T = \sum C_{acap} + C_{arep} + C_{amain} - C_{as} \quad (3.4)$$

where C_{acap}, C_{amain}, , C_{arep}, and C_{as} are the capital, O&M, replacement, and salvage costs of the component "a" respectively.

3.1.2.3 System technical reliability

Technical reliability criteria mean choosing optimal sizes of the system components such as PV, fuel cells, converter, electrolyser, hydrogen tank and supercapacitor to keep the balance between the supply and the load demand considering the system capacity shortage.

3.1.3 Inputs data

Based on the system configuration, input data including the weather resources of the site, load profile, technical specifications, costs data of the system components and other system constraints (project real discount rate, inflation rate, the system annual capacity shortage and the project lifetime) are required.

The project real discount rate 'i' is given by Equation 3.5 (Per.gov.ie, n.d.) as:

$$i = \frac{i' - f}{1 + f} \tag{3.5}$$

where i' is the nominal discount rate and f is the expected inflation rate over the project lifespan.

3.2 Simulation results

The simulation parameters are given in Table 3.1 (Longe et al., 2017; DOE, 2017; Singh et al., 2017). This simulation is carried out using an optimisation tool and based the algorithm in Figure 3.2. The system is designed to meet a DC load of 3 kW peak value as well as an AC load of 7 kW peak power. The profile of both loads is depicted in Figure 3.3. A constant irradiance of 500 Watt per metre square was assumed in the determination of the optimal configuration. The configuration is developed to operate with 0 % capacity shortage.

Table 3. 1: Simulation input parameters

Costs data of components			
Component	Capital costs (US $)	Replacement cost (US$)	O&M costs (US $)
PV panels	1000 per 1 kW	750	55 per year
Fuel cell (FC)	4000 per 1 kW	3000	0.01 per hour
Inverter	400 per 1 kW	300	10 per annum
Electrolyser	1100 per 1 kW	825	10 per annum
Supercapacitor	60 per 3000 F	45	0
H2 Tank	1000 per 1 kg	750	0

(a)

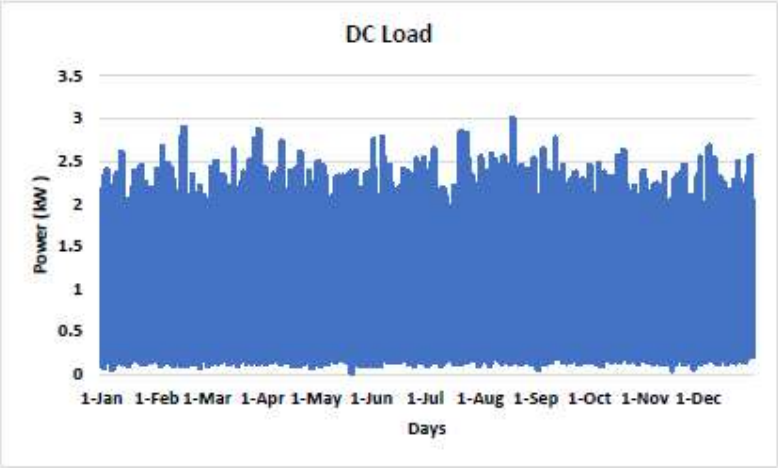

(b)

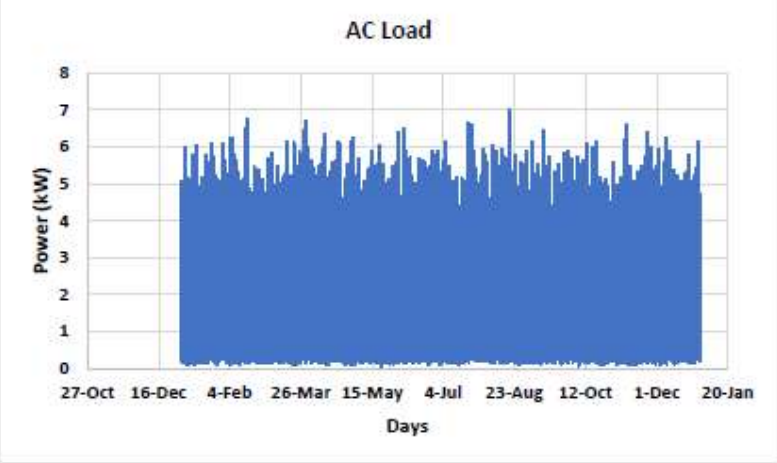

Figure 3. 3: (a) DC and (b) AC load profiles

Based on the solar radiation of the selected site, to meet the load demand with 0 % capacity shortage, the system must consist of 25 kW PV panels, 10 kW fuel cell, 15 kW electrolyser, 7 kg hydrogen storage tank, 320 supercapacitors and a power inverter of 7.6 kW (Table 3.2).

Table 3. 2: Optimisation results

Energy system component sizes	
Component	Size
PV generator	29.1 kW
Fuel Cell	10 kW
Inverter	7.6 kW
Electrolyser	15 kW
Supercapacitor	20 strings of 16 supercapacitors
Hydrogen tank	7 kg

The PV array with its capacity of 29.1 kW would produce a total of 96,656 kWh per annum to satisfy the load demand. Around 31 % of this generation is directly used by the load, while the remaining 69 % is utilised to produce hydrogen and charge the supercapacitor. The difference in the ratio of output power generated (Figure 3.4) and electricity load demand (10 kW) can be justified by the fact that the system needs to be sized above the load demand to permit capacity reserve to keep the 0 % of the capacity shortage.

The energy generated from the fuel cell is about 6,198 kWh per annum at a maximum power of 10 kW (Figure 3.5). The amount of hydrogen utilised to produce the above-mentioned energy is 1,302 kg, whereas the overall operating hours throughout the year are estimated to 4,271 hours. At this rate, the operational life of the fuel cell can be estimated to around 11 years 8 months and 12 days.

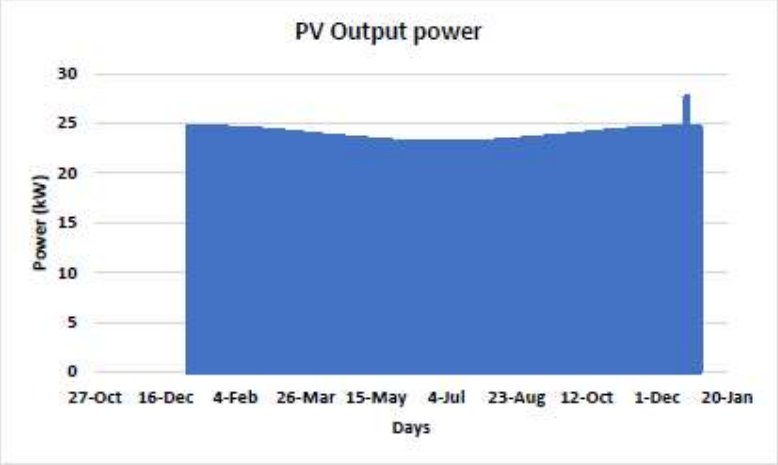

Figure 3. 4: Output power of photovoltaic arrays

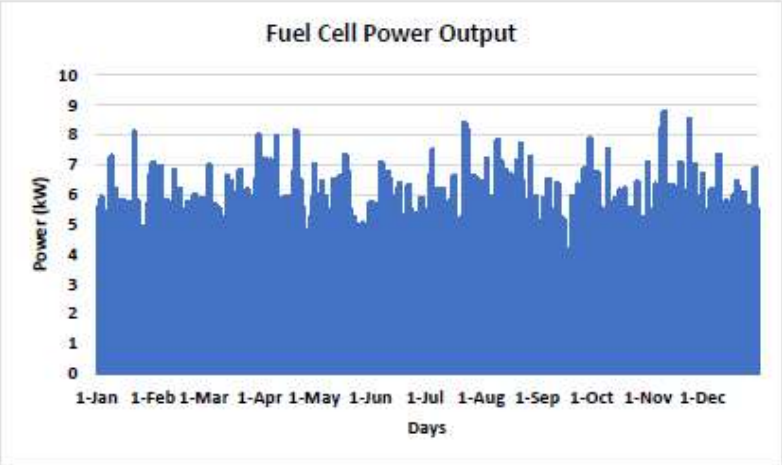

Figure 3. 5: Output power of fuel cell

The content of the hydrogen tank at the starting of the year is 0 kg (Figure 3.7), the tank is sized to accumulate up to 7 kg of hydrogen, subsequently permitting a capacity reserve operation of about 75.4 hours with a complete energy of 233 kWh. The total amount of hydrogen produced within the year is around 1,304 kg. The electrolyser needs a yearly energy of 60,512 kWh at the rated capacity of 15 kW to be able to produce this quantity of hydrogen. The maximum hydrogen production in an hourly basis is shown in Figure 3.6. Around 0.323 kg maximum quantity is produced each hour.

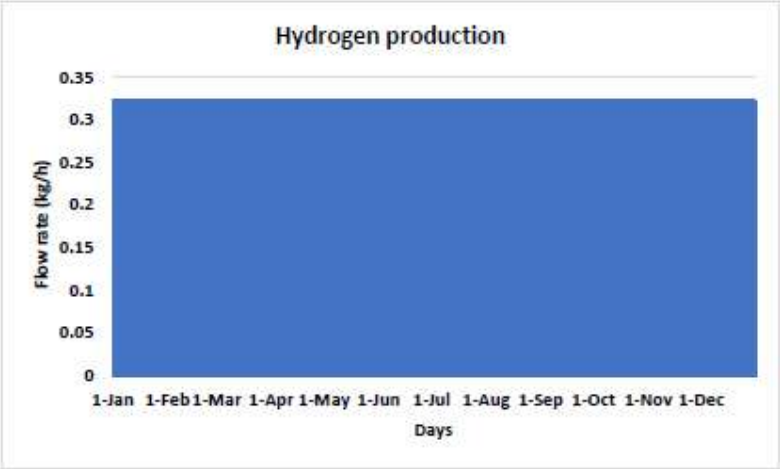

Figure 3. 6: Hydrogen production in the electrolyser

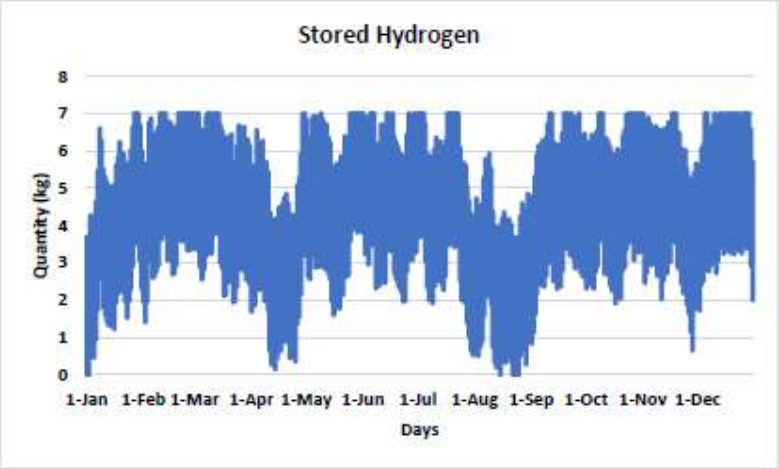

Figure 3. 7: Stored hydrogen

The initial state of charge of the supercapacitor unit is 100%. The supercapacitor unit has a nominal usable capacity of 1.2 kWh and can discharge at around 80 kW. The unit can manage the power demand for about 0.388 hours (23 minutes 17 seconds). The expected life of the unit is about 30 years. The yearly energy stored in the supercapacitors approaches 473 kWh/year, while the energy supplied to the load from the supercapacitor is 403 kWh/year. Hence, the storage depletion is 1.19 kWh/year with a 71 kWh losses every annum.

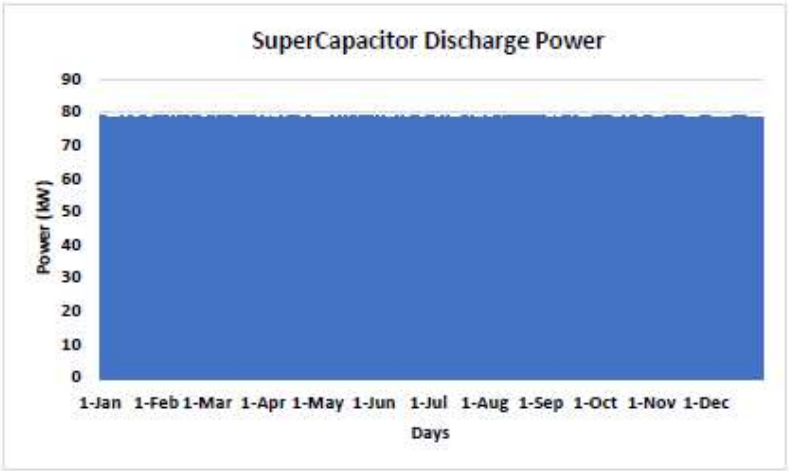

Figure 3. 8: Discharge power

3.3 Summary

In this chapter, an optimal sizing of a hybrid energy storage using a fuel cell system and supercapacitor for renewable off-grid applications was carried out. The objective was to determine a suitable system configuration with regard to the reliability to meet an overall load of 10 kW with 0 % capacity shortage. Based on the input data provided, the results show that, the optimal size of the system that meets the load requirement, given an irradiance of 850 Watts per metre square comprises 29.1 kW PV array, 10 kW fuel cell stack, 15 kW electrolysers, 7 kg hydrogen storage capacity, 7.6 kW converters and a total of 320 supercapacitors arranged in 16 strings of 20 supercapacitors each.

CHAPTER FOUR
SYSTEM COMPONENTS MODELLING

4.1 Introduction

This chapter deals with the mathematical modelling of individual components which are part of the system. These components include the photovoltaic array, a discrete reversible fuel cell, a hydrogen tank, the supercapacitor bank, and the power electronics converters such as DC to DC boost converter, DC-to-DC buck converter and voltage source inverter. The control schemes of power electronics converters devices mentioned above are also presented.

4.2 Component modelling

4.2.1 Model of a photovoltaic cell

The most widely used photovoltaic cell model is based on a one diode model depicted in the equivalent circuit in Figure 4.1. This circuit consists of a photon represented by a current source and a p-n junction represented by an antiparallel diode in parallel with a shunt and series internal resistances R_s and R_p. The parameters in the equivalent circuit are defined as follows:

- Series resistance R_s expresses the losses due to the electrical contact and the resistivity of the cell materiel
- Parallel resistance R_p is related to the losses produced by the p-n junction
- Diode current I_D is the current in the diode when it is directly polarised
- Photovoltaic current I_{Ph} is the current generated by the solar cell due to the sunlight incidence into it.
- Output current I is the existing current at the terminals of the solar cell

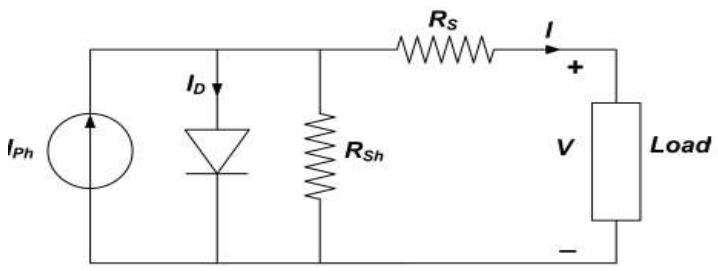

Figure 4. 1: Equivalent circuit of a photovoltaic cell

Based on the circuit in Figure 4.1, the output characteristics of a photovoltaic cell is described as:

$$I = I_{Ph} - I_S\left\{exp\left(\frac{V+IR_S}{A}\right) - 1\right\} - \frac{V+IR_S}{R_{Sh}} \quad (4.1)$$

$$A = \frac{mkT_c}{q} \quad (4.2)$$

where, A is the thermal voltage in V, m is the ideality factor, k is the Boltzmann's constant in J/K, T_c is the cell temperature in K, q is the electric charge and V is the voltage.

In Equation 4.1, the expression $\frac{V+IR_S}{R_{Sh}}$ is usually neglected as the shunt resistance is by far bigger than the series resistance. Based on that consideration, Equation 4.1 can be simplified as:

$$I = I_{Ph} - I_S\left\{exp\left(\frac{V+IR_S}{A}\right) - 1\right\} \quad (4.3)$$

Solving Equation 4.3 implies determining the parameters I_{Ph}, I_S, R_S and A, which can be obtained from manufacturers data, incidence irradiance and cell temperature. Data provided by the manufacturers gives generally the panel open and shorty circuit voltages, open and short current and maximum power at the standard test conditions (STC). This STC refers to a unified international test conditions adopted to determine the performance at a photovoltaic panel. It is defined as follows:

- Irradiation: 1000 W/m^2
- Temperature: 25^0 C
- Air mass: 1 at the equator, 1.5 in Europe

Other parameters such as temperature coefficient of the open-circuit voltage and temperature of short-circuit current might as well be provided by the manufacturer.

The cell operating temperature can be determined based on the Equation 4.4 as:

$$T_C = T_a + \frac{G}{G_{NOCT}}\left(NOCT - T_{a,NOCT}\right) \quad (4.4)$$

where T_a is the ambient temperature, G is the solar irradiance, $NOCT$ (nominal operating cell temperature) is usually provided by the manufacturer at an irradiance of $G_{NOCT} = 800\ W/m^2$, ambient temperature $T_{a,NOCT} = 20^o\ C$ and a wind speed of 1 m/s.

4.2.2 Parameters estimation

Parameters I_{Ph}, I_S, R_S and A are estimated as follows:

4.2.2.1 Determining the thermal voltage A

Thermal voltage defines the average energy of numerous particles travelling randomly at a certain temperature. This voltage can be obtained from the manufacturer data sheet at a set reference point from the Equation 4.5 as:

$$A_{ref} = \frac{\mu_{V_{OC}} T_{C,ref} - V_{OC,ref} + E_g N_S}{\frac{T_{C,ref} \mu_{I_{SC}}}{I_{Ph,red}} - 3} \tag{4.5}$$

where A_{ref} is the thermal voltage at the reference point, $T_{c,ref}$

$$I_{Ph,ref} = I_{SC,ref} \tag{4.6}$$

The thermal voltage is determined as:

$$A = A_{ref} \frac{T_C}{T_{C,ref}} \tag{4.7}$$

4.2.2.2 Determining the series resistance R_S

The value of the series resistance is either provided by the manufacturer or calculated based on the Equation 4.8 as:

$$R_S = \frac{A_{ref} ln\left(1 - \frac{I_{mpp,ref}}{I_{Ph,ref}}\right) - V_{mpp,ref} + V_{OC,ref}}{I_{mpp,ref}} \tag{4.8}$$

where $I_{mpp,ref}$ is the maximum current at the reference maximum power point and $V_{mpp,ref}$ the voltage at the reference maximum power point.

4.2.2.3 Determining the photon current I_{Ph}

The expression of the photon current is given as follows:

$$I_{Ph} = \frac{G}{G_{ref}} \left(I_{Ph,ref} + \mu_{I_{SC}} (T_C - T_{C,ref}) \right) \tag{4.9}$$

4.2.2.4 Determining the saturation current I_S

The saturation at a reference point is expressed as:

$$I_{S,ref} = I_{Ph,ref} exp\left(\frac{-V_{OC,ref}}{A_{ref}}\right) \tag{4.10}$$

The saturation current is determined based on Equation 4.10 as:

$$I_S = I_{S,ref}\left(\frac{T_C}{T_{C,ref}}\right)^3 x\ exp\left\{\left(\frac{N_S E_g}{A}\right)\left(1-\frac{T_{C,ref}}{T_C}\right)\right\} \quad (4.11)$$

4.2.3 Development of photovoltaic system Simulink model

Simulink model of the photovoltaic array is developed using parameters in Table 4.1. These parameters correspond to data of a BP Solar SX3200W PV panel. The resulting voltage versus current and voltage versus power curves are given in Figure 4.2 under an irradiation of 1000 Watts per m^2 and operating temperature of 25 and 45° C. A total of 15 strings of these panels are connected in parallel and each string comprises 12 series-connected modules. The maximum power of the photovoltaic array is 30 kW based on the design results obtained in chapter 3.

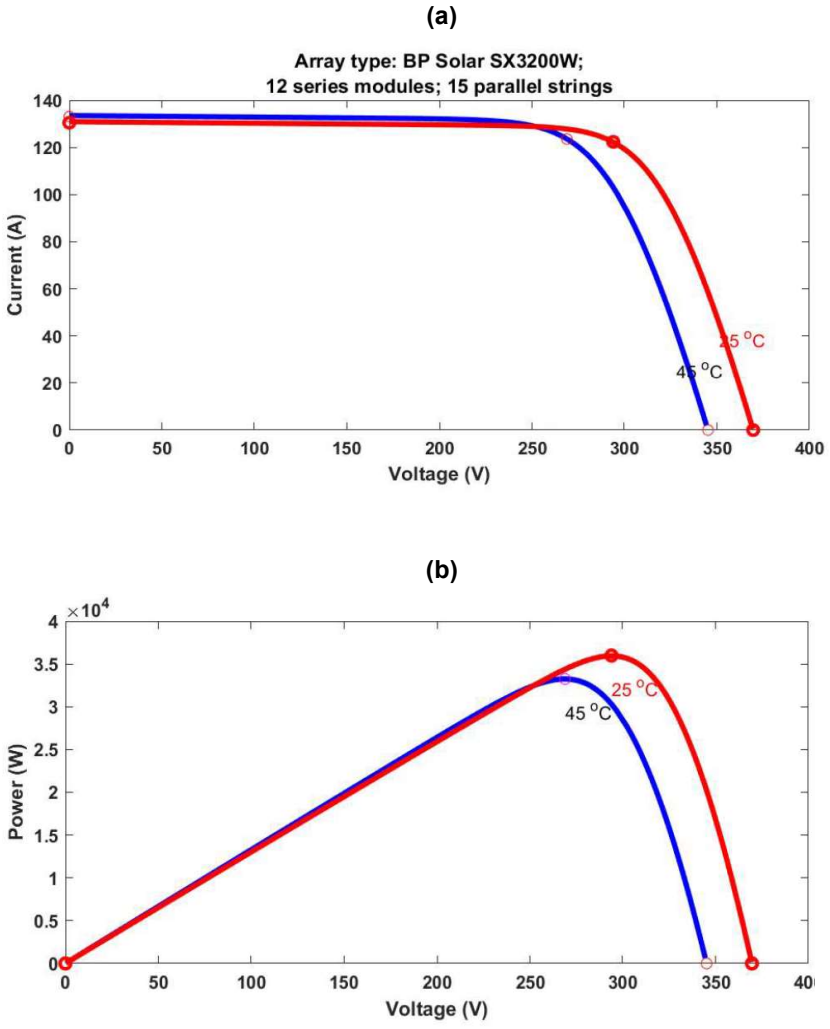

Figure 4.2: Photovoltaic module characteristics (a): Voltage versus the current, (b): Power versus voltage

Table 4.1: Photovoltaic array characteristics

Module data	
Type	BP Solar SX3200W
Maximum Power (Watts)	199.92
Open Circuit Voltage V_{oc} (Volts)	30.8
Voltage at maximum power point V_{mp} (Volts)	24.5
Temperature Coefficient of V_{oc} (% deg.C)	-0.33
Cells per module N_{cell}	50
Short-Circuit current I_{sc} (A)	8.7
Current at maximum power point I_{mp}	8.16
Temperature coefficient of I_{sc} (% deg.c)	0.1
Model Parameters	
Light-generated current I_L (A)	8.7449
Diode saturation current I_o (A)	1.0576e-10
Diode ideality factor	0.95448
Shunt resistance R_p (ohms)	190.2563
Series resistance R_s (ohms)	0.32982
Array Data	
Parallel strings	15
Series- connected modules per string	12

4.2.4 PV MPPT controller

As of now, diverse techniques are utilised to extract maximum power. Most of these techniques are used for photovoltaic and wind generators and vary from each other in several respects such as efficiency, convergence speed, complexity, sensors needed, cost, hardware implementation and many other aspects. (Karami et al., 2017) classified these methods in five categories listed in Table 4.2.

Table 4. 2: Maximum power point tracking methods

MPPT techniques and methods	
MPPT techniques	MPPT methods
Methods using predefined values characterising the Maximum Power Point	Constant voltage method Open-circuit voltage method Short-circuit current method Open-circuit voltage pilot PV cell method Temperature Gradient algorithm Temperature parametric method Feedback voltage or current method P-N junction drop voltage tracking technique
Method sensing the external parameters such as voltage, current etc., and comparing them with the pre-known values characterising the Maximum Power Point	Look-up table method Load current or load voltage maximisation Linear current control method
Method based on attempting to calculate and observe the result to determine the direction criteria for the next attempt to get to the Maximum Power Point	Only-current photovoltaic method PV Output Senseless control method Perturb and Observe method

	Three-point weight comparison method On-Line Maximum Power Point search method DC-Link capacitor droop control Array Reconfiguration method Maximum Power Point Tracking with variable inductorlevel-2 heading, left-justified
Method defining the Maximum Power Point based on mathematical calculation using available data	State-based Maximum Power Point Tracking method Linear reoriented coordinates method Curve-fitting method Differentiation method Slide control method Current sweep method dP/dV or dP/dI feedback control Incremental Conductance method Parasitic capacitance method Maximum Power Point Current and voltage computation method β method Methods by modulation Ripple correlation control
Method using intelligent learning process	Fuzzy logic method Neural network method Biological swarm chasing algorithm

The proposed PV MPPT tracker depends on Fuzzy Inference system and utilises the two inputs shown in Figure 4.3. Each input comprises five triangular membership functions with a normalised universe of discourse in the range of –2 to 2. These inputs are the error and change in error given in Equation 4.13 and Equation 4.14. The inputs consist of five variables namely negative big (NB), negative small (NS), zero (Z), positive small (PS) and positive big (PB). The error and change in error are given in Equation 4.12 and Equation 4.13 as follows (Doudou N. Luta & Raji, 2019a):

$$e(k) = \frac{p(k)-p(k-1)}{v(k)-v(k-1)} \tag{4.12}$$

where $\mathrm{p(k)}$, $\mathrm{p(k\text{-}1)}$, $\mathrm{v(k)}$ and $\mathrm{v(k\text{-}1)}$ are the powers and voltages at instant k and k-1 respectively

$$\Delta e_k = e_k - e_{k-1} \tag{4.13}$$

where e_k and e_{k-1} are the error at instant k and k-1 respectively.

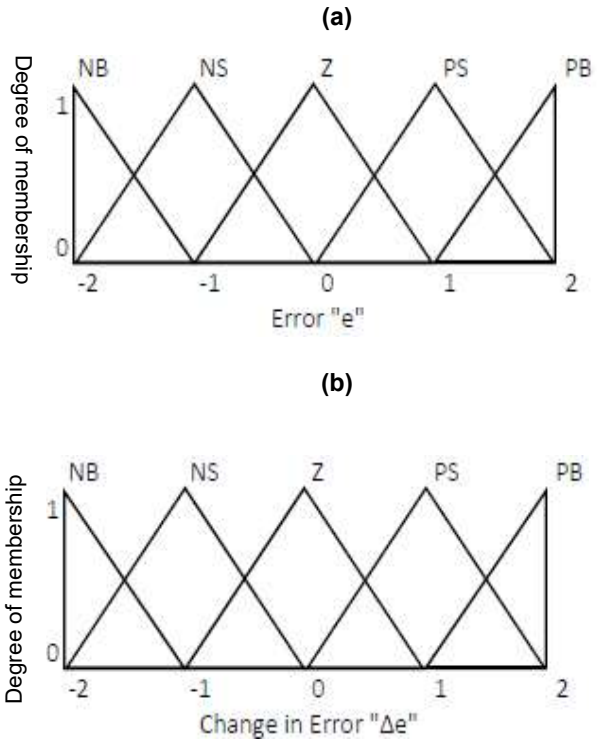

Figure 4. 3: Input membership functions

The output of Mamdani Inference Engine comprises five membership functions (two trapezoidal and three triangular membership functions) namely negative big (NB), negative small (NS), zero (Z), positive small (PS) and positive big (PB) (Figure 4.4). The universe of discourse ranges from 0 to 1.

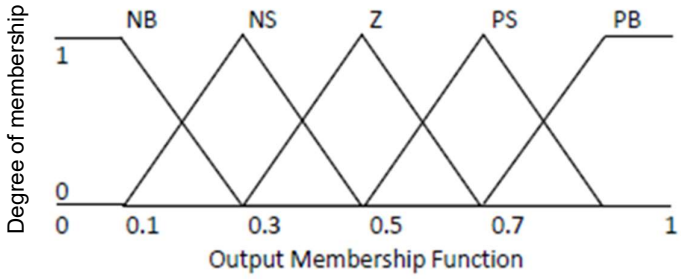

Figure 4. 4: Output membership function

Different number of subsets has been used for the rule settings, however, this work considers five subsets based on twenty-five rules (Table 4.3). These rule settings are obtained by analysing the behaviour of the system. Various operating conditions are considered to improve tracking performance of dynamic response of the system. The control algorithm operates as follows: The tracking process is started with an initial duty cycle of D=0. The converter input current and voltage are then determined and the duty

cycle that can provide maximum power of the converter based on predicted values that have already been set into fuzzy system is sensed. The operation is repeated continuously until the system becomes stable by reaching the maximum power.

Table 4. 3: Error and Change in error

Error \ Change in error	**E/ΔE**	**NB**	**NS**	**Z**	**PS**	**PB**
	NB	Z	Z	Z	PS	PB
	NS	Z	Z	NB	PS	PB
	Z	NB	NS	NS	PS	PB
	PS	NB	NS	NS	Z	Z
	PB	NB	NS	PS	Z	Z

4.3 Fuel cell system

Various models are proposed in the fuel cell research field; these models use a wide range of techniques and methods and focus on aspects such as chemicals, experimental and electrical. Chemical models deal with mass transport, heat transfer and diffusion of species inside the fuel cell. The major drawback with these types of model is their inability to be included into electrical simulation problems due to their excessive number of parameters.

Experimental modelling instead is based on experiments aiming to come up with empirical expressions representing fuel cells. However, most of these models do not include the thermodynamics of fuel cells and some effects caused by the operating parameters such gases inlet pressures, flow rate, compositions and temperature. On the other hand, electrical models use electrical elements to represent fuel cells behaviour without the inclusion of the chemical and thermodynamics aspects.

The electrical models of fuel cell can be either a steady-state model or a dynamic model. The steady-state model analyses the operation of a fuel cell at a particular point or at slow dynamic, while the dynamic model analyses the operation of a fuel cell in transient mode.

Besides the model mentioned above, other researchers present the fuel cell thermal modelling based on the thermal balance in both steady state and dynamic operating modes of fuel cells.

4.3.1 Fuel cell model

The type of fuel cell selected in this study is a PEMFC (proton exchange membrane fuel cell). The FC model adopted in this investigation is a modified version of the approach proposed by (Aslam et al., 2017), whereby the dynamics of the reactant flow are negligible.

Assuming that the fuel cell is supplied with pure hydrogen and oxygen gases, the temperature of the stack is controlled and unchanged at steady state, the system obeys the Nernst equation, the water by-product from the fuel cell stack is liquid, the gases used are ideal and obey the ideal gas law and a shocked orifice is assumed at the exhaust. The voltage resulting from the electrochemical reactions is expressed by the Nernst equation as (Doudou N. Luta & Raji, 2019c):

$$E_n = 1.229 + (\mathrm{T} - 298).\frac{-44.43}{2F} + \frac{RT}{2F} ln\left(P_{H_2} P_{O_2}^{\frac{1}{2}}\right) \tag{4.14}$$

where P_{H_2} and P_{O_2} are the hydrogen and oxygen partial pressures, respectively, T is the temperature, F is the Faraday constant and R is the ideal gas constant.

The partial pressures are defined as function of reactant utilisation by Equation 4.15 (Souleman et al., 2009):

$$P_{H_2} = \left(1 - U_{f_{H_2}}\right) x\% P_{fuel} \tag{4.15}$$

$$P_{O_2} = \left(1 - U_{f_{O_2}}\right) y\% P_{air}$$

where $U_{f_{H_2}}$ and $U_{f_{O_2}}$ are the hydrogen and oxygen utilisation, respectively, P_{fuel} and P_{air} are the supply pressures of the hydrogen and oxygen, respectively, and x and y are the percentages of hydrogen and oxygen compositions.

The rates of reactant utilisation are given as follows (Souleman et al., 2009):

$$U_{f_{H_2}} = \frac{60000RTi_{fc}}{2FP_{hydr}V_{hydr}x\%} \tag{4.16}$$

$$U_{f_{O_2}} = \frac{60000RTi_{fc}}{4FP_{oxyg}V_{oxyg}y\%}$$

where V_{hydr} and V_{oxyg} are the hydrogen and oxygen flow rates, i_{fc} is the cell current.

The lack of oxygen in the cell leads to the increase of its utilisation over the nominal value; hence, Equation (4.12) is adjusted as:

$$E_n = 1.229 + (\mathrm{T} - 298).\frac{-44.43}{2F} + \frac{RT}{2F} ln\left(P_{H_2} P_{O_2}^{\frac{1}{2}}\right) - K_u\left(U_{f_{O_2}} - U_{f_{O_{2nom}}}\right) \quad (4.17)$$

where K_u is the voltage undershoots constant and $U_{f_{O_{2nom}}}$ is defined as the nomination oxygen utilisation.

The open-circuit voltage of a single cell is given by Equation 4.18 as follows:

$$E_0 = K_c E_n \quad (4.18)$$

where K_c is the voltage constant.

Taking into consideration losses, including the activation losses and resistive and diffusion losses, the open-circuit voltage of a single cell is expressed as:

$$V = E_0 - V_{act} - V_r \quad (4.19)$$

where V_{act} and the V_r given as (Souleman et al., 2009):

$$V_{act} = \frac{RT}{2\alpha F} ln\left(\frac{i_{fc}}{\frac{2Fk\left(P_{H_2}+P_{O_2}\right)}{Rh}.exp\left(\frac{\Delta G}{RT}\right)}\right)\frac{1}{s\frac{T_d}{3}+1} \quad (4.20)$$

$$V_r = r_{ohm} i_{fc} \quad (4.21)$$

where T_d is the cell settling time to a current step and r_{ohm} is the cell resistance, α is the charge transfer coefficient, ΔG is the activation energy barrier, k is the Boltzmann constant and h is the Plank constant.

The complete PEMFC stack voltage is given as follows:

$$V_{fc} = N.V \quad (4.22)$$

Where N is the number of cells in the stack.

4.3.2 Fuel cell Polarisation curve

Simulink model of the fuel cell stack is developed using parameters in Table 4.3 and based on Equation 4.14 to Equation 4.22. The resulting voltage versus current and

voltage versus power curves are given in Figure 4.5. The maximum power of the stack is 10 kW based on the design results obtained in chapter 3.

Table 4. 4: Fuel cell stack characteristics

Fuel cell stack parameters	
Voltage at 0A and 1A [V_0(V), V_1(V)]	[52.2,52.46]
Nominal operating point [Inom(A), Vnom(V)]	[250,41.15]
Maximum Operating point [Iend(A), Vend(V)]	[320,39.2]
Number of cells	65
Nominal stack efficiency (%)	50
Operating temperature (Celsius)	45
Nominal Air flow rate	732
Nominal supply pressure [Fuel (bar), Air (bar)]	[1.16,1]
Nominal composition (%) [H2 O2 H2O (air)]	[9.95,21,1]

(a)

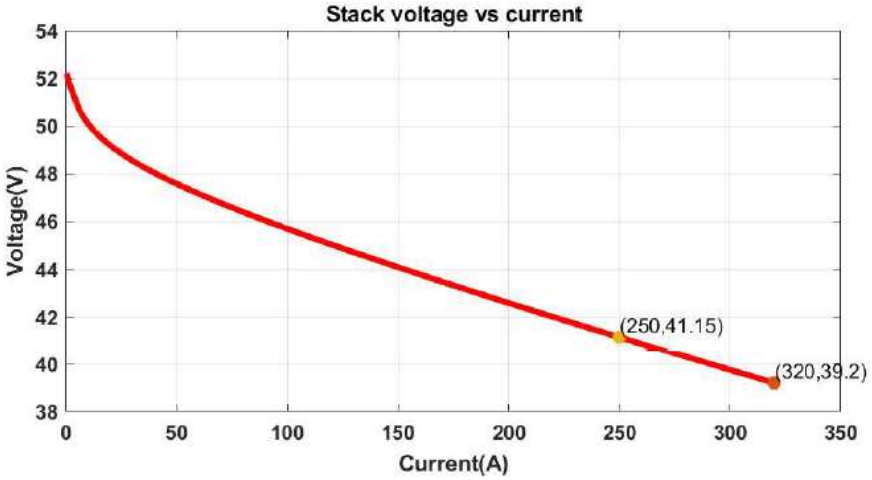

(b)

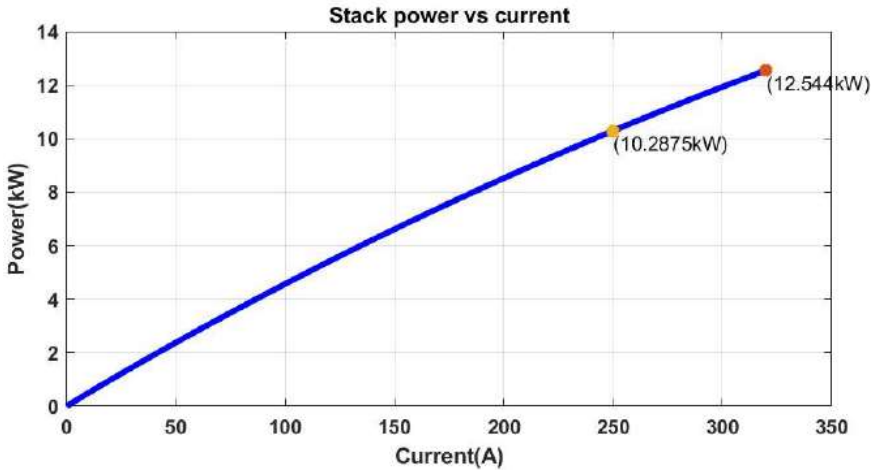

Figure 4. 5: Fuel cell stack characteristics (a): Voltage versus the current, (b): Power versus voltage

4.3.3 Fuel cell maximum power tracker

As it is the case for photovoltaic systems, a typical fuel cell stack shows a nonlinear power because of internal limitations and operating parameters which include the temperature, hydrogen and oxygen partial pressures, humidity levels, gas speed and stoichiometry, and membrane water content, leading to a reduced system performance. It is crucial to extract as much power as possible from the stack knowing that at any operating condition, there is only one Maximum Power Point. This prevents excessive fuel use and avoids low system efficiency. To ensure this, a switch mode power converter referred to as a Maximum Power Point Tracker (MPPT) is interfaced between the FC and the load and operates such that the converter's duty cycle is adjusted continuously, hence modifying the voltage and current depending upon the Maximum Power Point position. If a proper algorithm is used, the MPPT will be able to locate and track the PEMFC MPP.

As of now, diverse techniques are utilised to extract maximum power. Most of these techniques are employed for photovoltaic (Das et al., 2016) and wind generators and vary from each other in several respects such as efficiency, complexity, convergence speed, sensors needed, hardware implementation and cost, to name a few. This study considered and compared two maximum power point tracking approaches; one based on the Mamdani Fuzzy Inference System and the other on the Particle Swarm Optimisation algorithm to maintain the output power of a fuel cell stack as close as possible to its designed power.

Particle Swarm Optimisation (PSO) is nature-inspired optimisation method created by James Kennedy and Russell Eberhart in the year 1995 (Cheng et al., 2015). Recently, PSO has emerged as a promising algorithm to solve numerous optimisation problems in science and engineering. For MPPT applications, PSO algorithm is easy to execute, displays rapid computation abilities, and permits the determination of the MPP no matter the environmental conditions (Kumar & Chatterjee, 2016). The approach is based on the behaviour of bird flocks; lots of collaborative particles are used in an n dimensional space and each of them has a position pi (distributed randomly) and velocity vi (vi = 0 in initiation). The position of a particle is decided by the best position found by the particle up until this point P_{best}, and the best position of all particles so far G_{best}. The equations expressing the standards PSO methods are as follows (Doudou N. Luta & Raji, 2019c):

$$v_i(k+1) = wv_i(k) + c_1r_1\big(P_{best} - x_i(k)\big) + c_2r_2(G_{best} - x_i(k)) \tag{4.23}$$

$$x_i(k+1) = x_i(k) + v_i(k+1) \quad (4.24)$$

$$i = 1, 2, 3, \dots, N$$

where xi and vi are the velocity and position of a particle i, respectively, w is the inertia weight, k represents the iteration number. r_1 and r_2 are random variables uniformly distributed in the range of [0, 1], P_{best} is the best position of the particle I, G_{best} is the best position of all the particles in the swarm and $c1$ and $c2$ are the cognitive and social coefficients, respectively.

The operational strategy of a PSO algorithm shown in Figure 4.6 includes five following stages (Doudou N. Luta & Raji, 2019c):

- The first stage consists of randomly initialising the particles in a same distribution either over the search space or on grid nodes covering the search space in equidistant points.
- The second step concerns the evaluation of the fitness of particles one by one by giving the possible solution to the objective function.
- In the third step, individual and global best fitness values (P_{best} and G_{best}) are updated through the comparison of their previous values against the newly calculated and the replacement of P_{best} and G_{best} including their corresponding positions.
- The fourth step consists of updating the velocity and position of particles one after one in the swarm using equations (Venkateshkumar et al., 2013) and (Raj & Sreekumar, 2016).
- The last step involves verifying if the convergence criterion is met to end the process or increase the number of erations by 1 and move to the step 2.

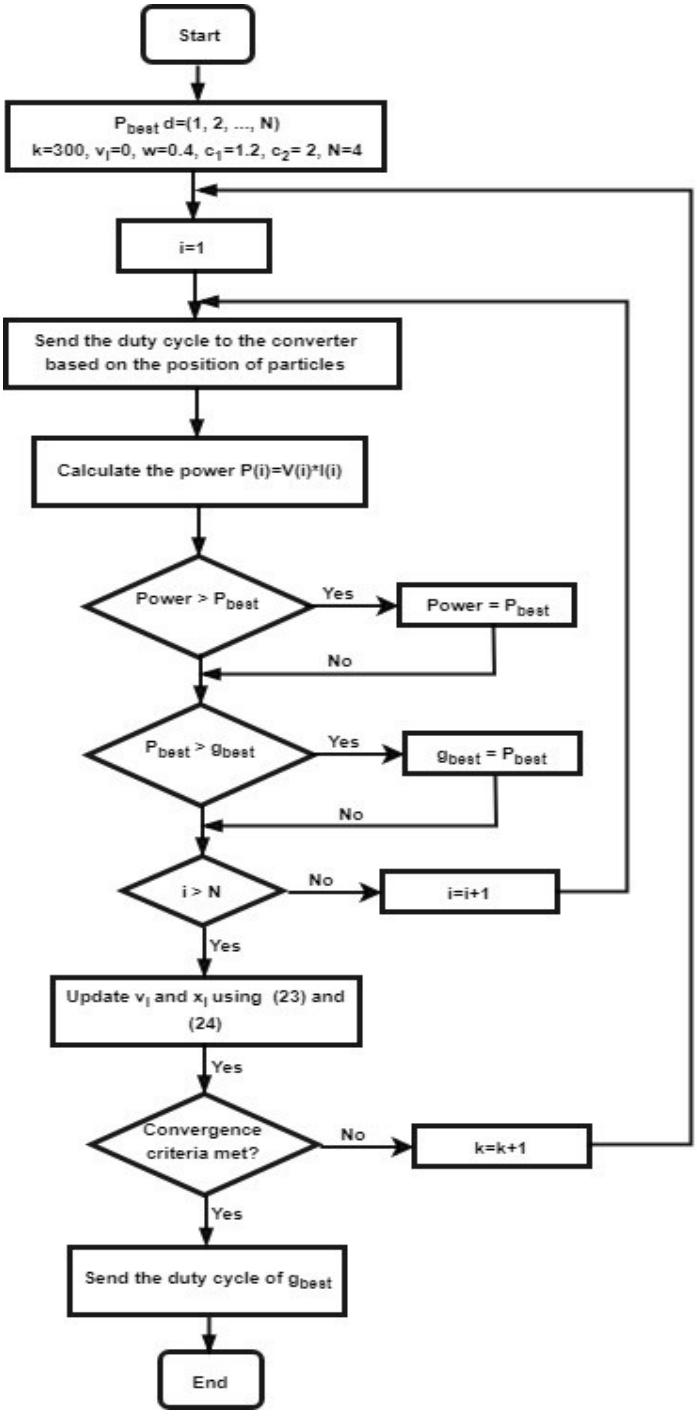

Figure 4. 6: Flowchart of PSO MPPT controller

4.4 Electrolyser

The type of electrolyser selected in this study is of alkaline type. The anode and cathode are submerged in the electrolyte. The reaction occurring in an alkaline electrolyser is illustrated in Figure 4.7 and expressed in Equation 4.25 as:

$$\text{Anode: } 2OH^- \rightarrow \frac{1}{2}O_2 + H_2O + 2e^-$$
$$\text{Cathode: } 2H_2O \rightarrow 2H^+ + 2OH^- \quad (4.25)$$

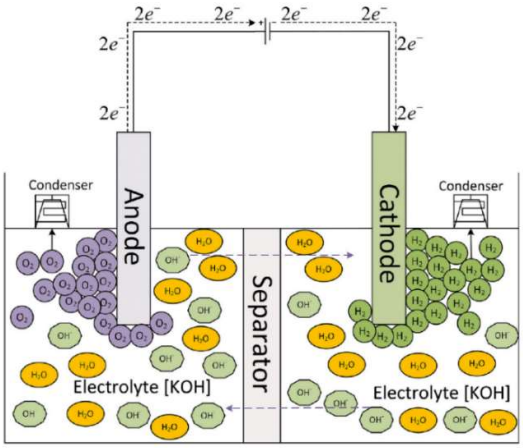

Figure 4.7: Alkaline electrolyser schematic

The operation of alkaline electrolyser is such that once a potential difference is applied at the terminal of the electrolyser, an electric field is developed, causing hydrogen ions (H^+) to move towards the cathode, while hydroxide ions (OH^-) migrate towards the anode. An ionic conductive gas separator is utilised to hinder the hydrogen and oxygen gases generated from combining, while gases receivers are utilised to gather the hydrogen and oxygen.

4.4.1 Electrolyser cell voltage

The performance of an alkaline electrolyser is assessed by plotting its current versus voltage characteristics (polarisation curve), drawn from the cell voltage against the current density. A common alkaline electrolyser polarisation curve is depicted in Figure 4.8.

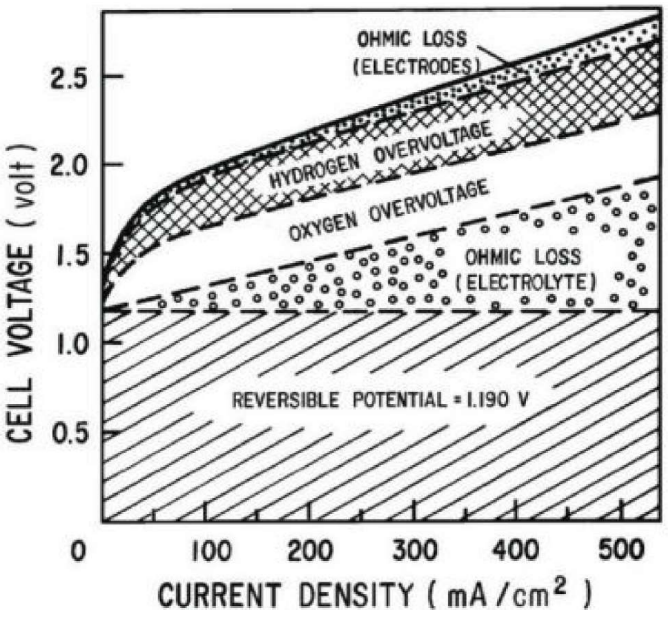

Figure 4. 8: System frequency tolerance requirements

It can be noted from Figure 4.8 that ohmic loss of electrolyte, overvoltage associated with oxygen, overvoltage associated with hydrogen and ohmic losses due to electric resistance of electrodes and circuitry increase the cell voltage over the reversible potential. The electrolyser cell voltage (V_{cell}) is given by Equation 4.26:

$$V_{cell} = V_{rev} + V_{act} + V_{ohm} + V_{con} \tag{4.26}$$

where V_{rev}, V_{act}, V_{ohm} and V_{con} are the reversible cell voltage, activation overvoltage, ohmic overvoltage and concentration overvoltage respectively.

The reversible cell voltage (V_{rev}) is identified as the minimum voltage required for the electrolysis to take place and determined by Gibbs equation as:

$$V_{rev} = \frac{\Delta G}{zF} \tag{4.27}$$

where ΔG, z and $F = 96485\ C/mol$ are the Gibbs energy, number of electrons and Faraday's constant respectively.

At 25^0 C and 1 bar which is the standard condition, the Gibbs energy to split water is equals to 237.2 kJ/mol, while $z = 2$. Therefore, by replacing those values into Equation 4.27, the corresponding value of V_{rev} is $= 1.229\ V$

In the same vein, the activation overvoltage is produced due to the electrochemical kinetics during simultaneous half reactions occurring at the anode and cathode. This activation overvoltage is expressed by Equation 4.28 as (Khan & Iqbal, 2009):

$$V_{act} = slog\left(\frac{t_1+\frac{t_2}{T}+\frac{t_3}{T^2}}{A}I + 1\right) \tag{4.33}$$

where s, t_1, t_2, t_3 are the overvoltage coefficient on electrodes, I, T and A are the current density, temperature of the cell and electrode area respectively.

The overvoltage ohmic is produced by the resistance of electrodes, interconnection and separating diaphragm to the electrons flow. This overvoltage is defined by Equation 4.34 as (Khan & Iqbal, 2009):

$$V_{ohm} = \frac{r_1+r_2T}{A}I \tag{4.34}$$

where r_1 and r_2 are parameters associated with ohmic resistance of the electrolyte.

The concentration overvoltage results generally from mass transport processes essentially convection and diffusion. For alkaline electrolysis the concentration overvoltage is by far smaller than the activation and ohmic overvoltage, thus negligible. Therefore, Equation 4.26 can be rewritten as:

$$V_{cell} = V_{rev} + V_{act} + V_{ohm} \tag{4.35}$$

Constants used in Equations 4.27 to 4.35 are listed in Table 4.5.

Table 4.5: Electrolyser parameters

	VALUE
Reversible voltage (V_{rev}) in volt	1.229
Area of Electrode (A) in cm^2	0.25
Faraday's Constant (F) in C/mol	96485
Number of Electrons (z)	2
Overvoltage coefficient on electrodes (t_1) in A^{-1}m^2	1.002
t_2 in A^{-1}m^2 ^{0}C	8.424
t_3 in A^{-1}m^2 ^{0}C	247.3
r_1 in Ωm^2	8.05e^{-5}
$r_2$in Ωm^2 ^{0}C	-2.5e^{-7}

Owing to the presence of a logarithmic function in Equation 4.33, a close examination is required to eliminate negative values that can provide unrealistic results. This can occur for low currents as the model parameters might not adequately follow the

electrolyser response. In the same manner, for the input current equal to zero in Equation 4.35, the electrolyser cell voltage is equal to the reversible voltage and may potentially operate as a voltage source, thus supplying current to other elements of the electrical circuit.

4.4.2. Hydrogen production rate

Hydrogen production rate is associated to the input current using Faraday law such that it is proportional to the transfer rate of electrons to both electrodes. The equation describing the hydrogen production is known as Faraday's efficiency defined as (Khan & Iqbal, 2009):

$$\eta_F = \frac{\left(\frac{I}{A}\right)^2}{f_1 + \left(\frac{I}{A}\right)^2} f_2 \tag{4.36}$$

where f_1 and f_2 are parameters associated with Faraday efficiency and often assumed constant for the overall model. These parameters are defined as:

$$f_1 = 2.5T + 50 \tag{4.37}$$

$$f_2 = 1 - 6.25 \times 10^{-6} T \tag{4.38}$$

Therefore, the total hydrogen production rate in an electrolyser is given as (Khan & Iqbal, 2009):

$$\dot{n}_{H_2} = \eta_F \frac{n_c I}{zF} \tag{4.39}$$

$$\dot{n}_{H_2} = \dot{n}_{H_2O} = \dot{n}_{O_2} \tag{4.40}$$

where $\dot{n}_{H_2}$, $\dot{n}_{H_2O}$ and $\dot{n}_{O_2}$ are the molar flow rate per second of hydrogen, water and oxygen respectively.

In the same vein, the volume flow rate of hydrogen is defined as:

$$Q = \dot{n}_{H_2} \times 3600 \times 0.022414 \tag{4.41}$$

Parameters used to develop the 15 kW electrolyser stack Simulink model are given in Table 4.6.

Table 4.6: Electrolyser parameters (Letcher, 2016)

	VALUE
Reversible voltage (V_{rev}) in volt	1.229
Area of Electrode (A) in cm^2	0.25
Faraday's Constant (F) in C/mol	96485
Number of Electrons (z)	2
Overvoltage coefficient on electrodes (t_1) in A^{-1}m^2	1.002
t_2 in A^{-1}m^2 ^{0}C	8.424
t_3 in A^{-1}m^2 ^{0}C	247.3
r_1 in Ωm^2	8.05e^{-5}
$r_2$in Ωm^2 ^{0}C	-2.5e^{-7}
Cell current mA/cm^2	0.2-0.4
Cell voltage V	1.8-2.4
Cell area m^2	0.1
Cells in series	170
Cells in parallel	140

4.5 Hydrogen storage tank

Hydrogen can be stored using different methods, the most common storage approaches include compressed hydrogen storage, liquid hydrogen storage, and metal hybrid storage. The dynamics of hydrogen stored into the tank is given by Equation 4.42 as (Lajnef et al., 2013):

$$P_f - P_i = z\frac{q_{H_2}RT_f}{M_{H_2}V_f} \tag{4.42}$$

P_f and P_i tank pressure and tank initial pressure respectively, q_{H_2} is the volume flow rate of hydrogen, z is the compressibility factor, R is the gas constant, M_{H_2} is the molar mass of hydrogen, and T_f and V_f are the final temperature and volume respectively.

Based on the system configuration obtained in chapter 3, the capacity of the hydrogen tank is 7 kg. This value corresponds to a volume of 83.901 cubic metres at standard temperature and pressure (1 atm and 21° C).

4.6 Supercapacitor

The supercapacitor voltage is given by Stern Equation as (Mathworks, 2013):

$$V_{SC} = \frac{N_s Q_T d}{N_p N_e \varepsilon_o \varepsilon A_i} + \frac{2N_e N_s RT}{F} sinh^{-1}\left(\frac{Q_T}{N_p N_e^2 \sqrt{8RT\varepsilon\varepsilon_o c}}\right) - R_{SC} i_{SC} \tag{4.43}$$

where i_{SC} is obtained from Equation 4.44 expressed as:

$$Q_T = \int i_{SC} dt \tag{4.44}$$

For the self-discharge phenomenon, Equation 4.44 is modified as:

$$Q_T = \int i_{self\_dis} dt \tag{4.45}$$

with

$$i_{self\_dis} = \begin{cases} \frac{C_T a_1}{1+sR_{SC}C_T} \; if \; t - t_{oc} \leq t_3 \\ \frac{C_T a_2}{1+sR_{SC}C_T} \; if \; t_3 < t - t_{oc} \leq t_4 \\ \frac{C_T a_3}{1+sR_{SC}C_T} \; if \; t - t_{oc} > t_4 \end{cases} \tag{4.46}$$

where a_1, $a_2$and a_3 are change rate of the Supercapacitor voltage at the intervals (t_{oc}, t_3), $(t_3, t_4)$and (t_4, t_5) respectively.

The characteristics of the supercapacitor used in this study are given in Table 4.7. A total of 320 supercapacitors are considered to form the supercapacitor bank. They are connected such that 16 of them are in series and 20 in parallel. On the other hand, the charge characteristics of a single supercapacitor is shown in Figure 4.9.

Table 4.7: Supercapacitor characteristics (Maxwell, 2007)

Parameters	
Characteristics of a single supercapacitor	
Rated Capacitive (F)	3000
Equivalent DC series resistance (ohms)	27e-3
Rated Voltage (V)	3
Operating temperature (°C)	25
Initial Voltage (V)	3
Characteristics of the supercapacitor bank	
Number of series capacitors	16
Numbers of parallel capacitors	20

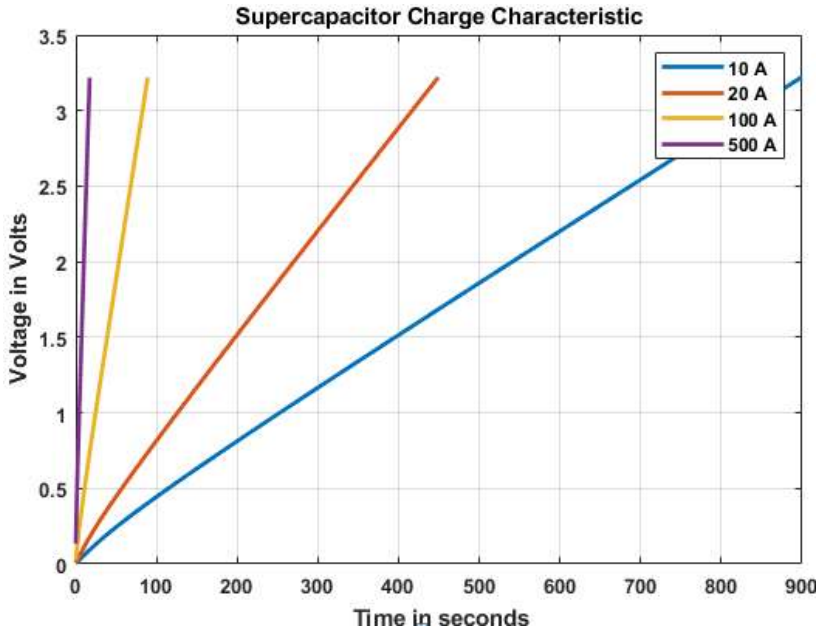

Figure 4.9: Charge characteristics of a single supercapacitor

4.7 Power electronics converters

The role of power electronics converters is to control the flow of power from the generation to a load such that the load is supplied with a suitable current, voltage and/or frequency. This is achieved by reducing as much as possible power losses to obtain a higher conversion efficiency. Power electronic converters are categorised in different sorts depending on the type of conversion. The type of conversion includes DC-to-AC, AC-to-DC, DC-to-DC or AC-to-AC.

In general, the design of power electronic converters is based on components such as inductors, capacitors and semiconductor switches. These switches can be either uncontrolled for instance diodes, semi-controlled (thyristors) or fully controlled (BJTs, MOSFETs, IGBTs, GTOs, etc.). Controlled semiconductor devices are driven by circuits using control signals while the uncontrolled ones are line commutated.

This section is dedicated to the modelling of DC-to-DC and DC-to-AC converters used in this thesis. Three boost converters and a buck converter are used in the system modelling. The voltage of the photovoltaic array is boosted from 294 V to 350 V, that of the fuel cell is boosted from 41.15 V to 350 V and lastly, the supercapacitor bank voltage is increased from 48 V to 350 V. In order to charge the supercapacitor bank, a buck converter is used to convert the 350 V from the photovoltaic system to 48 V to meet the voltage of the bank as shown in Table 4.7.

The control of the photovoltaic boost converter is achieved using a maximum power tracking algorithm based on fuzzy, whereas that of the fuel cell stack utilises PSO (Particle swarm Optimisation) algorithm. On the other hand, the control of the boost and buck converters for the supercapacitor banks are based on the single loop voltage mode control.

Similarly, a three-phase DC-to-AC converter is used to convert the 350 DC V from the DC link to an AC voltage to supply the 7 kW AC load at 350 Volts.

4.7.1 DC to DC converters

The role of DC-to-DC converters is to condition the voltage and control power flow in the PV array, fuel cell and supercapacitor. Converters used in practical systems are more complex, however, basic DC-to-DC converter topologies can as well be used in the simulation to achieve the same objective. This subsection focuses on the modelling of converters such as boost and buck converters including the closed loop control systems used.

4.7.1.1 Boost converter

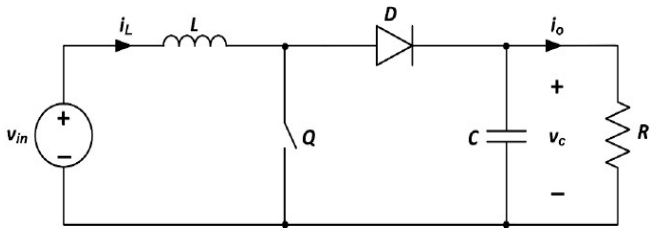

Figure 4.10: Boost converter

The basic model of a boost converter is shown in Figure 4.10 where the semiconductor devices Q and D are assumed ideal. The boost converter operating modes are defined by the states of the inductor current. The converter is said to be in continuous conduction mode (CCM) if the inductor current does not go to zero and otherwise, it is in discontinuous conduction mode (DCM).

At steady state, the converter operation is such that when the semiconductor device Q is on, the input voltage V_{in} charges the inductor L while the capacitor supplies the load R. During the off state of Q, the inductor discharges its stored energy to the load through the diode.

By assuming that the capacitor voltage ripple is much smaller than its DC value V_c, Equation 4.47 expressing the relationship between V_c and V_{in} can be written as:

$$\frac{V_c}{V_{in}} = \frac{1}{1-D} \tag{4.47}$$

with the duty cycle D defined as:

$$D = \frac{T_{on}}{T_s} \tag{4.48}$$

where T_{on} and T_s are the fraction of Q is on and the switching period respectively.

At steady state operating state, the value of the critical inductance L that defines the limit between continuous conduction mode (CCM) and discontinuous conduction mode (DCM) is defined by Equation 4.49 as:

$$L_c = \frac{(1-D)^2 D \times R}{2f_s} \tag{4.49}$$

with f_s, the switching frequency defined as:

$$f_s = \frac{1}{T_s} \tag{4.50}$$

To maintain continuous conduction for different voltages and loads, the inductance is often selected 10 times the calculated value.

The capacitance required to minimise the peak to peak voltage ripple variation in the output voltage is given by Equation 4.51 as:

$$C_{min} = \frac{DV_c}{\Delta V_c R f_s} \tag{4.51}$$

The parameters of DC-to-DC boost converters used in this study are given in Tables 4.8, 4.9 and 4.10.

Table 4.8: PV boost converter parameters

PV boost converter parameters	
Input voltage (Volts)	294
Output voltage (Volts)	350
Duty cycle (%)	24
Switching frequency (kHz)	5
Inductance (Henry)	98.07 e-6
Capacitance (Farads)	81 e-3
Load (Ohms)	8.587
Steady-state dc operating point	
Average inductance current (A)	48.523
Maximum inductance current (A)	96.4887
Minimum inductance (A)	557.22 e-3
Operating current (A)	40.7593

Table 4.9: Fuel cell boost converter parameters

Fuel cell boost converter parameters	
Input voltage (Volts)	41.15
Output voltage (Volts)	350
Duty cycle	88
Switching frequency (kHz)	5
Inductance (Henry)	15 e-6
Inductance resistance (Ω)	1 e-9
Capacitance (Farads)	59 e-3
Capacitance resistance (Ω)	1 e-2
Load (Ohms)	12.25
Steady-state dc operating point	
Average inductance current (A)	243.013
Maximum inductance current (A)	492.977
Minimum inductance (A)	0
Operating current (A)	28.5714

Table 4.10: Supercapacitor boost converter parameters

Supercapacitor bank boost converter parameters	
Input voltage (Volts)	48
Output voltage (Volts)	350
Duty cycle	86
Switching frequency (kHz)	5
Inductance (Henry)	2.5e-6
Inductance resistance (Ω)	1e-9
Capacitance (Farads)	45800e-6
Capacitance resistance (Ω)	45.8e-3
Load (Ohms)	1.5
Steady-state dc operating point	
Average inductance current (A)	1.70139 e3
Maximum inductance current (A)	3.35808 e3
Minimum inductance (A)	44.7039
Operating current (A)	233.333

4.7.1.2 Buck converter

The simple model of a buck converter is shown in Figure 4.11 where the semiconductor devices Q and D are assumed ideal.

At steady state, the converter operation is such that when the semiconductor device Q is on, the diode D is reverse biased, and the input voltage V_{in} charges the inductor L while supplying the load R. When Q is off, the energy stored in the inductor is discharged to the load through the diode.

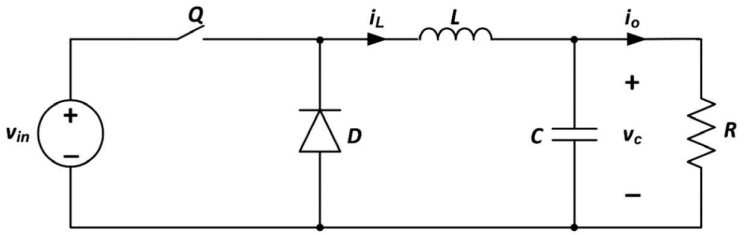

Figure 4.11: Buck converter

For the capacitor voltage ripple is much smaller than its DC value V_c, Equation 4.52 expressing the relationship between V_c and V_{in} can be written as:

$$\frac{V_c}{V_{in}} = D \tag{4.52}$$

At steady state operating state, the value of the critical inductance L that defines the limit between continuous conduction mode (CCM) and discontinuous conduction mode (DCM) is defined by Equation 4.53 as:

$$L_c = \frac{(1-D)\times R}{2f_s} \tag{4.53}$$

To minimise the peak to peak voltage ripple variation in the output voltage, the minimal capacitance is given by Equation 4.54 as:

$$C_{min} = \frac{(1-D)V_c}{8\Delta V_c L {f_s}^2} \tag{4.54}$$

The supercapacitor buck converter parameters are given in Table 4.11, the charging power is set to 4.8 kW.

Table 4. 11: Supercapacitor buck converter parameters

Supercapacitor bank buck converter parameters	
Input voltage (Volts)	350
Output voltage (Volts)	48
Duty cycle %	14.2
Switching frequency (kHz)	5
Inductance (Henry)	415 e-6
Inductance resistance (Ω)	1 e-9
Capacitance (Farads)	1042 e-6
Capacitance resistance (Ω)	50 e-3
Charging power (Watts)	4800
Steady-state dc operating point	
Average inductance current (A)	100
Maximum inductance current (A)	109.98
Minimum inductance (A)	90.02
Operating current (A)	100

As stated earlier in this section, the switching of both the boost and buck converters for the charging and discharging of the supercapacitor bank are controlled using voltage control mode. The technique consists of controlling the output voltage via a voltage loop. Figure 4.12 shows the voltage control mode for both the boost and the buck converters.

The control scheme consists of a negative feedback that sense the output voltage of the converter to determine the error voltage and control the duty cycle. This error voltage is used as input to the controller which is an inverting closed loop operational amplifier. The controller generates a control voltage applied to the non-inverting input of the comparator and a sawtooth voltage is applied to the inverting input of the comparator to determine the converter pulse wide modulation signal.

The closed loop parameters used for both the boost and buck converters are given in Table 4.12.

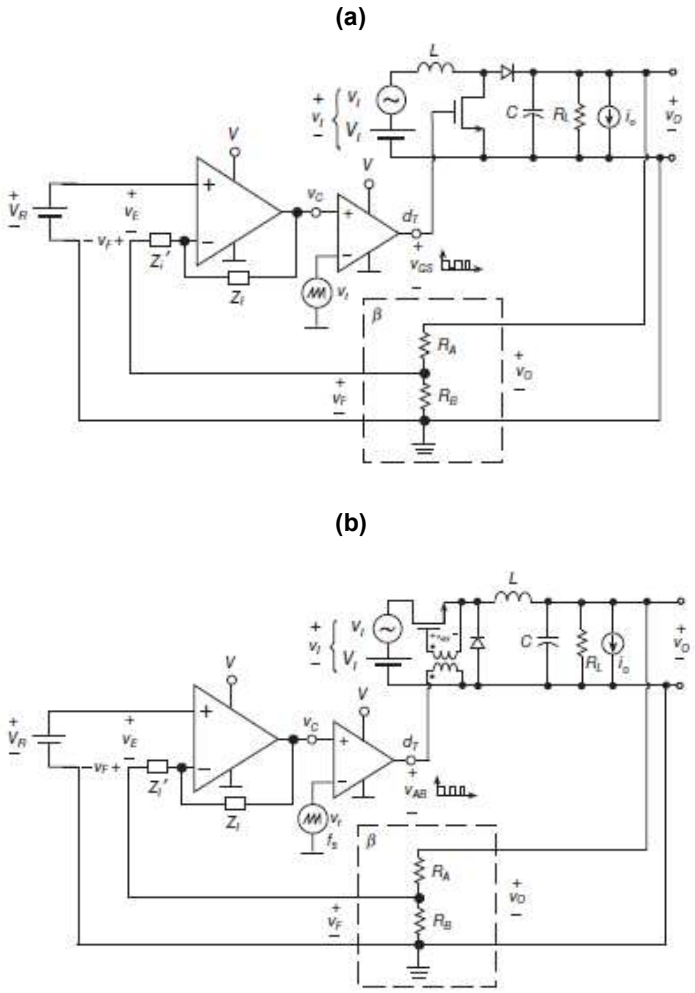

Figure 4. 12: (a) Boost converter and (b) buck converter with voltage mode control

Table 4. 12: Feedback loop design parameters

Boost converter closed loop control parameters	
Sensor type	Voltage divider
V_{ref}/V_o	0.00714286
PI controller	
k_p	40.1121 e-3
k_i	6.06742 e-3
Buck converter closed loop control parameters	
Sensor type	Voltage divider
V_{ref}/V_o	0.0520833
PI controller	
k_p	176.315 e-3
k_i	1.55988 e-3

The frequency response can be defined as a complex function expressed by Equation 4.55 as follows:

$$H(j\omega) = M(\omega)e^{j\varphi(\omega)} \tag{4.55}$$

where $M(\omega)$ and $\varphi(\omega)$ are the magnitude and the phase response respectively.

In this study, the bode graph is used to characterise the frequency response of the power electronics converters. It comprises two curves namely the gain versus the frequency and the phase versus the frequency.

The frequency response of the open-loop transfer functions of both the boost and buck converters are given in Figure 4.13 and Figure 4.14 respectively. Looking at the open-loop frequency response of the boost converter, it can be observed that for frequencies between 0 and 8 Hz (Figure 4.13(a)), the response of the converter decreases linearly to reach a gain of zero decibel. The amplitude of zero decibel implies that the output of the converter will have the same value as the input. The output will lag the input with a phase of about 80° (Figure 4.13(b)).

Similarly, for frequencies between 8 Hz and 54 Hz, the gain of the system will be in the range of 0 to – decibel with respect to the input voltage. For frequencies between 75 Hz and 1000 Hz, the gain of the system is in the range of 0.369 to -49 decibels, thus the output voltage of the converter is far smaller than 350 V, moreover, the output will lag the input with a phase angle between 50 to 71°.

Lastly, for frequency ranges between 1 kilo and 1 MHz, the gain of the system is between -49 and -53 decibels, thus the output voltage of the converter will be in close to zero volt.

(a)

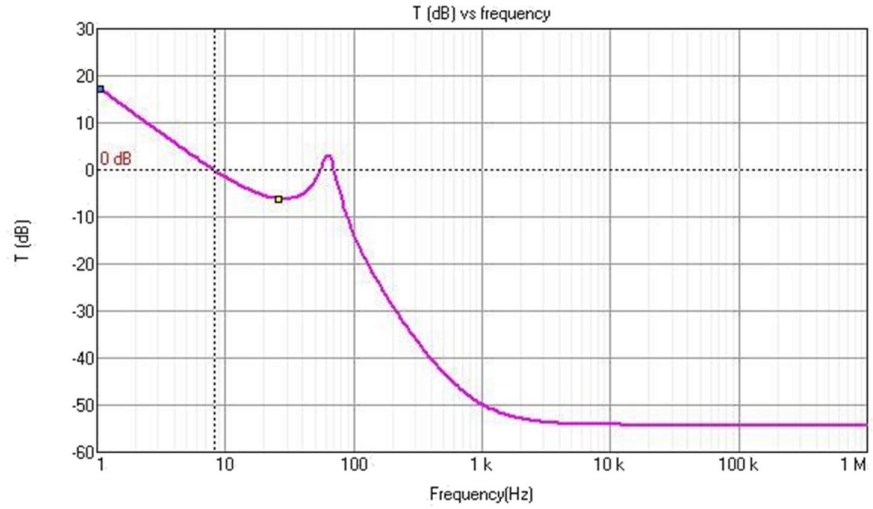

(b)

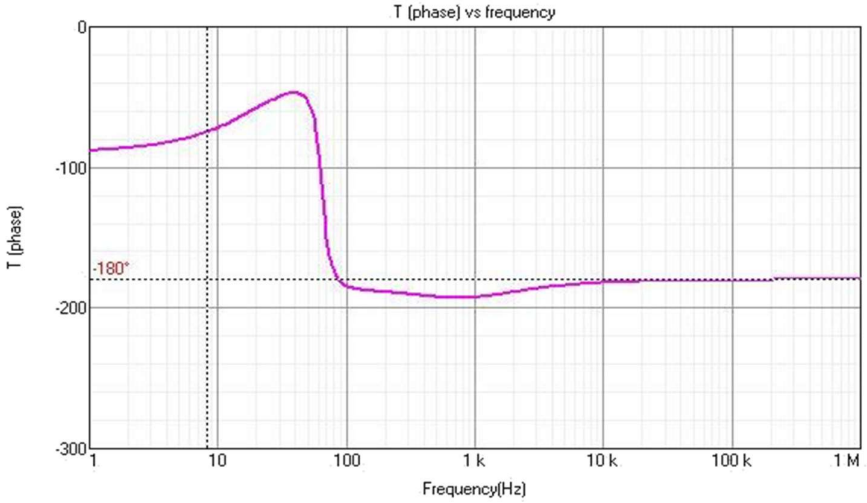

Figure 4. 13: (a) Boost converter open loop transfer function gain and (b) Phase

On the other hand, looking at the open loop frequency response of the buck converter, it can be observed that for frequencies between 0 and 241 Hz (Figure 4.14(a)), the response of the converter decreases linearly to reach a gain of zero decibel. The amplitude of zero decibel implies that the output of the converter will have the same value as the input. The output corresponding to these frequencies is such that it lags the input with a phase 77 to 90^{o} (Figure 4.14(b)).

Similarly, for frequencies between 241 Hz and 1 MHz, the gain of the system will be in the range of 0 to – 92 decibels with respect to the input voltage. Hence, the output voltage will be far lesser than 48 V and behind the input with a phase between 90 to 150^{o} (Figure 4.14(b)).

(a)

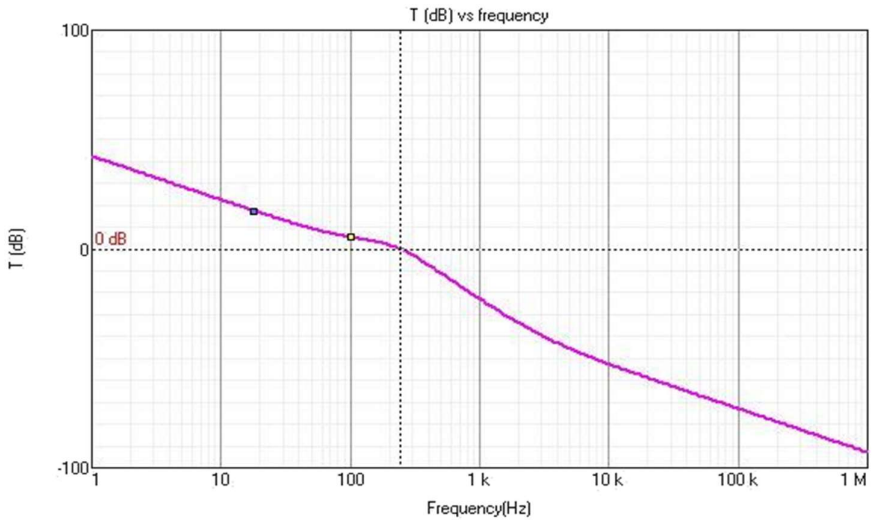

(b)

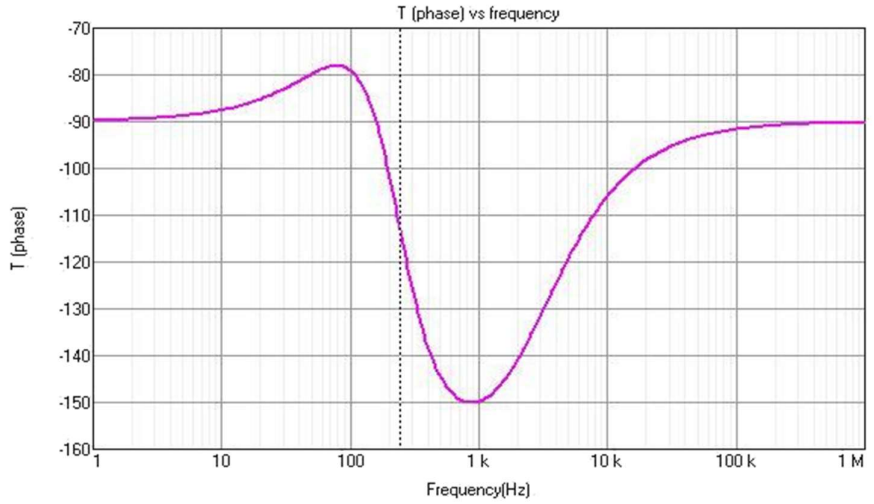

Figure 4. 14: (a) Buck converter open loop transfer function gain and (b) Phase

The purpose of a typical closed-loop control system is to ensure the closed-loop stability, fast rejection of disturbances, track rapidly the setpoint and its ability in processing changes and system's uncertainty. The frequency response of the closed-loop transfer functions of both the boost and buck converters are given in Figure 4.15 and Figure 4.16 respectively. Looking at the closed-loop frequency response of the boost converter, it can be noted that for frequencies between 0 and 75.24 Hz (Figure 4.15(a)), the response of the converter increases to reach a peak gain 77.39 decibel, however, from 75.25 Hz, this gain decreases to get to a stable value of 17.882 decibel for frequencies between 4.11 kHz to 1 MHz. The output voltage of the converter for this frequency range is about 350 V with a phase angle of -180° (Figure 4.15(b)).

(a)

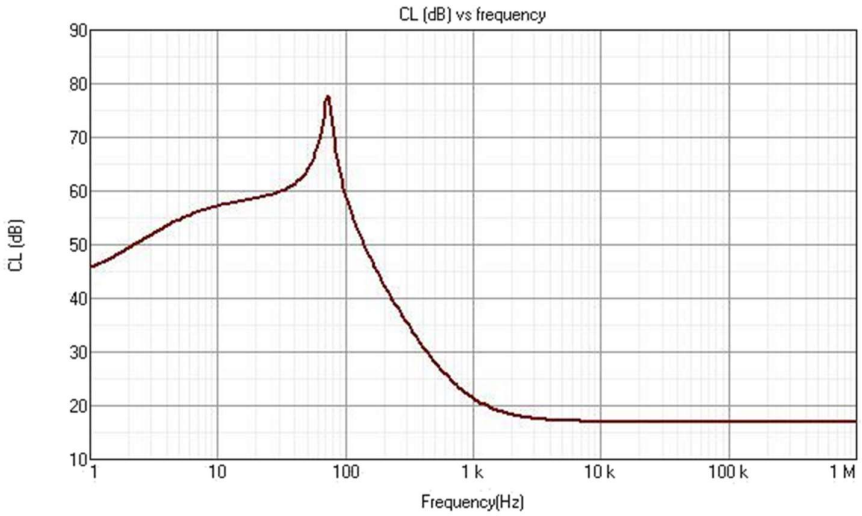

(b)

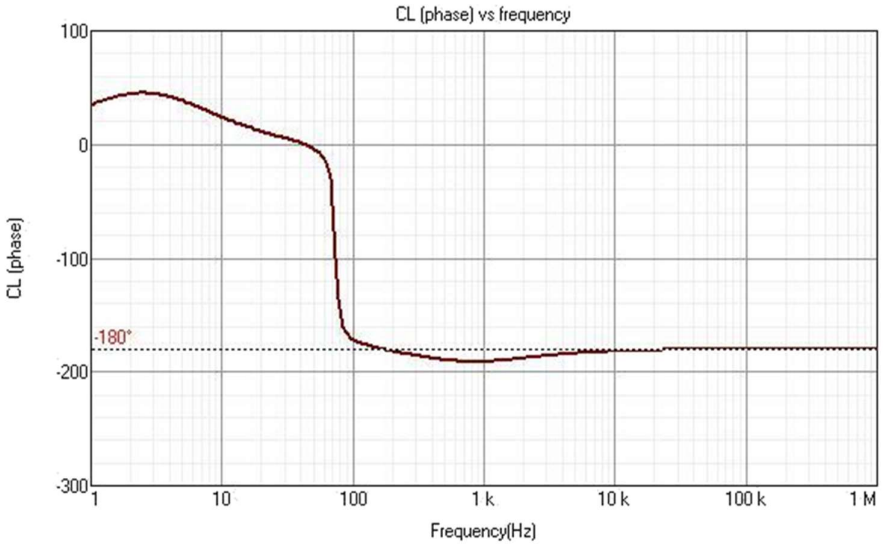

Figure 4. 15: (a) Boost converter closed loop transfer function gain and (b) Phase

Figure 4.16 shows the frequency response of the buck converter, for frequencies between 0 and 279 Hz (Figure 4.16(a)), the response of the converter has a gain in the range of 26 decibels to 41 decibels, while the phase varies between 3^{o} and -55^{o} (Figure 4.16(b)). The response of the converter gets into the stable region in the frequency range between 279 Hz and 1 MHz where the gain decreases drastically to -50 decibels for phases ranging between -55^{o} and -89^{o}.

(a)

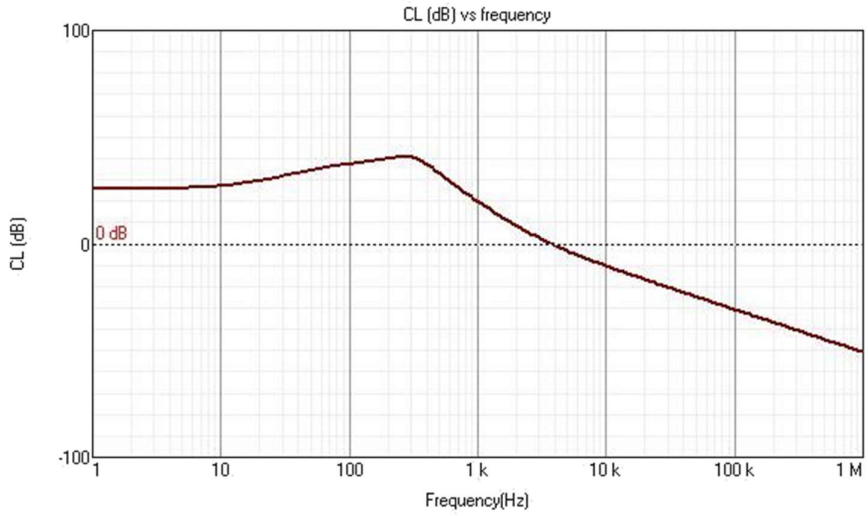

(b)

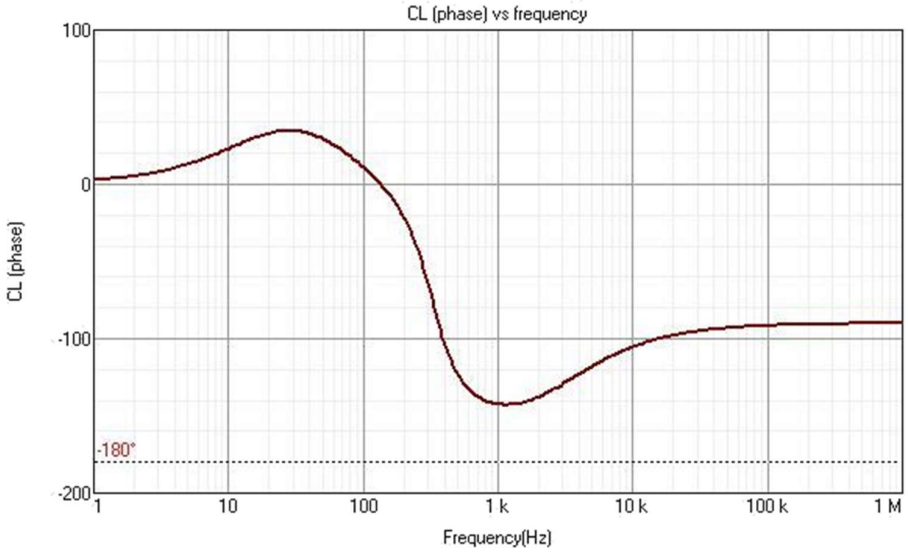

Figure 4. 16: (a) Buck converter closed loop transfer function frequency response and (b) Phase

4.7.2 DC to AC converters

A typical three phase inverter shown in Figure 4.17 consists of six switches, with the switching of which depending on the modulation scheme. The inverter has eight switch states given in Table 4.13. Both switches in the same leg cannot be turned ON at the same time, as it would short the input voltage violating the Kirchhoff Voltage Law. Hence, the nature of the two switches in the same leg is complementary.

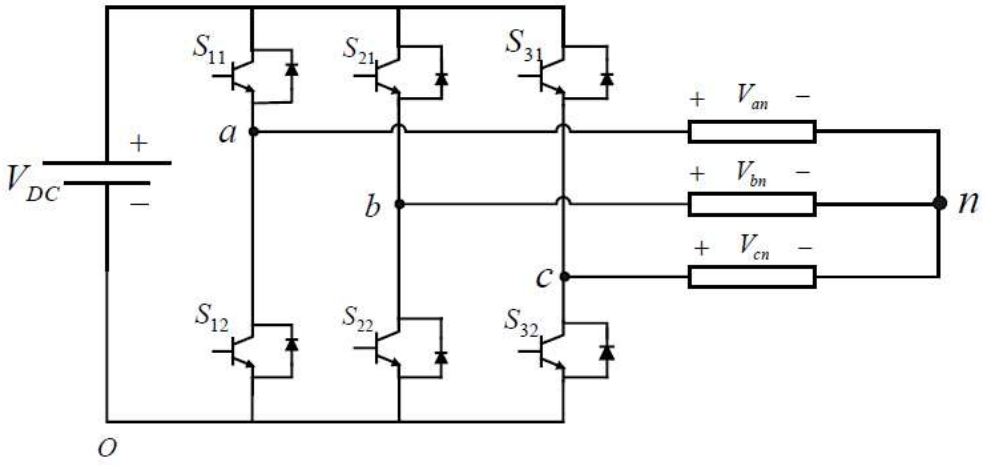

Figure 4.17: Three-phase full bridge inverter (Elbaset et al., 2017)

Table 4. 13: Switching states in a three-phase inverter

S_{11}	S_{12}	S_{31}	V_{ab}	V_{bc}	V_{ca}
0	0	0	0	0	0
0	0	1	0	$-V_{DC}$	V_{DC}
0	1	0	$-V_{DC}$	V_{DC}	0
0	1	1	$-V_{DC}$	0	$-V_{DC}$
1	0	0	$-V_{DC}$	0	$-V_{DC}$
1	0	1	$-V_{DC}$	$-V_{DC}$	0
1	1	0	0	V_{DC}	$-V_{DC}$
1	1	1	0	0	0

The DC link capacitors at the input of the inverter is determined using Equation 4.56 given as:

$$C_{DC} = \frac{P}{2\pi f V_{DC} \Delta V_{DC}} \tag{4.56}$$

Where P is the power from the renewable generator, f is the inverter frequency, V_{DC} is the DC voltage and ΔV_{DC} is the capacitor DC voltage ripple.

The role of this capacitor is to store energy during excess power periods and supplies it back during insufficient generation to maintain the capacitor's power flow.

The harmonics generated by the inverter are reduced using a LC filter shown in Figure 4.18.

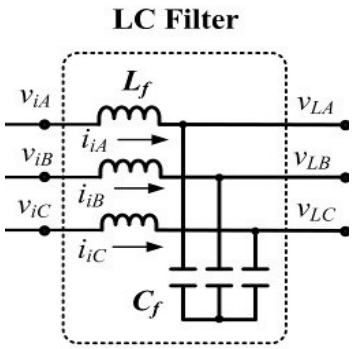

Figure 4. 18: Three-phase LC filter

The choice of the capacitor C_f depends on the capacitor reactive power at fundamental frequency and the inductance. The efficiency of the inverter may be reduced in case of a high value of capacitance, while a reduced capacitance may increase the inductance. In most cases, the value of the reactive power of capacitor is selected as less than 15% of the inverter rated power. In this study, the capacitor is considered as 10% of the inverter rated power. The capacitor C_f is selected based on Equation 4.57 given as:

$$C_f = \frac{10\,\% \times P}{2\pi f \times V^2} \tag{4.57}$$

where P is the power from the renewable generator, f is the frequency and V is the line to line AC voltage.

On the other hand, the choice of the inductance L_f is determined by considering the resonance frequency of filter which is often set to be greater than or equal to the 10th of the AC side frequency to avoid resonance. The selection of L_f is defined by Equation 4.58 which is expressed as follows:

$$L_f \leq \frac{1}{100 \times (2\pi f)^2 \times C_f} \tag{4.58}$$

A typical control scheme of a voltage source inverter is shown in Figure 4.19. A phase locked Loop (PLL) is used to maintain proper frequency and phase angle of the voltage. The control scheme consists of voltage and current regulators to provide good power factor. The voltage regulator reduces changes in the DC voltage through a PI controller and generates a current I_d^* by comparing the DC voltage V_{dc} and the DC reference voltage V_{dc}^*. The current regulator comprises PI controllers for the I_d and I_q currents. The ΔI_d signal is processed in the PI controller to reduce the error and generate an

adding signal with V_d for comparison with ωL to obtain the signal V_d^*. On the other hand, the current I_q^* is set to zero for the inverter power factor improvement.

ΔI_q is processed through the PI controller to generate an adding signal with V_q and ωL to obtain the signal V_q^*. The $dq0$ frame is converted back into three-phase (abc) for the PWM generation.

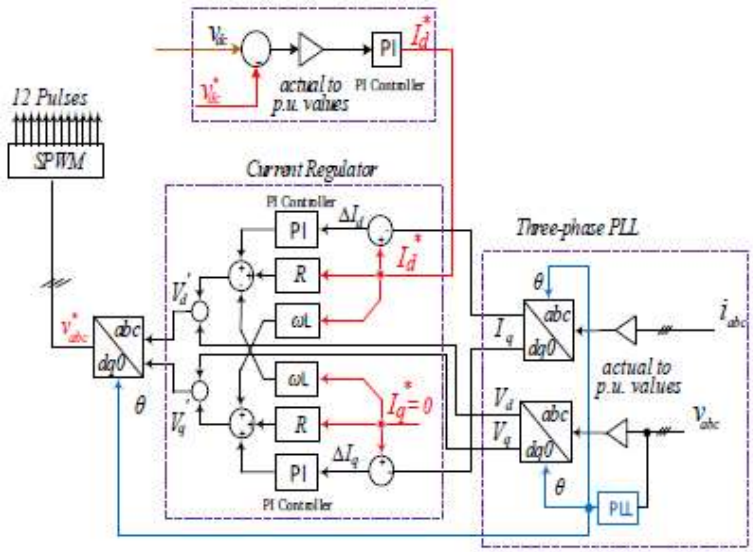

Figure 4. 19: Voltage source inverter control scheme

The PI controller equation is given as:

$$R(s) = k_p + \frac{k_i}{s} = k_p\left(\frac{1 + T_i s}{T_i s}\right) \tag{4.59}$$

where k_p is the proportional gain, k_i is the integral gain and $T_i = {k_p}/{k_i}$ is the integral time constant.

Teodorescu et al gives the value of k_p, k_p and T_i as expressed in Equation 4.60 (Teodorescu et al., 2011):

$$k_p = 0.12.\frac{C}{T_s}$$
$$k_i = \frac{k_p}{T_i} \quad (4.60)$$
$$T_i = 17.T_s$$

where C is the DC link capacitor and T_s is the sampling time defined as:

$$f_s = \frac{f_c}{0.1} \quad (4.61)$$

where f_c is the cross-over frequency obtained from the frequency response of the controller.

Parameters used in the AC side are given in table 4.14

Table 4. 14: AC side parameters

AC side parameters	
DC link voltage	350 V
DC link capacitor	2600 µF
AC voltage	
Frequency	50 Hz
Switching frequency	5 kHz
LC filter	
C_f	16e-6 µF
L_f	6340 µH
PI controller	
k_p	15.6
k_i	45882.4
T_i	0.00034

4.8 Summary

This chapter dealt with the mathematical modelling of individual components which are part of the system. These components included the photovoltaic array, a discrete reversible fuel cell, a hydrogen tank, the supercapacitor bank, and the power electronics converters such as DC to DC boost converter, DC to DC buck converter and voltage source inverter. The control schemes of power electronics converters devices mentioned above were also presented.

CHAPTER FIVE
DEVELOPMENT OF ENERGY MANAGEMENT ALGORITHM

5.1 Introduction

Conventional power systems are organised to operate as single direction power flow systems with unified generation sources, long transmission lines and distribution networks. These power systems are generally based on generators using fossil fuels as the primary energy sources. However, the negative environmental effects associated with the use of fossil fuels and the necessity for improving the reliability of the power systems have led to the use of renewable generators. Thus, several distributed generation units including renewable generators are now integral parts of the power systems making the overall system more complex sets of interacting new generation technologies aiming to improve the generation, increase the system efficiency and demand side flexibility.

A unique control and management strategy would not have the capacity to decide on the development and operation of these complex power systems, the sets of functions for operation and development of such power systems have been set up under hierarchical dependence (Vandoorn et al., 2013; Guerrero et al., 2013; Guerrero et al., 2011). The hierarchical control strategies for the operation of renewable power systems are shown in Figure 5.1 and consists of three levels of control namely energy management, power management and local controllers. The energy management is related to decision-making for the operation of renewable power systems with activity times of hours to days. At this level, the operation of the power systems is planned in an optimal manner considering the available renewable resources, the operational cost of the units, power generation and utilisation and the best time to complete actions. Therefore, energy management systems are predominantly centred around economics based on factors such as fuel costs, capital costs, support costs, mission profiles, lifetimes, and so forth (Kanchev et al., 2011). In addition, the structure of energy management systems should look at the variability of renewable resources, the unpredictability of the load, generation capacity, and power exchange with the electric network that may cause energy unbalances in case of grid-connected systems (Luta & Raji, 2016; Doudou N. Luta & Raji, 2019b).

On the other hand, power management is required for appropriate operation of a renewable power system by acting on the prompt operational conditions toward certain ideal parameters such as voltage, current, power, and frequency (Nejabatkhah & Li,

2015). The hierarchical control of power management involves four control stages namely the inner control loops, primary control, secondary control and tertiary control.

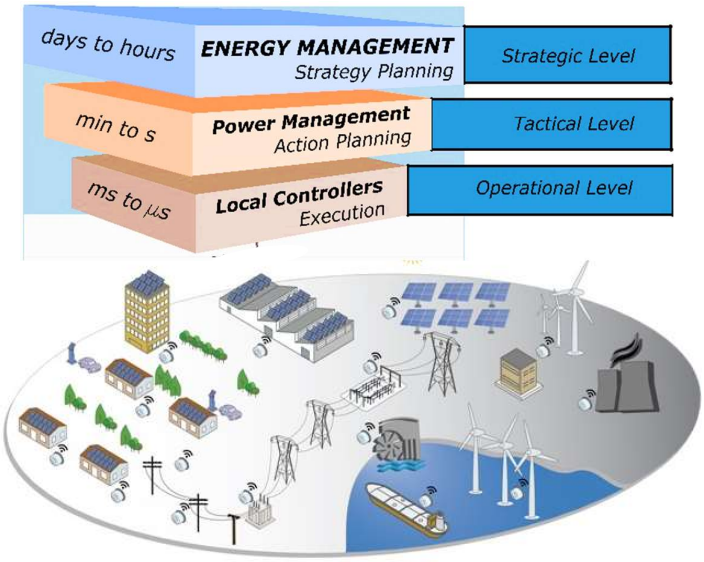

Figure 5. 1 Management and Control of Renewable Power Systems

The inner control loops can regulate the voltage and current of every module, while the primary control modifies the frequency and voltage references provided to the inner control loops. In the same vein, the secondary control manages the control of power quality, and voltage unbalance and compensation of harmonics. The tertiary control directs the power flow between the electric network and the renewable power systems at the point of common coupling (PCC) for grid connected systems or between areas inside renewable power systems (Guerrero et al., 2011). This control level is related to supervisory control and acquisition systems.

5.2 Concepts of energy management systems

An energy management system is defined by IEC 61970 as a computer unit consisting of a software that provides key support services and applications offering required functionalities for viable operation of electrical generation and transmission systems to ensure satisfactory security of energy supply at less cost (Byeon et al., 2013). Therefore, in the context of renewable power systems, the energy management systems serve to operate, control and coordinate distributed generations, loads, power electronics converters, energy storage units and grid parts in case of grid-connected renewable power systems to provide sustainable, reliable and clean energy in optimal manner (Malysz et al., 2014; Katiraei et al., 2008). For grid connected renewable power systems, the energy management systems can operate to enhance self-consumption

or take part in the electricity market, whereas, for 100% renewable power systems, the energy management systems can execute tasks such as economic dispatch and load control.

5.3 Problem formulation

The proposed energy management of the system is performed by deciding on the operating priority of each generator and the load conditions. For 100 % renewable power systems, renewable resource availability is an important parameter. In the development of the energy management algorithm, the following limits for the operating parameters are considered:

- Minimum state of charge of the supercapacitor bank ($SOC_{SP_{Min}}$): 20%
- Maximum state of charge of the supercapacitor bank ($SOC_{SP_{Max}}$): 95%
- Minimum allowable power of the electrolyser:
- Maximum allowable power of the electrolyser: 15 kW
- Minimum volume of hydrogen in the tank (V_{H_2Min}): 0 cubic metre
- Maximum volume of hydrogen in the tank (V_{H_2Max}): 83 cubic metres

The equation governing the energy management system can be written as:

$$P_{PV} + P_{FC} + P_{SP} = P_L + P_{LSP} + P_{LEL} \tag{5.1}$$

where P_{PV}, P_{FC}, P_{SP}, P_L, P_{LSP} and P_{LEL} are the power generated from the photovoltaic system, power output of the fuel cell, charging power of the supercapacitor, power demand of the load, discharging power of the supercapacitor and the power consumed by the electrolyser respectively.

The maximum charging power P_{SPMax} and discharging power P_{LSPMax} of the supercapacitor bank are defined by Equation 5.2 and Equation 5.3 respectively as follows:

$$P_{SP} \leq P_{SPMax} \tag{5.2}$$

$$P_{LSP} \leq P_{LSPMax} \tag{5.3}$$

On the other hand, the state of charge of the supercapacitor is limited by Equation 5.4 given as:

$$SOC_{SP_{Min}} \leq SOC_{SP} \leq SOC_{SP_{Max}} \tag{5.4}$$

Similarly, the volume of hydrogen stored in the tank is defined based on two limits as expressed in Equation 5.5:

$$V_{H_2Min} \leq V_{H_2} \leq V_{H_2Max} \tag{5.5}$$

The maximum power to operate the electrolyser is required to be less or equal to a set limit defined by Equation 5.6 as:

$$P_{LEL} \leq P_{LELMax} \tag{5.6}$$

In the same vein, the net power of the system is given by Equation 5.7 as the difference between the power generated and the overall load.

$$P_{Net} = P_{PV} - P_L \tag{5.7}$$

where the switching operations considered in the energy management algorithm are as follows:

If the net power of the system is less than zero, depending on the stored hydrogen into the tank, three scenarios can occur:

- If the photovoltaic power cannot fully meet the power request by the load, the fuel cell provides the rest of the power. Therefore, the fuel cell is used during low irradiance time. Thus, the power balance equation is given as:

$$P_{PV} + P_{FC} = P_L \tag{5.8}$$

- If the stored hydrogen into the tank falls beneath its minimum value, the supercapacitor begins discharging to keep up the power supply to the load until the condition of the state of charge of supercapacitor becomes less than its minimum value. Therefore, the supercapacitor serves to supply shorter and strong peak power demands that may occur in the system. The power balance in this case is expressed by Equation 5.9 as:

$$P_{PV} + P_{SC} = P_L \tag{5.9}$$

Figure 5.2 shows the energy management algorithm developed based on equations 5.1 to 5.9, while Figure 5.3 depicts the Simulink model of the system.

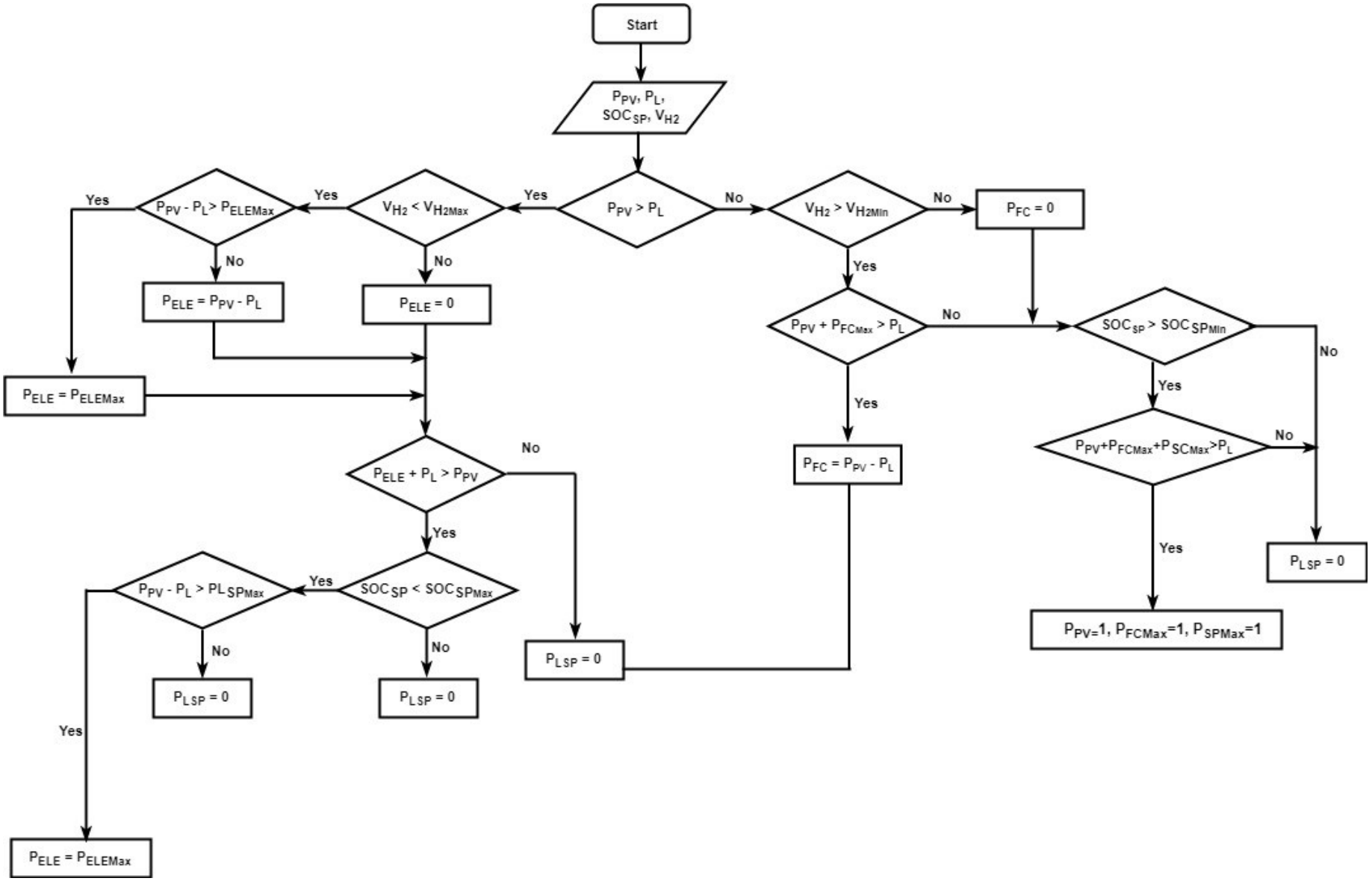
Start
P_{PV}, P_L, SOC_{SP}, V_{H2}
$P_{PV} > P_L$
Yes
$V_{H2} < V_{H2Max}$
Yes
$P_{PV} - P_L > P_{ELEMax}$
Yes
$P_{ELE} = P_{ELEMax}$
No
$P_{ELE} = P_{PV} - P_L$
No
$P_{ELE} = 0$
No
$V_{H2} > V_{H2Min}$
No
$P_{FC} = 0$
Yes
$P_{PV} + P_{FCMax} > P_L$
No
$SOC_{SP} > SOC_{SPMin}$
No
$P_{LSP} = 0$
Yes
$P_{PV+}P_{FCMax}+P_{SCMax}>P_L$
No
$P_{LSP} = 0$
Yes
$P_{PV=}1$, $P_{FCMax}=1$, $P_{SPMax}=1$
Yes
$P_{FC} = P_{PV} - P_L$
$P_{ELE} + P_L > P_{PV}$
No
$P_{LSP} = 0$
Yes
$SOC_{SP} < SOC_{SPMax}$
Yes
$P_{PV} - P_L > PL_{SPMax}$
Yes
$P_{ELE} = P_{ELEMax}$
No
$P_{LSP} = 0$
No
$P_{LSP} = 0$

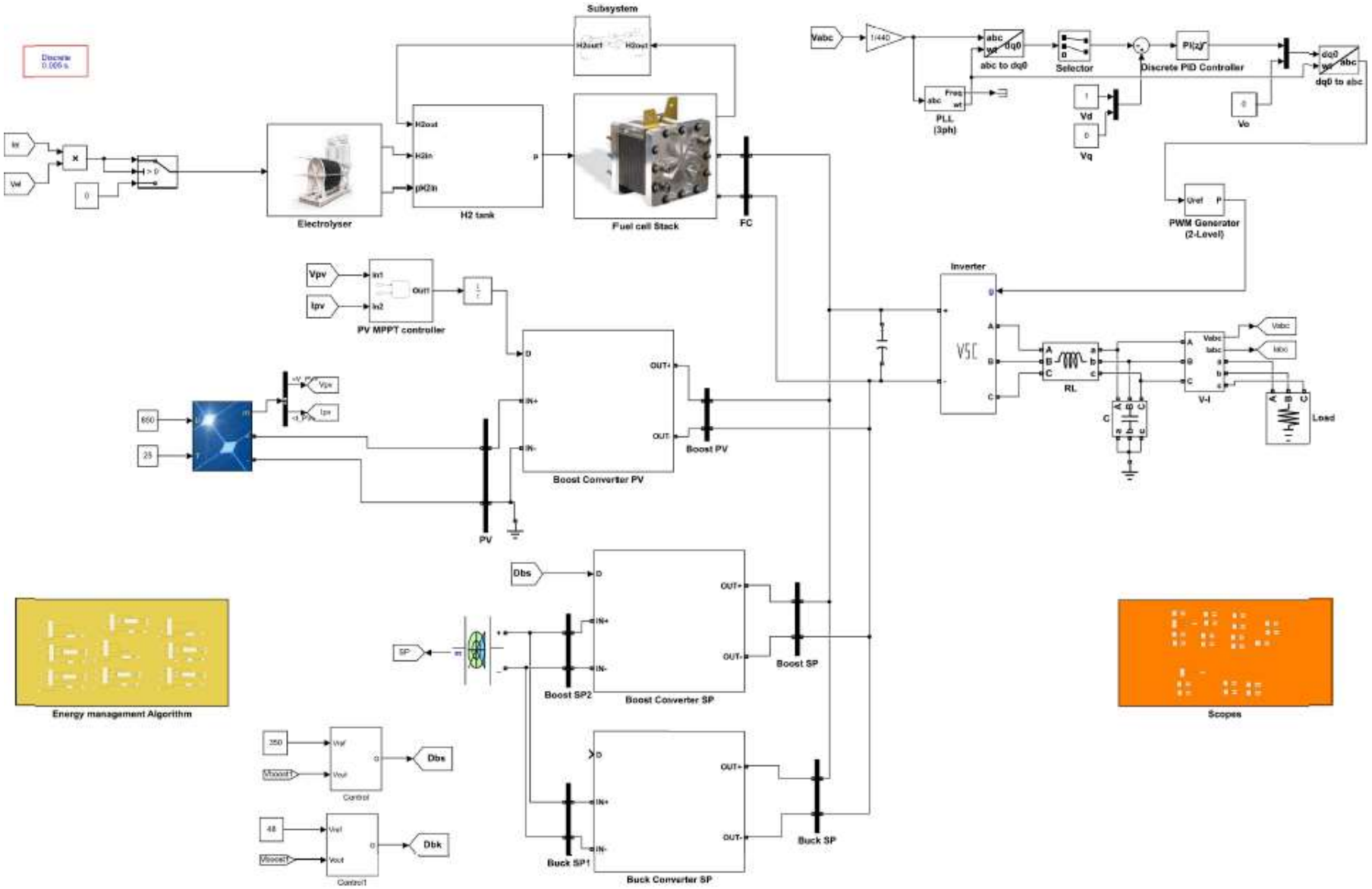

Figure 5. 3: Simulink model of the system

5.4 Simulation results and discussion

The system in Figure 5.3 was simulated using Matlab/Simulink environment, based on the energy management algorithm proposed in Figure 5.2. A DC load of 3 kW peak value as given in section 3.2 is connected to the DC side of the 100 % renewable power system. This DC load is considered to vary randomly and may become greater than 3 kW depending upon the demand conditions. An AC load of 6.99 kW is as well connected to the AC side through a three-phase inverter. Due to the high-performance computing system requirement, a simulation was carried out only for a duration of 500 seconds and different scenarios are presented. The reversible fuel cell used in this study is assumed to be on a discrete reversible type, furthermore, It was assumed that the initial level of hydrogen in the tank is 50 % of the tank total volume.

5.4.1 Scenario 1

In the first scenario, the photovoltaic system generates around 28.9 kW to meet the load demand, produce hydrogen and charge the supercapacitor. Figure 5.4 shows the voltage, current and power output of the photovoltaic system. It is connected to the DC link capacitor through a DC/DC boost converter that converts the 294 V from the photovoltaic array to 350 V, while the electrolyser received its power from the PV 294 volts bus in case there is any excess of power. The switching of the DC/DC boost converter on the photovoltaic side is controlled using a pulse-width modulation (PWM) generated from a maximum power point tracking (MPPT) algorithm based on incremental conductance technique. Similarly, the fuel cell is connected to a DC/DC boost converter that the 250 V from the fuel cell to 350 V.

Like for the photovoltaic array, the switch DC/DC boost converter on the fuel cell side is also controlled by a PWM produced by an incremental conductance MPPT algorithm. On the other hand, the supercapacitor is connected to the DC link capacitor through a DC/DC boost converter as well as a DC/DC buck converter. The DC/DC boost converter boosts the input voltage of the supercapacitor to accommodate the 350 V of the DC link for the discharging of the supercapacitor, whereas the DC/DC buck converter step downs the 350 V of the DC link capacitor to charge the supercapacitor. The PWM to drive the supercapacitor DC/DC boost converter is generated from a feedback control loop using a reference voltage of 350 V, in the same vein, the PWM driving the supercapacitor buck converter is produced from feedback control loop using 48 V as a reference voltage.

The 28.9 kW generated from the photovoltaic plant corresponds to the irradiance of 850 W/m^2 (Figure 5.4 (c)). Under the normal test conditions which correspond to an

irradiance of 1000 W/m^2 and a temperature of 25^o. It was considered that the solar radiation remains unchanged, thus no power fluctuation is observed in the plant.

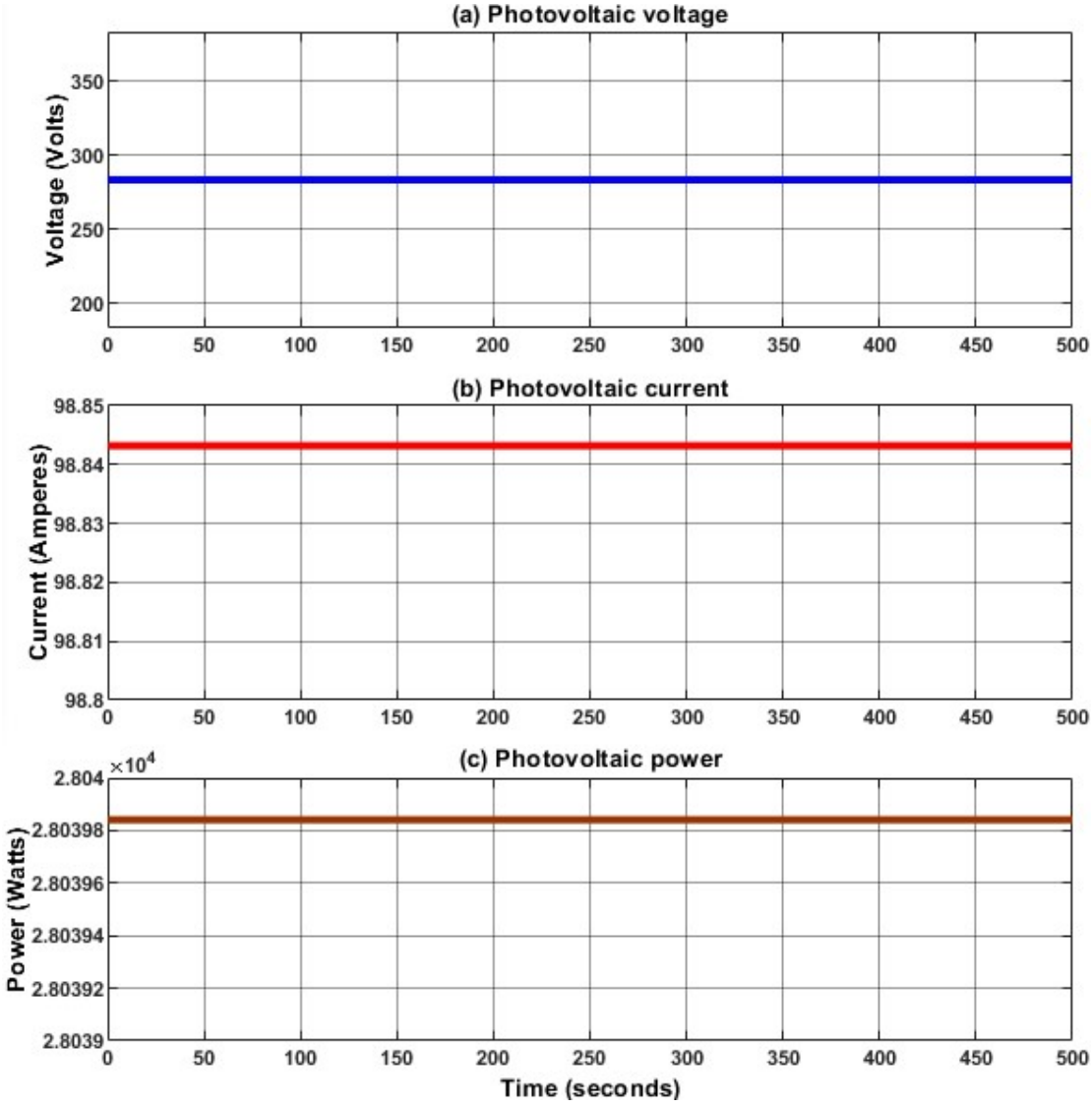

Figure 5. 4: Photovoltaic (a) voltage, (b) current and (c) power

Under a constant solar radiation of 850 W/m^2, the photovoltaic array is likely to generate about 693.6 kWh per day to meet the load demand, produce hydrogen and charge the supercapacitor. Based on the energy management algorithm, this energy is split to supply the load, produce hydrogen through the electrolyser depending on the quantity of hydrogen stored and charge the supercapacitor.

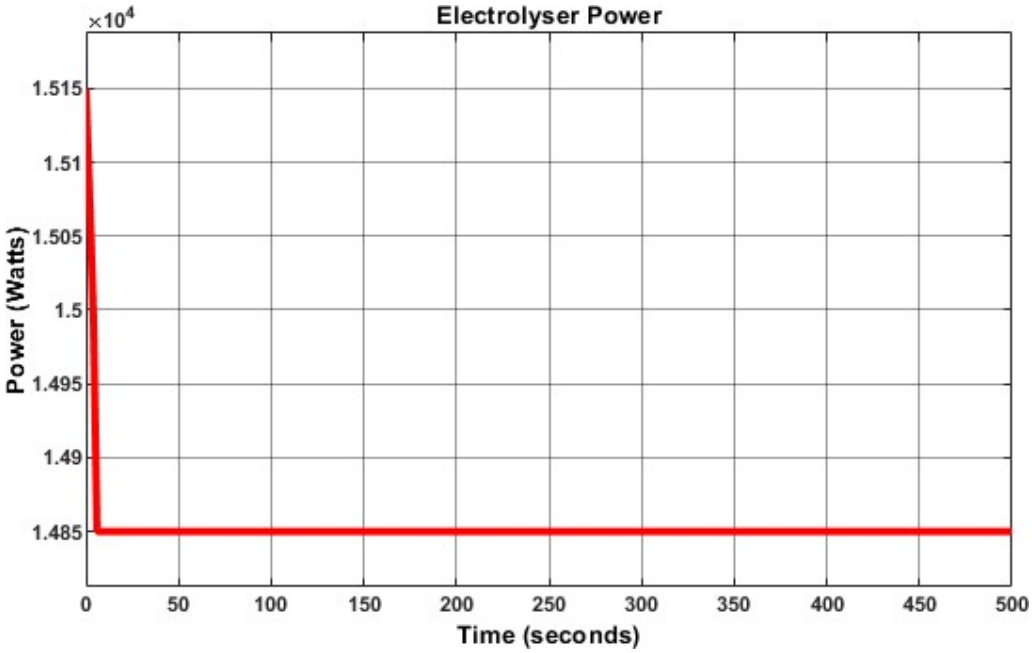

Figure 5. 5: Input power to the electrolyser

The 15 kW of the generated power is used to power the electrolyser as shown in Figure 5.6, this electrolyser is connected to the photovoltaic array via a 290 V DC bus.

The hydrogen produced in the electrolyser and that consumed in the fuel cell are depicted in Figure 5.6 (a) and Figure 5.6 (b) respectively. Since the power generated by the photovoltaic system can handle the load demand, the energy storage is unused, thus no hydrogen is consumed in the fuel cell. On the other hand, the hydrogen is produced in the electrolyser at a constant flow rate of 0.01813 mol per seconds. Bearing in mind that a mole of hydrogen molecule is comparable to 22.4 litres hydrogen at standard conditions for temperature and pressure (STP) described as a temperature equal to 273.15^{o}K and an absolute pressure of 10^5 Pascals, the total number of litres of hydrogen produced per second in the electrolyser is about 0.4144. Regarding the weight, this quantity of hydrogen corresponds to approximately 0.037 g, as the mass of 22.4 litres of hydrogen molecule is around 2 g.

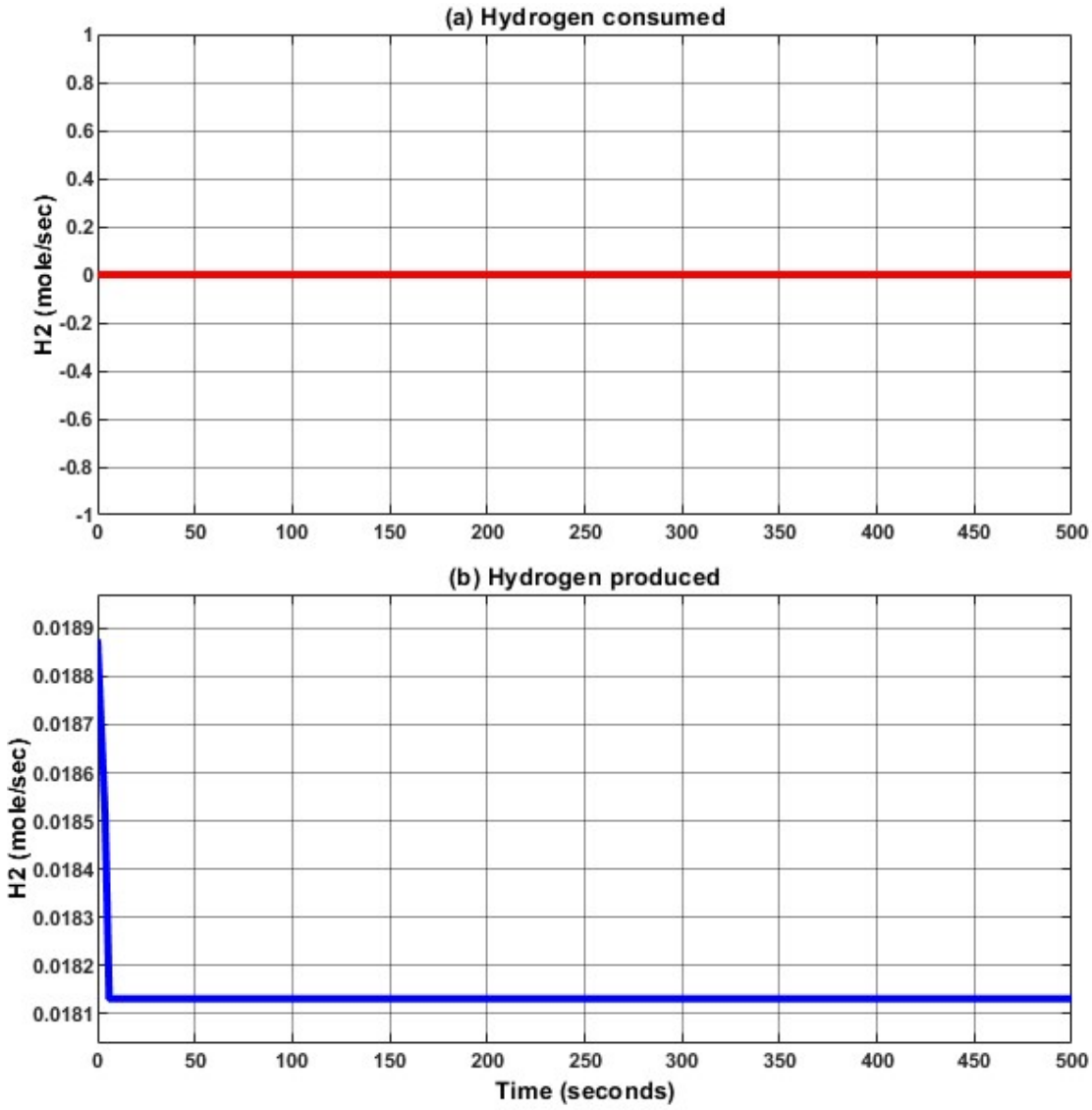

Figure 5. 6: (a) Hydrogen consumed in the fuel (b) hydrogen produced in the electrolyser

On the other hand, the characteristics of the supercapacitor such as current, voltage and state of charge are depicted in Figure 5.7, it can be noted that the current in the supercapacitor has a negative value of 50 A, this sign expresses the charging state of the supercapacitor as the supercapacitor is being charged from the photovoltaic array. The corresponding charging voltage is 48 V, which is consistent with the supercapacitor normal voltage. The initial state of charge of the supercapacitor is around 51.5 % and its final value is slightly above 54 %. No random change of the load is observed in the load profile and since the photovoltaic array generates electricity to meet the load requirement, the supercapacitor is operating in charging mode.

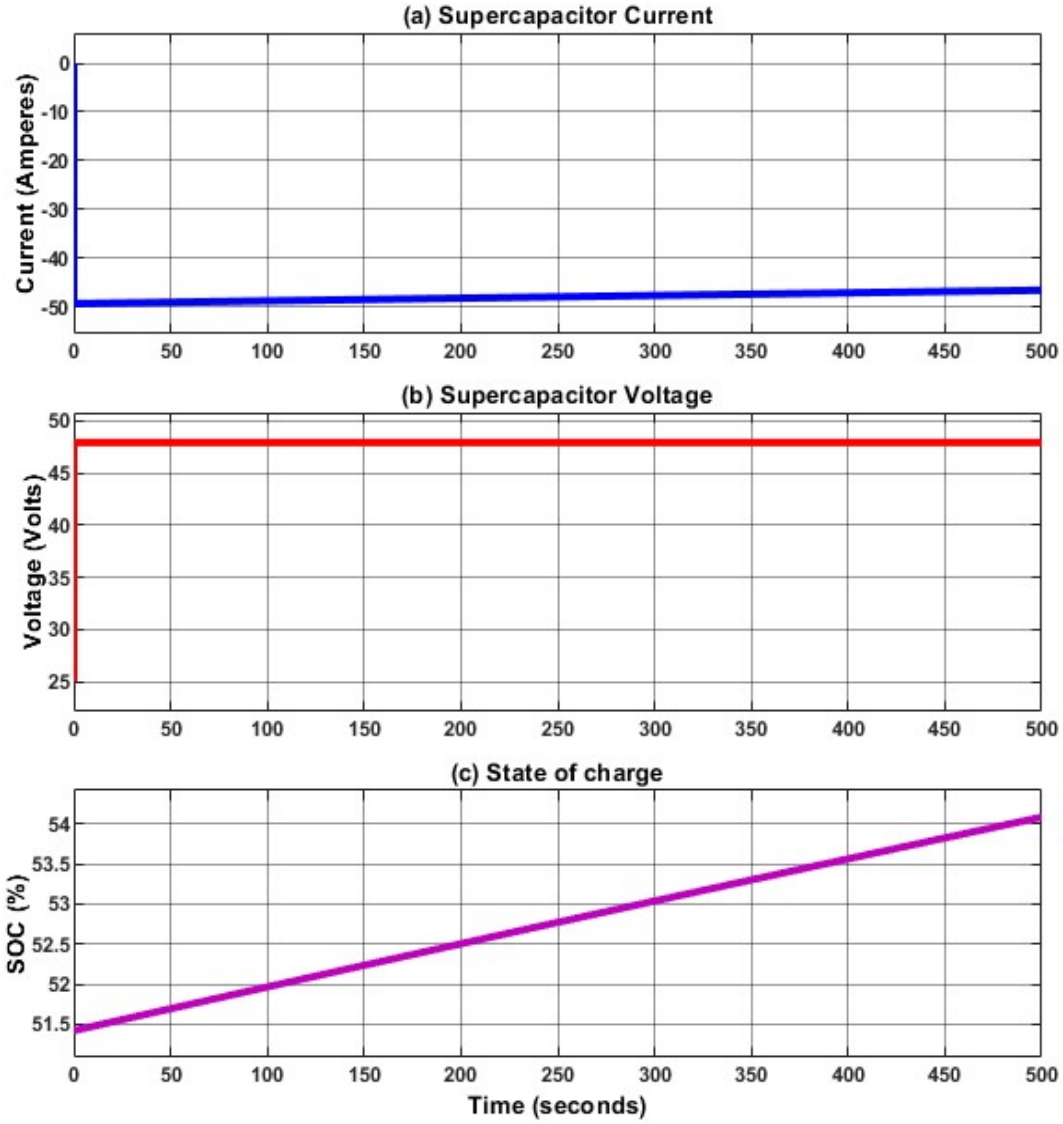

Figure 5. 7: Supercapacitor (a) current, (b) voltage and (c) state of charge

The characteristics of the DC load which include the current, voltage and power are depicted in Figure 5.8. The current feeding the load is about 11.45 A (Figure 5.8 (c)), thus the power required to supply the load is 3000 W (see Figure 5.8 (d)). The voltage at the load terminal is depicted in Figure 5.8(b), this voltage remains 348 V. In this scenario, this load is kept constant.

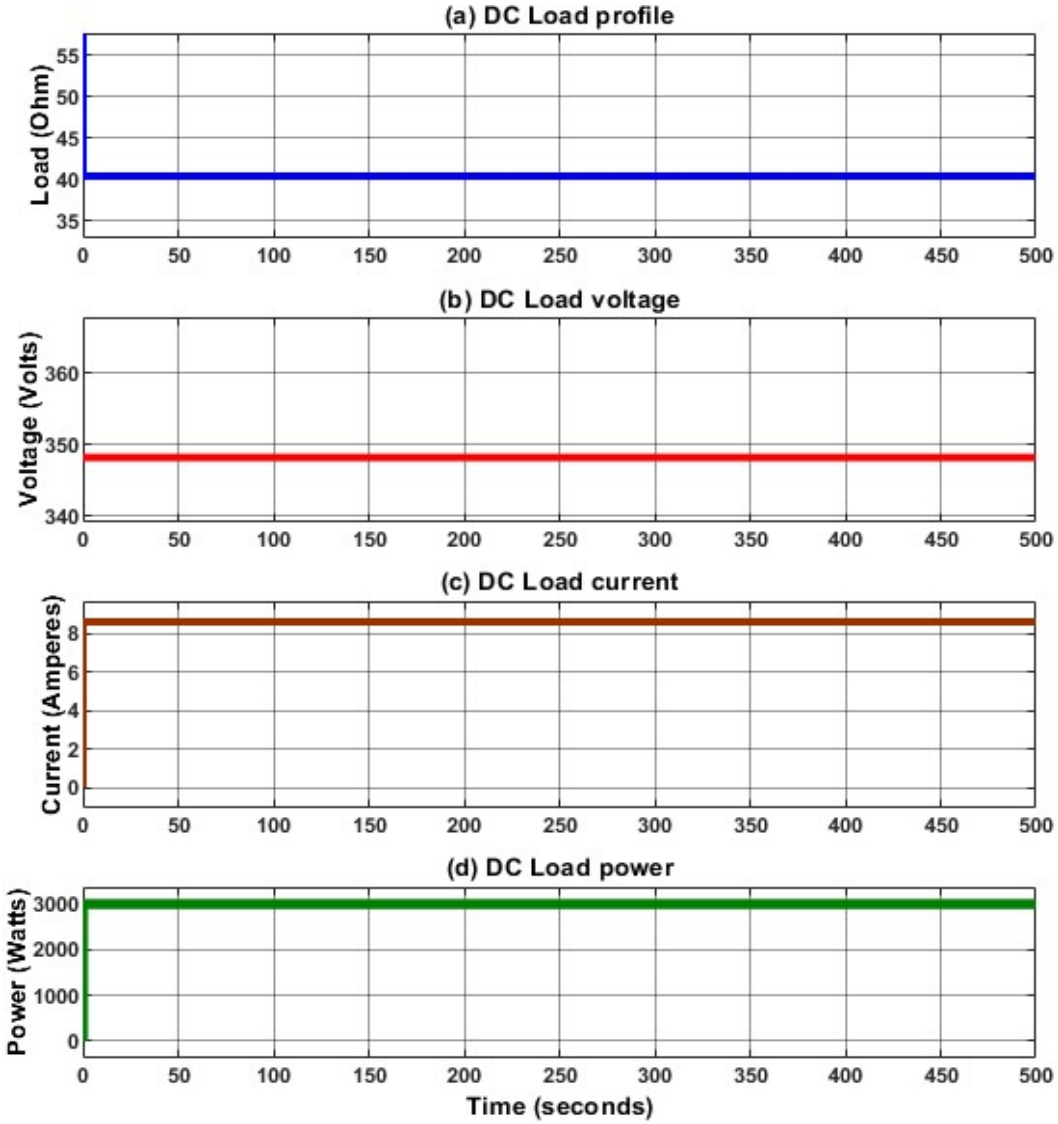

Figure 5. 8: (a) Load profile, (b) load current, (c) load voltage and (d) load power

5.4.2 Scenario 2

In the second scenario, the solar radiation which is one of the inputs to the photovoltaic is decreased to 344 W/m^2, then slightly increased to 359 W/m^2 and goes down again around 348 W/m^2, causing the power generated from the photovoltaic system to fluctuate around 12 kW. 10 kW of this power serves to meet both the DC and AC load demands and the remaining portion is used to produce hydrogen and charge the supercapacitor, however, based on the energy management algorithm, the priority in this case is given to the electrolyser. Therefore, the remaining power is used to produce hydrogen.

The characteristics of the photovoltaic array in this scenario is given in Figure 5.9, consisting of the voltage, current and power generated.

The voltage profile of the photovoltaic array is such that, initially it sat around 186 Volts, then decreases moderately to 183 V for a solar radiation equivalent to 344 W/m^2. With a rising of the solar radiation to 359 W/m^2, this output voltage stands around 187 Volts, to finally drop to around 184 V for a corresponding solar radiation equal to 348 W/m^2 (Figure 5.9 (a)).

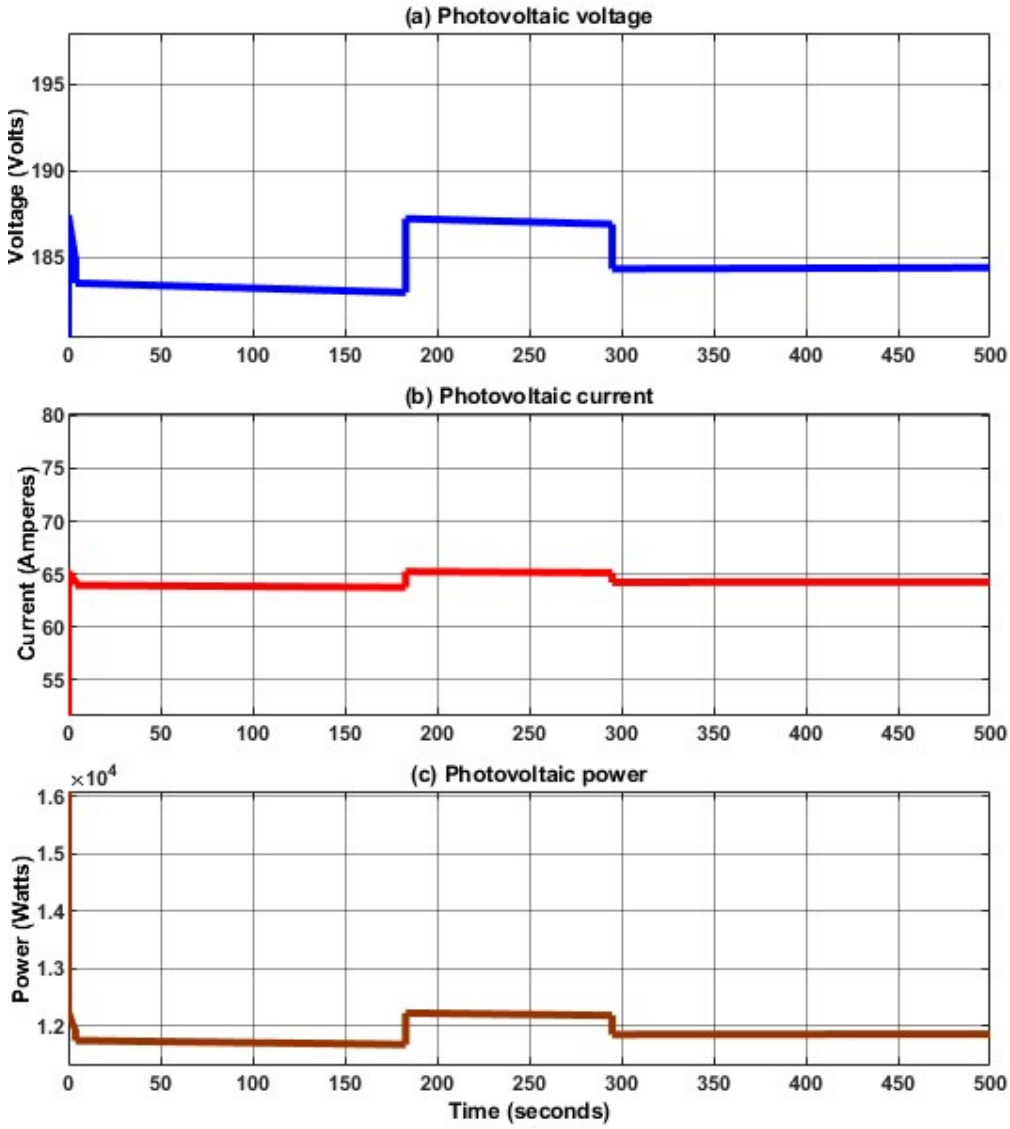

Figure 5. 9: Photovoltaic (a) voltage, (b) current and (c) power

Similarly, the current profile of the photovoltaic array originally sat around 63 to 65 A for a solar radiation equal to 344 W/m^2. With a rising of the solar radiation to 359 W/m^2, the resulting current still stands around 65 Amperes, to finally decrease to 64 Amperes when the solar radiation is 348 Watts/m^2 (Figure 5.9 (b)).

Therefore, depending on the value of the voltage and current, the power generated from the photovoltaic system may vary between 11.7 to 12.2 kW. Thus, the resulting energy will range between 280.8 to 292.8 kW per day.

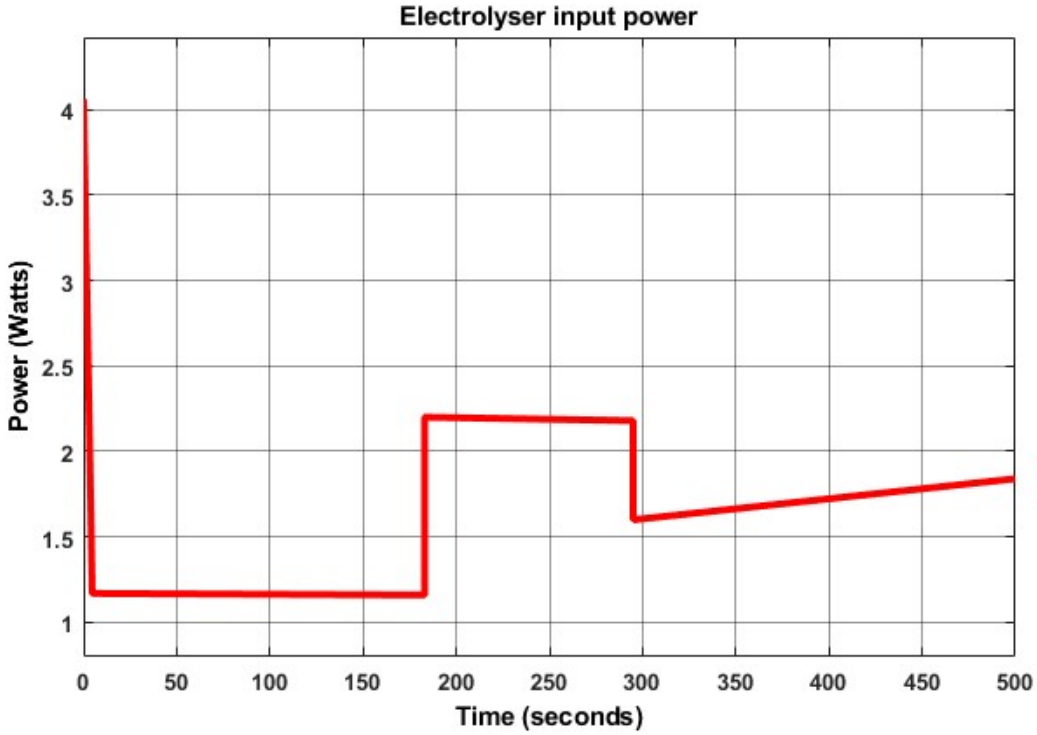

Figure 5. 10: Electrolyser input power

The electrolyser is supplied from 2 kW excess power generated from the photovoltaic array as shown in Figure 5.10. The hydrogen produced in the electrolyser as well as that consumed in the fuel cell are shown in Figures 5.11 (a) and 5.11 (b) respectively. Like in the first scenario, since the power generated by the photovoltaic system can handle the load demand, the energy storage is unused, thus no hydrogen is consumed in the fuel cell. On the other hand, the hydrogen is produced in the electrolyser at a flow rate varying between 4.5 10^{-14} to about 3 10^{-13} mol per seconds depending on the excess power.

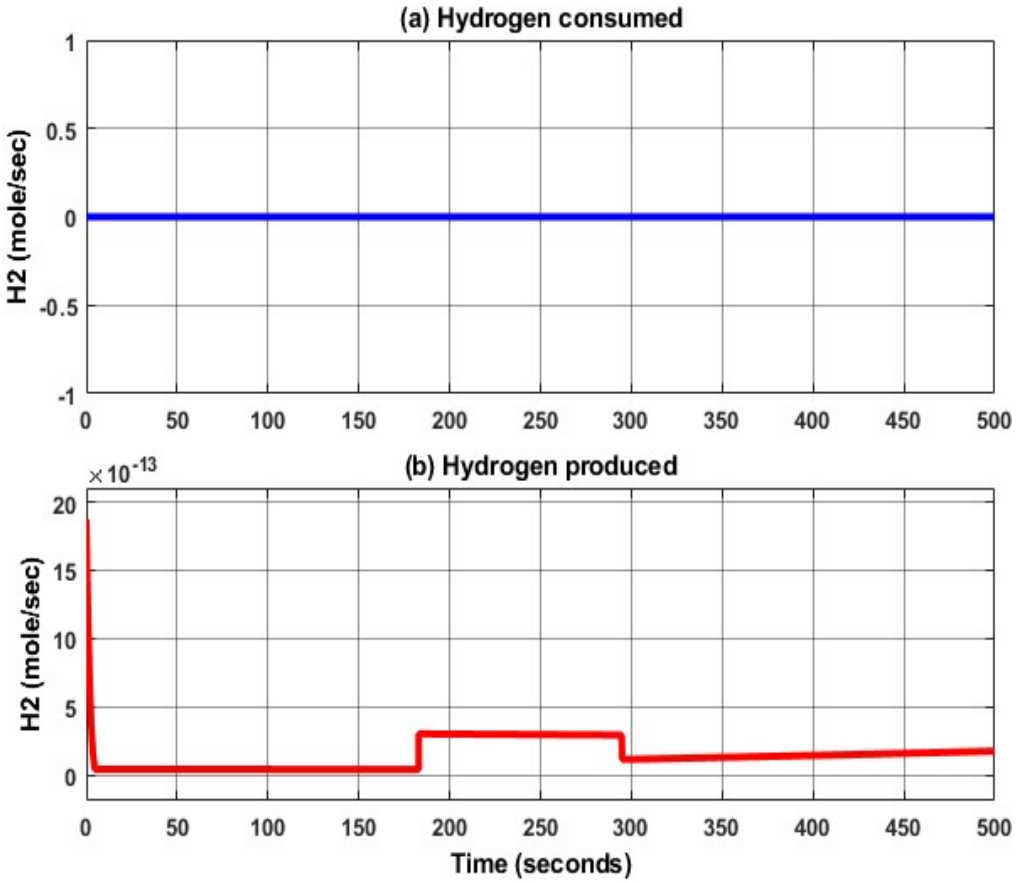

Figure 5. 11: (a) Hydrogen consumed in the fuel (b) hydrogen produced in the electrolyser

On the other hand, the characteristics of the supercapacitor such as current, voltage and state of charge are depicted in Figure 5.12, it can be noted that the current in the supercapacitor is zero amperes, implying that the supercapacitor is not charging or discharging. The corresponding voltage is around 42 V, while the state of charge ranges around 53 to 54 %.

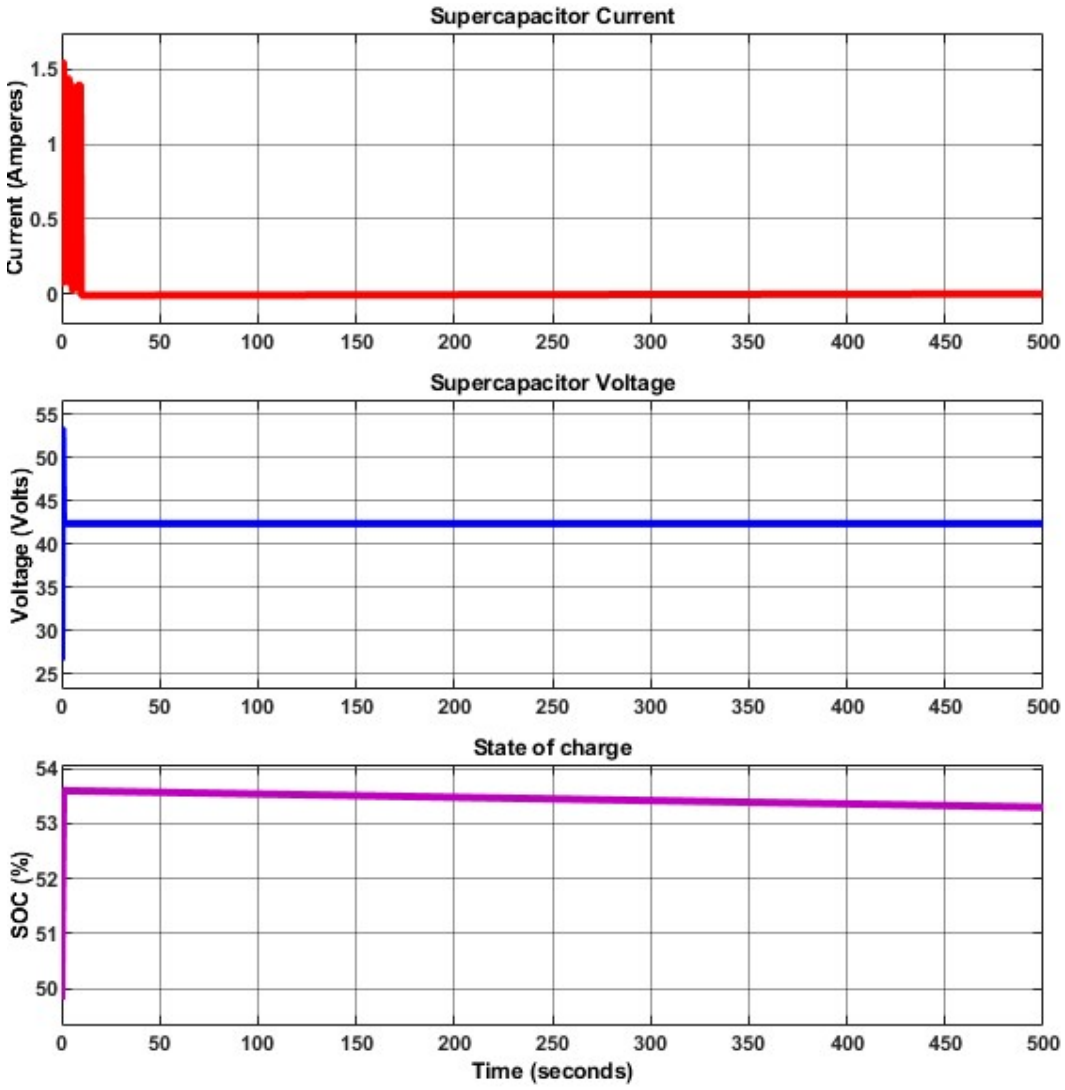

Figure 5. 12: (a) Supercapacitor current, (b) voltage and (c) state of charge

The load considered in this scenario is of a resistive nature changing randomly between 38 and 42 ohms (Figure 5.13(a)). Its characteristics include the current, voltage and power as are depicted in Figure 5.12. The current fluctuates around 8 A (Figure 5.12 (c)), thus the power required to supply the load varies slightly around 3 kW (see Figure 5.12 (d)). The voltage at the load terminal is depicted in Figure 5.12(b), this voltage remains 350 V.

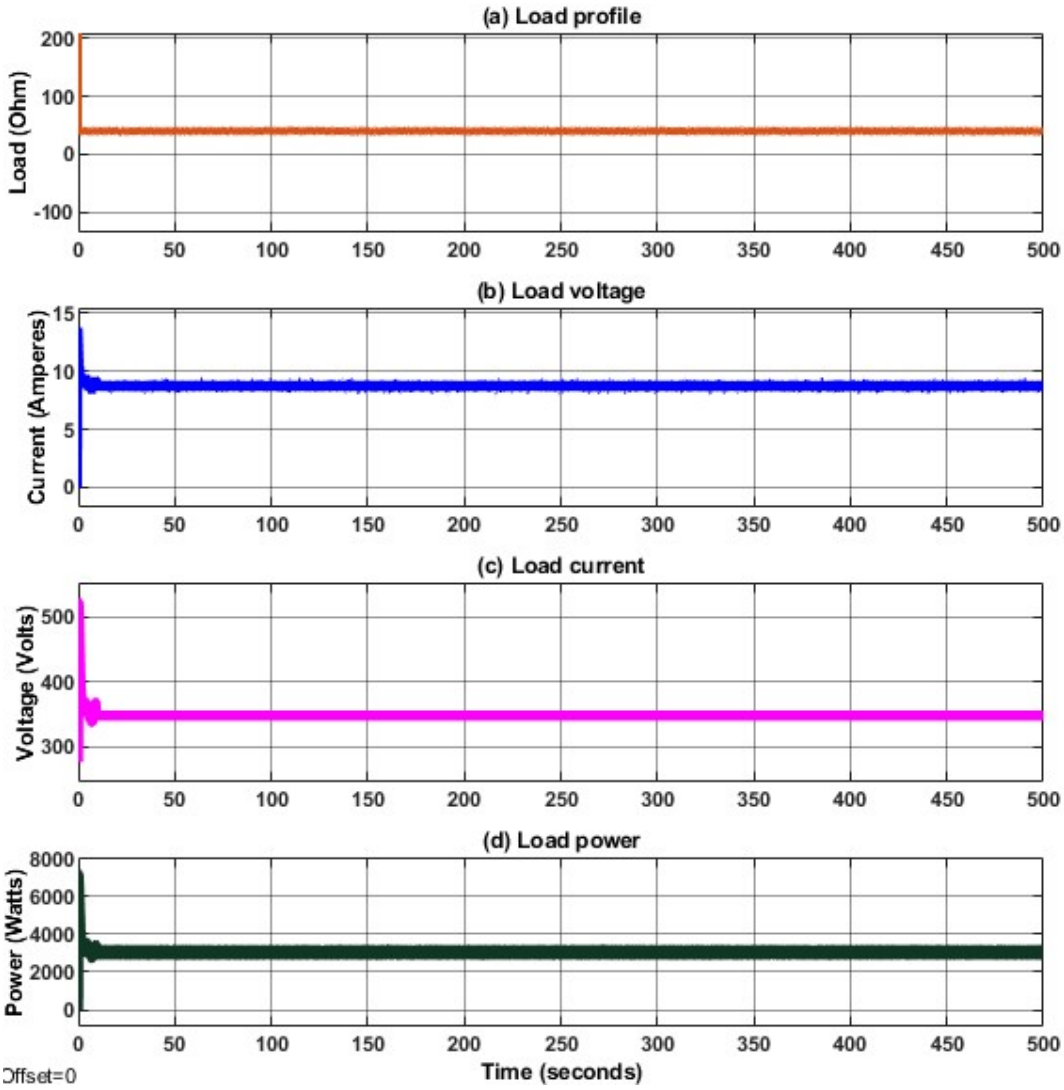

Figure 5. 13: (a) DC Load profile, (b) voltage, (c) current and (d) power

5.4.3 Scenario 3

Another scenario is that of the photovoltaic system supplying power to the load only as the solar radiation is at a low value (333 W/m^2), however, during a short period, it generates some excess which in this case is used to charge the supercapacitor as the level of hydrogen in the tank was assumed to be full. The voltage, current and power of the photovoltaic array from the boost converter side are given in Figure 5.14

The voltage profile is such that, initially it sat around 338 V, then increases moderately around 341 V due to a short increase of the solar radiation, then goes down to 338 V (Figure 5.14(a)).

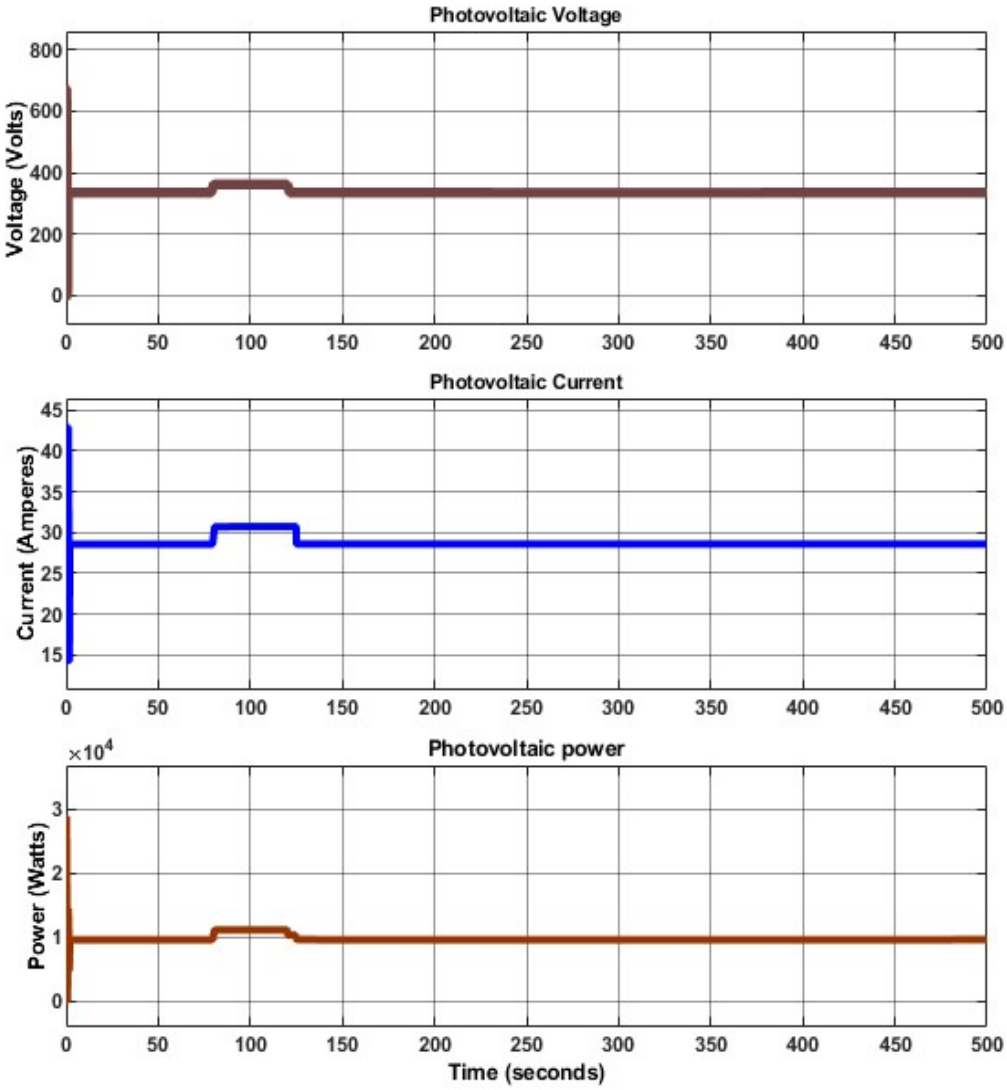

Figure 5. 14: (a) Photovoltaic voltage, (b) current and (c) power

Similarly, the current of the photovoltaic array at the boost converter output side is around 28 A, then increases slightly to 31 Amperes as the solar radiation has increased to finally get back to 28 A. (Figure 5.14 (b)).

With regards to the power, due to the available solar radiation, an average of 10 kW is generated from the photovoltaic array, thus, only enough to supply the loads (Figure 5.14(c)). The resulting energy produced daily from the photovoltaic system is around 240 kWh. No hydrogen is produced from the electrolyser as shown in Figure 5.15 and Figure 5.16(b), thus the level of hydrogen stored in the tank will remain the same. In the same vein, no hydrogen is used in the energy system as the overall energy can meet the load demand (Figure 5.16(a)), hence the fuel cell is unused.

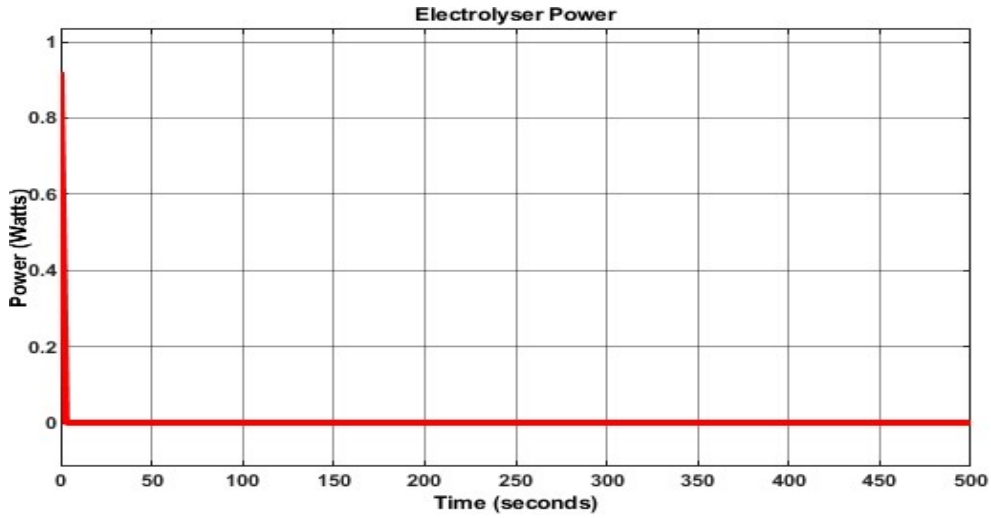

Figure 5. 15: Electrolyser power

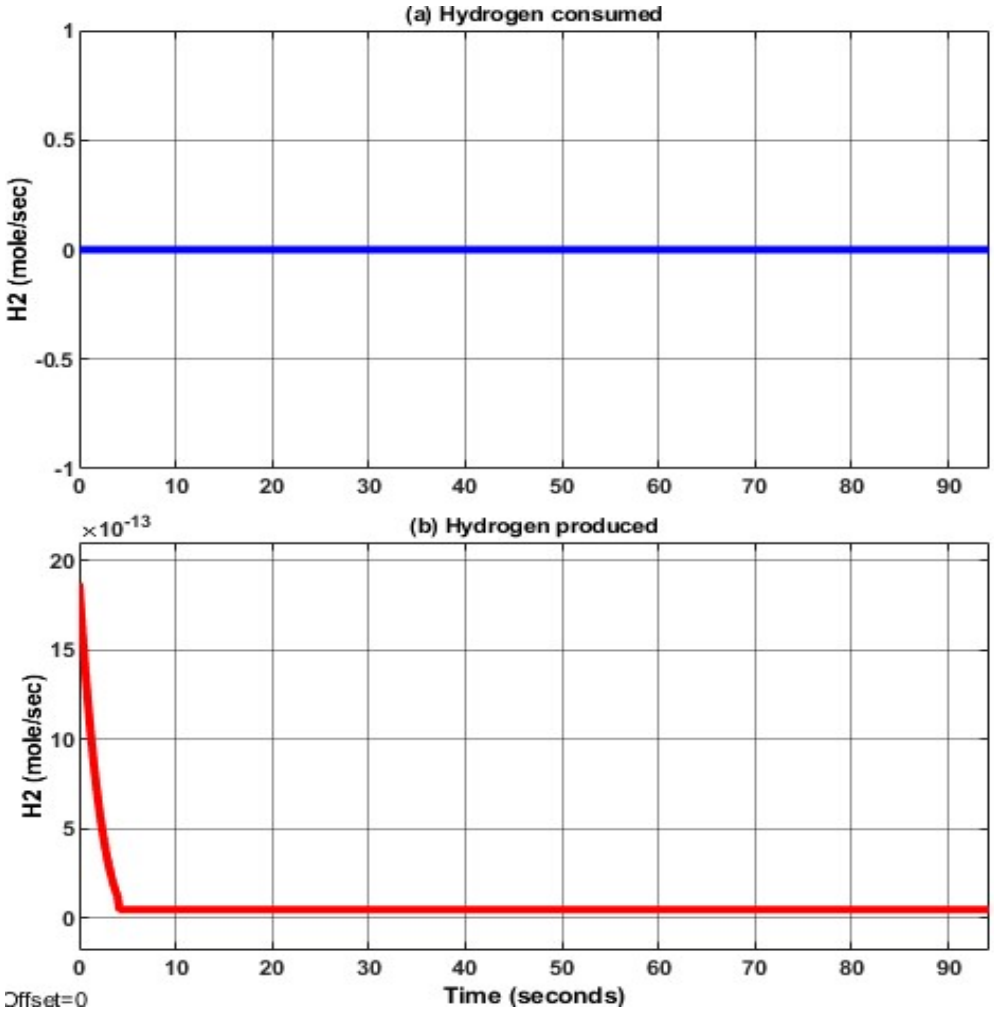

Figure 5. 16**: (a) hydrogen produced and (b) hydrogen consumed**

Figure 5.17 depicts the supercapacitor current, voltage and power; initially the current is around zero as the supercapacitor is not charging or discharging (Figure 5.17(a)), however, due to a short excess power generated by the photovoltaic system, it is observed a negative current which shows that the charging of the supercapacitor. The resulting undershoot and overshoot are caused by the high-charging current and can be perceived as the switching of the supercapacitor from its initial state to the charging state.

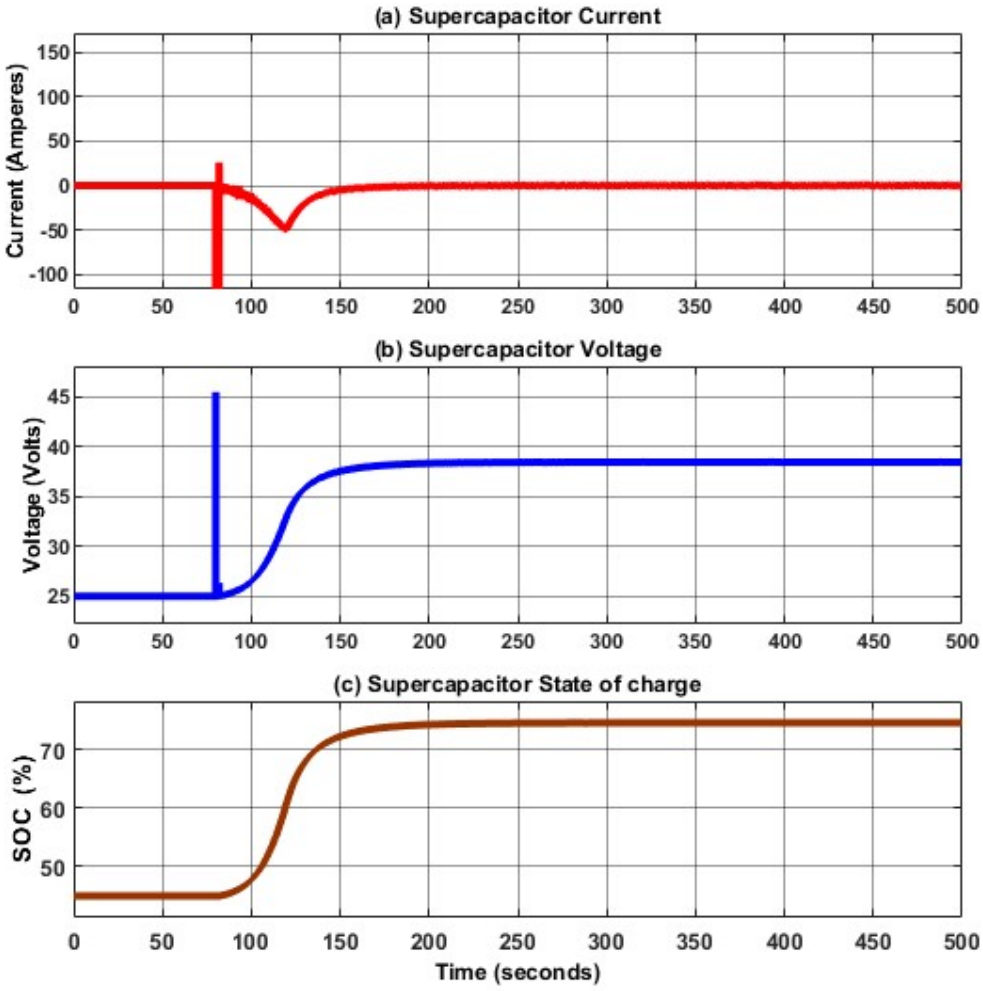

Figure 5. 17: (a) Supercapacitor current, (b) voltage and (c) state of charge

Regarding the voltage, at first, it is 25 V, however, it increases to around 38 V due to the charging of the supercapacitor (Figure 5.17(b)). The overshoot in the supercapacitor voltage profile results from the sudden change of the supercapacitor from rest to the charging state.

In the same manner, the state of charge of the supercapacitor is initially at 45 %, then increases to over 75 % due to the charging of the supercapacitor.

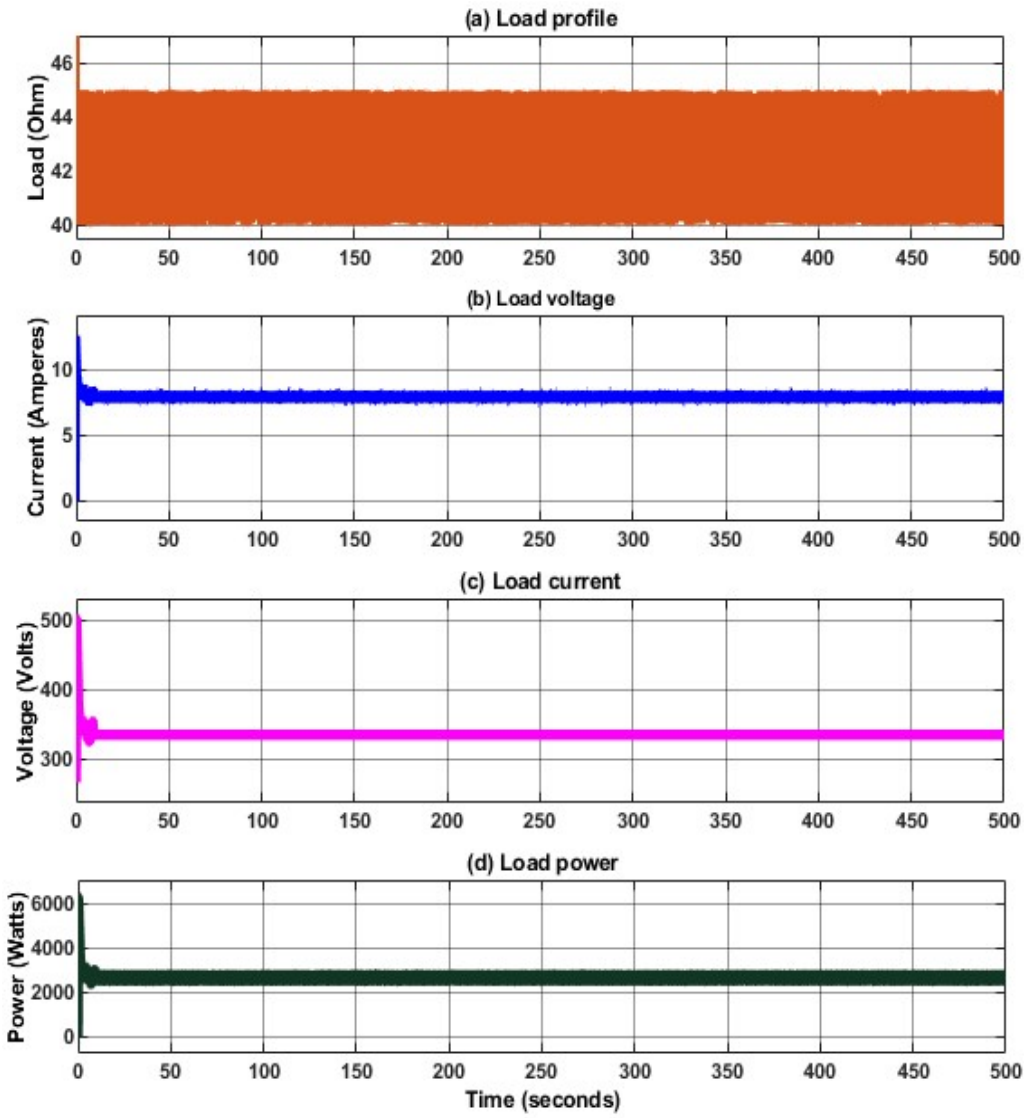

Figure 5. 18: (a) Supercapacitor current, (b) voltage and (c) state of charge

The load characteristics are shown in Figure 5.18; this load varies randomly between 40 and 45 ohms (Figure 5.18(a)) depending on the demand, however, the photovoltaic system generates enough to meet that load. The current required by the DC load is around 8 A (Figure 5.18(b)), while the voltage is about 345 V (Figure 5.18(c)). Depending upon the load demand, the power required may vary between 2.645 and 2.975 kW. With such a load profile, the daily energy needed to maintain the supply in the DC side is around 71.4 kWh per day.

5.4.4 Scenario 4

The last scenario considered is that of the photovoltaic array generating power during a short period only to meet the load demand without producing hydrogen or charging the supercapacitor, thereafter, the photovoltaic system is not able to generate power due to the absence of solar radiation. Therefore, the load demand is met the fuel cell and the supercapacitor depending upon the load condition. The supercapacitor is used only when there is sudden variation of the load as the fuel cell time response is slow.

The voltage, current and power generated from the photovoltaic array from the boost converter side are depicted in Figure 5.19; the voltage profile is such that, initially it sat around 338 V, then drops to zero due to insufficient solar radiation (Figure 5.19(a)).

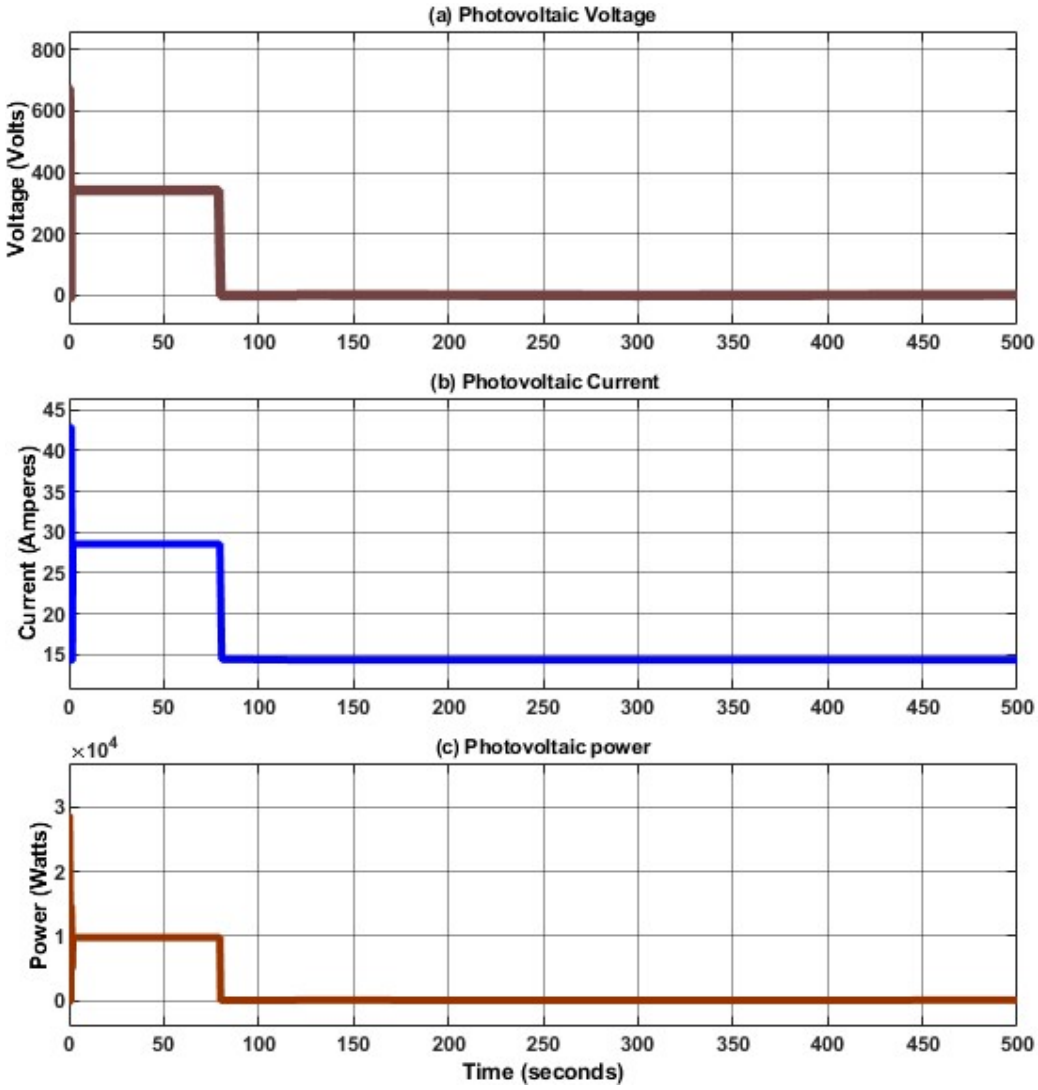

Figure 5. 19: Photovoltaic (a) voltage, (b) current and (c) power

In the same manner, the current of the photovoltaic array at the boost converter output side is around 28 Amperes, then decreases to zero as a result of lack of solar radiation (Figure 5.19 (b)).

As the power generated from the photovoltaic system is insufficient to meet the demand (Figure 5.19(c)), the load energy requirement is met through the hybrid energy storage system. Thus, the reversible fuel cell (Electrolyser-fuel cell system) and the supercapacitor operate to maintain the balance. Figure 5.20(a) shows the hydrogen consumed in the fuel cell, whereas that of produced in the electrolyser is zero (Figure 5.20(b)). To produce 10 kWh of energy, a typical fuel cell will require about 300 grams of hydrogen as hydrogen has the highest energy content by mass. This quantity of hydrogen is equivalent of around 30 moles of hydrogen. Thus, to meet the load demand 10 kW, the fuel cell needs 30 moles of hydrogen per hour.

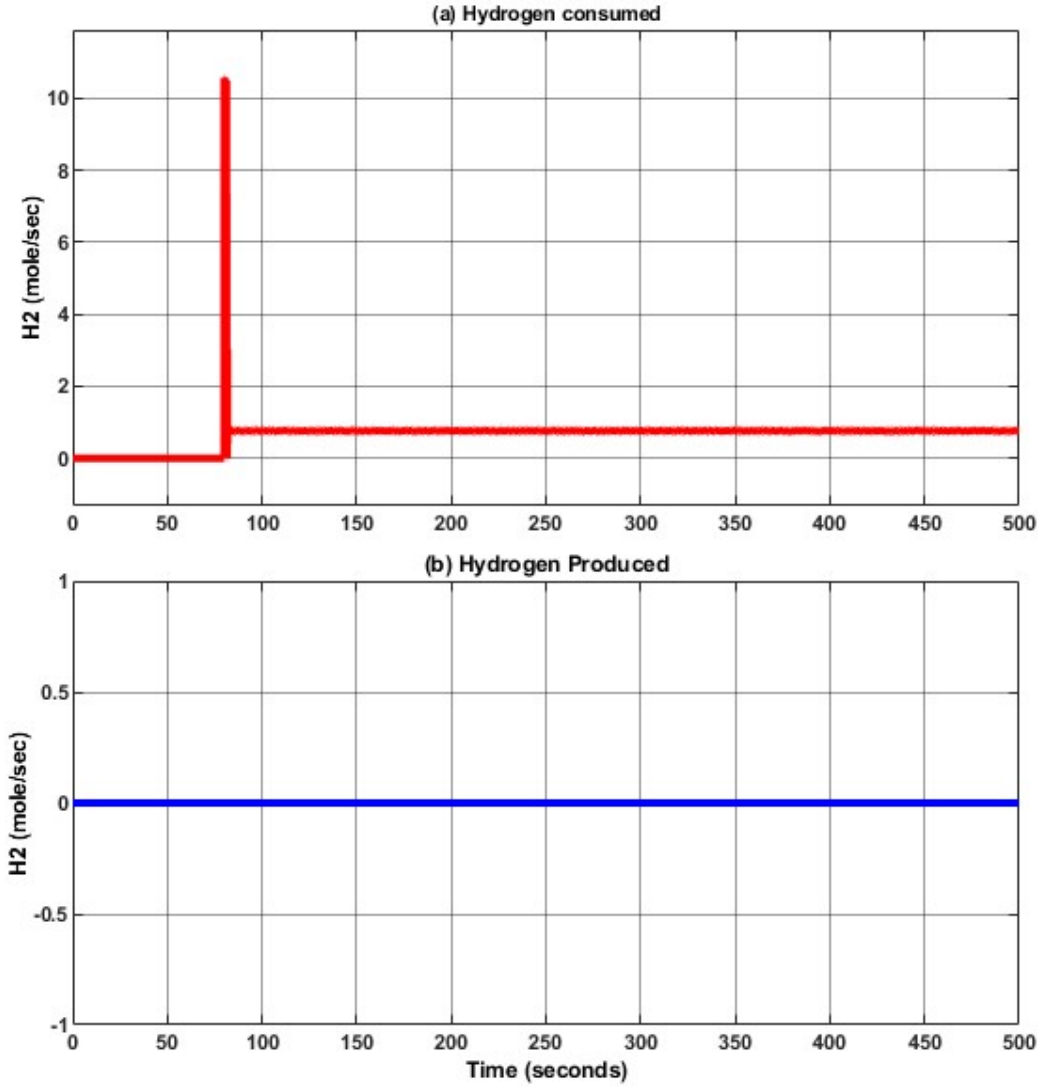

Figure 5. 20: (a) hydrogen consumed and (b) hydrogen produced

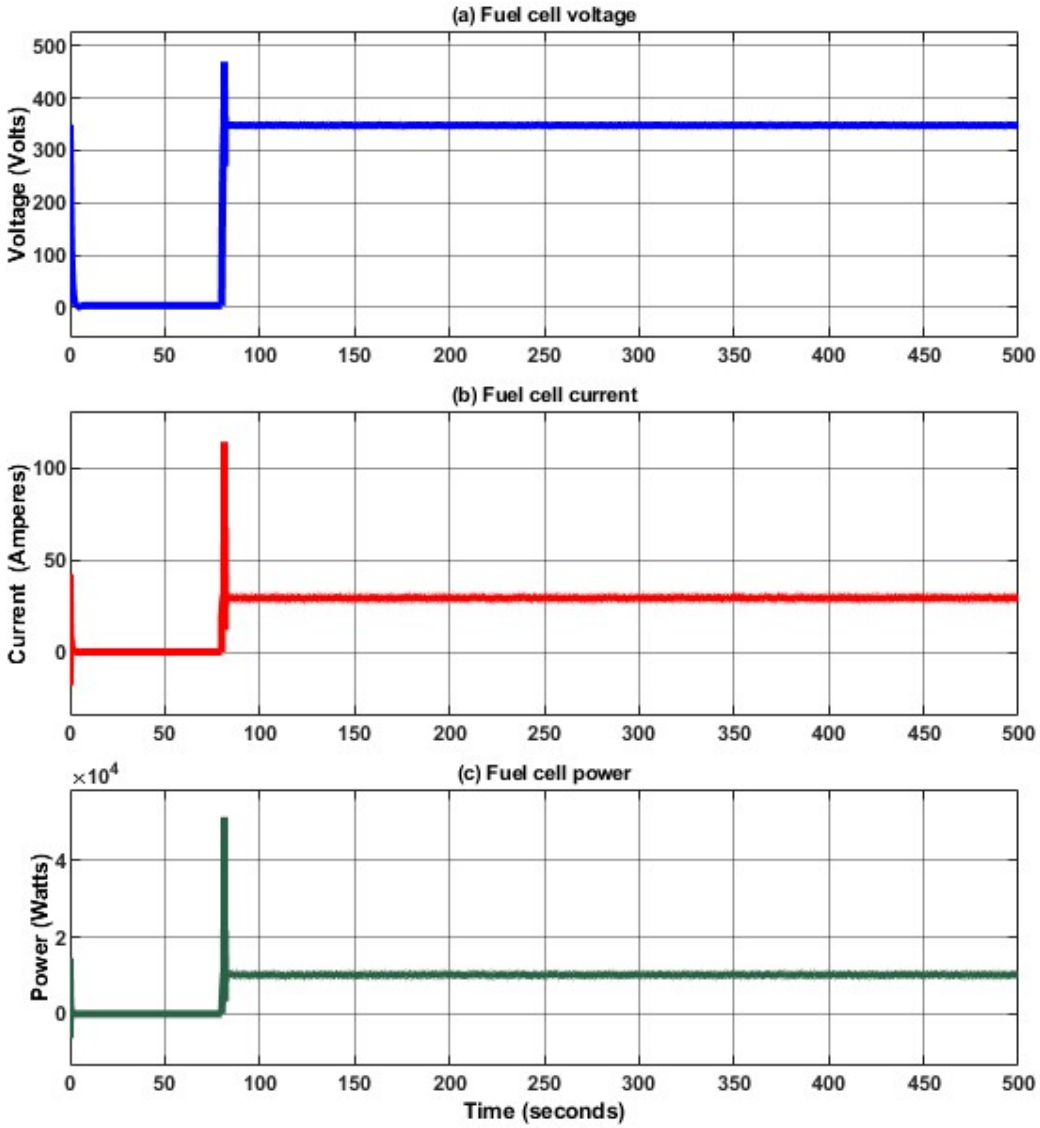

Figure 5. 21: Fuel cell (a) voltage, (b) current and (c) power

The voltage, current and power generated in the fuel cell from the boost converter side are depicted in Figure 5.20; the voltage profile is such that, initially it sat around zero Volts, then augments to around 350 V as at that stage, the load is fully met from the fuel cell (Figure 5.20(a)). The overshoot depicted in Figure 5.20(a) results from the sudden change of state of the fuel cell from rest to the generation mode.

In the same manner, the current of the fuel cell at the boost converter output side is around zero Amperes, then increases to 28 A as a result of the fuel cell supplying the load (Figure 5.19 (b)). Both the fuel cell voltage and current determine its power depending upon the load (Figure 5.20(c)).

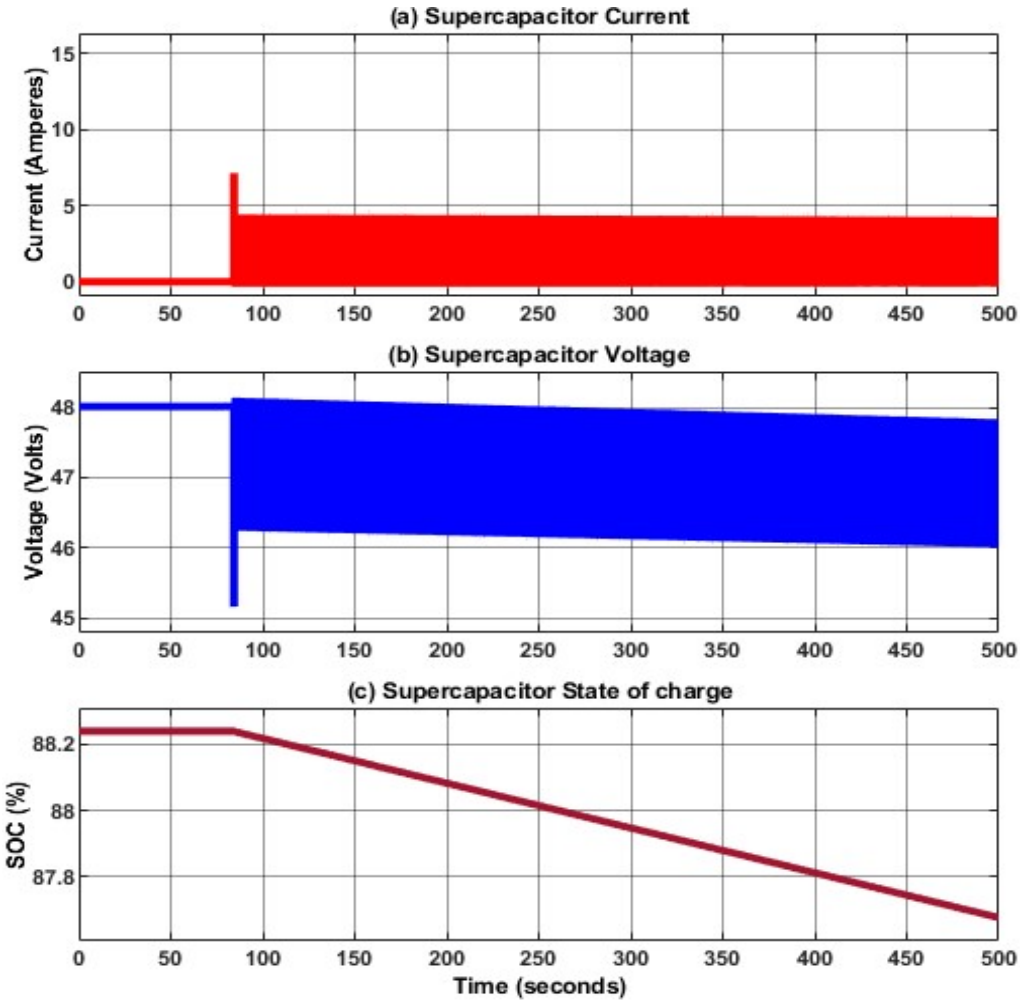

Figure 5. 22: (a) Supercapacitor current, (b) voltage and (c) state of charge

Figure 5.22 shows the characteristics of the supercapacitor bank, in this scenario, the supercapacitor current is initially equal to zero, thereafter it increases to about 4 A (Figure 5.22 (a)) to support the fuel cell depending on the load fluctuation. The corresponding voltage is equal to 48 V at the earlier stage of the simulation, then drops slightly to around 47.8 V (Figure 5.22 (b)). The power provided by the supercapacitor bank to handle the load variation is about 200 W, which corresponds to an energy supply of about 84 KWs (kilo watt second). The state of charge of supercapacitor bank begins around 88.2 %, then decreases to about 87.4 % (Figure 5.22 (c)).

5.5 Summary

This chapter was dedicated to the development of the energy management algorithm. The first step consisted of formulating the energy management problem based on the objectives of the research. Thereafter, an energy management algorithm based on a set of rules was established. A Simulink model integrating models of each components involved in system and including the energy management algorithm was developed. The resulting system was simulated, and the findings were presented in four scenarios which demonstrated the ability of the developed energy management system to handle the load.

CHAPTER SIX
CONCLUSION AND FUTURE WORK

6.1 Conclusion

This research dealt with the development of an energy management algorithm for a hybrid reversible fuel cell-supercapacitor in a 100 % renewable power system to maintain the balance between the supply and the load demand and manage sudden load fluctuations. Hydrogen is expected to play a key role in the concept of low-carbon power generation in support to renewable energy systems as it is available, clean, efficient and potentially more cost-effective than fossil fuels on condition that the engineering challenges associated with its safe infrastructure development, economical extraction and storage are solved. In 100% renewable power systems, a hydrogen production unit can be utilised together with a fuel cell to form an energy storage system for power balancing and energy shifting to hinder any mismatch caused by potential variation of renewable resources. The only drawback when using fuel cells is their slow time response which may reduce their lifetime in case of many occurrences of rapid load fluctuations above the fuel cell nominal load. In this study, a hybrid energy storage unit comprises of a renewable hydrogen fuel cell system and a supercapacitor bank was proposed. In such configuration, the hydrogen fuel cell system is meant to shift the energy availability over time, while the supercapacitor bank plays the role of managing rapid load variations and peak power occurrences. The challenges when dealing with a 100 % renewable power system including variation renewable resources and a hybrid energy storage system are the system design and the energy management system. On the one hand, a well-designed renewable power system implies a reliable system, while, on the other hand, a renewable power system with several energy sources necessitate an energy management system to coordinate the supply of energy from the different sources to the load. Therefore, the aim of this research was to design an optimal renewable power system based on photovoltaic system, renewable hydrogen fuel cell system and supercapacitors and propose an energy management algorithm able to maintain the balance between the renewable power system and load and manage sudden load variations. To achieve the given objectives, the research was subdivided in five chapters. Besides the introductory and the conclusive chapters, the rest of the study can be summarised as follows:

Chapter two concerned the literature survey on the concept of 100 % renewable power systems, different types of energy storage technologies, types of fuel cell systems and electrolysers including their characteristics and operating principles, a review on

supercapacitors and key drivers in the development of 100 % renewable power systems.

It was reported that key drivers for the expansion of 100 % renewable power systems include elements such as demand side management, expansion and liberalisation of markets, grid support services from renewable energy, diversifying renewable resources, bulk energy storage, transmission network efficiency and flexibility, role of smart grids, power system stability with non-synchronous generators and effective utilisation of excess generations. In addition, various forms of energy storage technologies such as mechanical, electrochemical, electrical, thermochemical, chemical and thermal were presented. Their characteristics and specific applications were as well considered. Furthermore, a section focusing on supercapacitors was also considered. It presented the different types of supercapacitors, their main characteristics and part involved. Lastly, a brief review of photovoltaic systems; starting from their history, evolution, operating principle, technology classification and characteristics were presented.

In chapter three, an optimal sizing of a hybrid energy storage using a fuel cell system and supercapacitor for renewable off-grid applications was carried out. The objective was to determine a suitable and reliable configuration to meet an overall load of 10 kW with 0 % capacity shortage. Based on the input data provided, the results show that, the optimal size of the system that meets the load requirement, given an irradiance of 850 Watts per metre square comprises 29.1 kW PV array, 10 kW fuel cell stack, 15 kW electrolysers, 7 kg hydrogen storage capacity, 7.6 kW converters and a total of 320 supercapacitors arranged in 16 strings of 20 supercapacitors each.

Chapter four dealt with the mathematical modelling of individual components which are part of the system. These components included the photovoltaic array, a discrete reversible fuel cell, a hydrogen tank, the supercapacitor bank, and the power electronics converters such as DC to DC boost converter, DC to DC buck converter and voltage source inverter. The control schemes of power electronics converters devices mentioned above were also presented.

Chapter five focused on the development of the energy management algorithm. Based on the given objectives, an energy management problem was formulated and using a set of rules, an algorithm was developed. A system based on mathematical models of each component and integrating the energy management algorithm was developed and simulated using Matlab/Simulink environment. Due to high computing performance requirements, the obtained Simulink model was simulated for a short duration to evaluate the effectiveness of the developed energy management algorithm. The results

are presented in four different scenarios demonstrating the ability of the system to maintain the balance between the supply and the demand and to manage sudden peak power occurrences.

In the first scenario, the photovoltaic system generated about 28.9 kW under an irradiance of 850 W/m^2 to meet the load demand, produce hydrogen and charge the supercapacitor. It was considered that the solar radiation remained unchanged, hence, no power variation observed. The photovoltaic array was expected to generate about 693.6 kWh per day to meet the load demand, produce hydrogen and charge the supercapacitor. The energy storage system was unused as the photovoltaic system was able to meet the complete load demand.

In the second scenario, the solar radiation was decreased to 344 W/m^2, then slightly increased to 359 W/m^2 and then decreased again to 348 W/m^2, causing the power generated from the photovoltaic system to fluctuate around 12 kW. 10 kW of this power served to meet both the DC and AC load demands and the remaining portion was used to produce hydrogen and charge the supercapacitor, with the priority on producing hydrogen.

In the third scenario, the photovoltaic system was able to supply load only as the solar radiation was set to 333 W/m^2, however, during a short period, it generated some excess which in this case was used to charge the supercapacitor as the level of hydrogen in the tank was assumed to be full.

The last scenario was that of the photovoltaic array generating power during a short period only to meet the load demand without producing hydrogen or charging the supercapacitor, thereafter, the photovoltaic system is not able to generate power due to the absence of solar radiation. Therefore, the load demand was met the fuel cell and the supercapacitor depending upon the load condition. The supercapacitor was used only when there was sudden load variation.

6.2 Future work

Further research will focus on:

- Validating the developed energy management system using a testbench;
- Validating the developed energy management system using a real time simulator platform;
- Developing the energy system using more advanced approaches.

REFERENCES

Akinyele, D.O. & Rayudu, R.K. 2014. Review of energy storage technologies for sustainable power networks. *Sustainable Energy Technologies and Assessments*, 8: 74–91.

Alotto, P., Guarnieri, M. & Moro, F. 2014. Redox flow batteries for the storage of renewable energy : A review. *Renewable and Sustainable Energy Reviews*, 29: 325–335.

Alva, G., Lin, Y. & Fang, G. 2018. An overview of thermal energy storage systems. *Energy*, 144: 341–378. https://doi.org/10.1016/j.energy.2017.12.037.

Alva, G., Liu, L., Huang, X. & Fang, G. 2017. Thermal energy storage materials and systems for solar energy applications. *Renewable and Sustainable Energy Reviews*, 68(August 2016): 693–706. http://dx.doi.org/10.1016/j.rser.2016.10.021.

Amin, N., Ahmad Shahahmadi, S., Chelvanathan, P., Rahman, K.S., Istiaque Hossain, M. & Akhtaruzzaman, M.D. 2017. *Solar Photovoltaic Technologies: From Inception Toward the Most Reliable Energy Resource*. Elsevier. http://dx.doi.org/10.1016/B978-0-12-409548-9.10092-2.

Aneke, M. & Wang, M. 2016. Energy storage technologies and real life applications – A state of the art review. *Applied Energy*, 179: 350–377.

Aslam, M., Tariq, A., Hameed, S. & Bin, M.S. 2017. Comparative assessment of maximum power point tracking procedures for photovoltaic systems. *Green Energy and Environment*, 2(1): 5–17. http://dx.doi.org/10.1016/j.gee.2016.11.001.

Aslan, M., Weingarth, D., Jäckel, N., Atchison, J.S., Grobelsek, I. & Presser, V. 2014. Polyvinylpyrrolidone as binder for castable supercapacitor electrodes with high electrochemical performance in organic electrolytes. *Journal of Power Sources*, 266: 374–383. https://reader.elsevier.com/reader/sd/pii/S0378775314007137?token=BD670A43D4251628AD12AF2B79BD457E743072325BF05BB508EECE3FC3B025CC1C6BDE82BD54BE88BA1292D261474E02.

Bahar, H. 2019. Solar PV, Tracking Clean Energy Progress. https://www.iea.org/tcep/power/renewables/solarpv/ 1 July 2019.

Balogun, M.S., Qiu, W., Wang, W., Fang, P., Lu, X. & Tong, Y. 2015. Recent advances in metal nitrides as high-performance electrode materials for energy storage devices. *Journal of Materials Chemistry A*, 3(4): 1–72.

https://reader.elsevier.com/reader/sd/pii/S037877530100903X?token=8B3FFAE32CDF03F4139DCE8BCFDD25EBC70242EE2906EA9C7D97537D9CF6C3918C3A03E0A28F07655DC5B8BF24BD5B7B.

Barbir, F., Basile, A. & Veziroğlu, T.N. 2016. *Compendium of Hydrogen Energy : Hydrogen Energy Conversion*. 1st ed. B. Frano, B. Angelo, & V. T.Nejat, eds. Woodhead Publishing Limited. https://bu.unistra.fr:443/.do?idopac=BUS2129273%5Cnhttp://files/1581/do.html.

Barranco, V., Pico, F., Ibañez, J., Lillo-Rodenas, M.A., Linares-Solano, A., Kimura, M., Oya, A., Rojas, R.M., Amarilla, J.M. & Rojo, J.M. 2009. Amorphous carbon nanofibres inducing high specific capacitance of deposited hydrous ruthenium oxide. *Electrochimica Acta*, 54: 7452–7457. https://reader.elsevier.com/reader/sd/pii/S0013468609010329?token=6AD71C4B3E507B967C9CDAC07607E034CE9A06AC8CAFBFD8C6B82725C751BD0D007C687E63A2D63297B083FE07A8EFE6.

Bhuiyan, F.A. & Yazdani, A. 2012. Energy storage technologies for grid-connected and off-grid power system applications. In *IEEE Electrical Power and Energy Conference*. IEEE: 303–310.

Bito, A. 2005. Overview of the sodium-sulfur battery for the IEEE Stationary Battery Committee. *IEEE Power Engineering Society General Meeting, 2005*: 1–4.

Bocklisch, T. 2015. Hybrid energy storage systems for renewable energy applications. *Energy Procedia*, 73: 103–111. http://dx.doi.org/10.1016/j.egypro.2015.07.582.

Bolund, B., Bernhoff, H. & Leijon, M. 2007. Flywheel energy and power storage systems. *Renewable and Sustainable Energy Reviews*, 11(2): 235–258.

Bouhtiyya, S., Lucio-Porto, R., Ducros, J.., Boulet, P., Capon, F., Brousse, T. & Pierson, J.. 2012. Transition metal nitrides thin films for supercapacitor applications. *The Electrochemical Society*: 2019. http://ma.ecsdl.org/content/MA2012-02/6/494.abstract.

Brandt, A., Ramirez-Castro, C., Anouti, M. & Balducci, A. 2013. An investigation about the use of mixtures of sulfonium-based ionic liquids and propylene carbonate as electrolytes for supercapacitors. *Journal of Materials Chemistry A*, 1: 12669–12678. https://sci-hub.tw/10.1039/C3TA12737K.

Breyer, C., Birkner, C., Meiss, J., Goldschmidt, J.C. & Riede, M. 2013. A top-down analysis: Determining photovoltaics R&D investments from patent analysis and R&D headcount. *Energy Policy*, 62: 1570–1580.

Brown, M.A. 2014. Enhancing efficiency and renewables with smart grid technologies and policies. *Futures*, 58: 21–33. http://dx.doi.org/10.1016/j.futures.2014.01.001.

Budischak, C., Sewell, D., Thomson, H., MacH, L., Veron, D.E. & Kempton, W. 2013. Cost-minimized combinations of wind power, solar power and electrochemical storage, powering the grid up to 99.9% of the time. *Journal of Power Sources*, 225: 60–74. http://dx.doi.org/10.1016/j.jpowsour.2012.09.054.

Byeon, G., Yoon, T., Oh, S. & Jang, G. 2013. Energy management strategy of the DC distribution system in buildings using the EV service model. *IEEE Transactions on Power Electronics*, 28(4): 1544–1554.

Caisheng, W., Nehrir, M.H. & Shaw, S.R. 2005. Dynamic models and model validation for PEM fuel cells using electrical circuits. *IEEE Transactions on Energy Conversion*, 20(2): 442–451. https://ieeexplore.ieee.org/stamp/stamp.jsp?tp=&arnumber=1432859.

Chatzivasileiadi, A., Ampatzi, E. & Knight, I. 2013. Characteristics of electrical energy storage technologies and their applications in buildings. *Renewable and Sustainable Energy Reviews*, 25: 814–830. http://dx.doi.org/10.1016/j.rser.2013.05.023.

Chen, H., Cong, T.N., Yang, W., Tan, C., Li, Y. & Ding, Y. 2009. Progress in electrical energy storage system: A critical review. *Progress in Natural Science*, 19(3): 291–312. http://dx.doi.org/10.1016/j.pnsc.2008.07.014.

Cheng, P., Peng, B., Liu, Y., Cheng, Y. & Huang, J. 2015. Optimization of a Fuzzy-Logic-Control-Based MPPT Algorithm Using the Particle Swarm Optimization Technique. *MDPI energies*, 8: 5338–5360.

Child, M., Kemfert, C., Bogdanov, D. & Breyer, C. 2019. Flexible electricity generation, grid exchange and storage for the transition to a 100% renewable energy system in Europe. *Renewable Energy*, 139: 80–101. https://doi.org/10.1016/j.renene.2019.02.077.

Cho, H.W., Hepowit, L.R., Nam, H.S., Kim, S.H., Lee, Y.M., Kim, J.H., Kim, K.M. & Ko, J.M. 2012. Synthesis and supercapacitive properties of electrodeposited polyaniline composite electrode on acrylonitrile-butadiene rubber as a flexible current collector. *Synthetic Metals*, 162: 410–413. http://dx.doi.org/10.1016/j.synthmet.2011.12.025.

Choi, C., Kim, Soohyun, Kim, R., Choi, Y., Kim, Soowhan & Jung, H. 2017. A review of vanadium electrolytes for vanadium redox flow batteries. *Renewable and Sustainable Energy Reviews*, 69(March 2016): 263–274. http://dx.doi.org/10.1016/j.rser.2016.11.188.

Chong, L.W., Wong, Y.W., Rajkumar, Rajprasad Kumar, Rajkumar, Rajpartiban Kumar & Isa, D. 2016. Hybrid energy storage systems and control strategies for stand-alone renewable energy power systems. *Renewable and Sustainable Energy Reviews*, 66: 174–189. http://dx.doi.org/10.1016/j.rser.2016.07.059.

Chua, N. 2016. Edmond Becquerel: The Man Behind Solar Panels. *Solenergy Systems Inc.* http://solenergy.com.ph/solar-panel-philippines-edmond-becquerel/ 15 August 2019.

Clemente, A., Panero, S., Spila, E. & Scrosati, B. 1996. Solid-state, polymer-based, redox capacitors. *Solid State Ionics*, 85: 273–277. https://reader.elsevier.com/reader/sd/pii/016727389600070?token=F51E348BDBF8D41DAF5CE6E62E7DC96238F9EB3B500EDE064495C225E41AF751B7E6CB328E2107400D78B114AEEBF670.

Cochran, J., Bird, L., Heeter, J. & Arent, D.J. 2012. *Integrating Variable Renewable Energy in Electric Power Markets: Best Practices from International Experience*. http://www.osti.gov/bridge 25 April 2019.

Comello, S., Reichelstein, S. & Sahoo, A. 2018. The road ahead for solar PV power. *Renewable and Sustainable Energy Reviews*, 92(April): 744–756. https://doi.org/10.1016/j.rser.2018.04.098.

Das, N., Wongsodihardjo, H. & Islam, S. 2016. A Preliminary Study on Conversion Ef fi ciency Improvement of a Multi-junction PV Cell with MPPT.

Das, V., Padmanaban, S., Venkitusamy, K., Selvamuthukumaran, R., Blaabjerg, F. & Siano, P. 2017. Recent advances and challenges of fuel cell based power system architectures and control – A review. *Renewable and Sustainable Energy Reviews*, 73(March 2016): 10–18. http://dx.doi.org/10.1016/j.rser.2017.01.148.

Díaz-González, F., Sumper, A. & Gomis-Bellmunt, O. 2015. *Energy Storage in Power Systems*. John Wiley & Sons Ltd.

DOE. 2017. Progress in Hydrogen and Fuel Cells. *US Department of Energy*: 2. https://www.energy.gov/sites/prod/files/2017/10/f37/fcto-progress-fact-sheet-august-2017.pdf 28 March 2018.

Edition, S. & Virginia, W. 2004. *Fuel Cell Handbook*. 7th ed.

Elbaset, A.A., Hassan, M.S. & Ali, H. 2017. Performance analysis of grid-connected PV system. *2016 18th International Middle-East Power Systems Conference, MEPCON 2016 - Proceedings*, (1): 675–682.

Esmaili, A., Novakovic, B., Member, Student, Nasiri, A., Member, Senior & Abdel-baqi, O. 2013. A Hybrid System of Li-Ion Capacitors and Flow Battery for Dynamic Wind Energy Support. *IEEE Transactions on Industry Applications*, 49(4): 1649–1657. file:///C:/Users/Acer/Downloads/A Hybrid System of Li-Ion Capacitors and Flow Battery for Dynamic Wind Energy Suppor.pdf.

Etxeberria, A., Vechiu, I., Camblong, H., Vinassa, J.M. & Camblong, H. 2010. Hybrid Energy Storage Systems for renewable Energy Sources Integration in microgrids: A review. *2010 Conference Proceedings IPEC*: 532–537. http://ieeexplore.ieee.org/document/5697053/.

Fan, L.Z. & Maier, J. 2006. High-performance polypyrrole electrode materials for redox supercapacitors. *Electrochemistry Communications*, 8: 937–940. https://reader.elsevier.com/reader/sd/pii/S1388248106001330?token=11884EC8DE580891AEB30A7B81081653D967BD66610F131F645B9FCAD9A21F2CADB9B8FBCFAF5B3C58B3F7680571DFD6.

Farhoodnea, M., Mohamed, A., Shareef, H. & Zayandehroodi, H. 2012. Power quality impact of grid-connected photovoltaic generation system in distribution networks. *SCOReD 2012 - 2012 IEEE Student Conference on Research and Development*: 1–6. https://ieeexplore-ieee-org.libproxy.cput.ac.za/stamp/stamp.jsp?tp=&arnumber=6518600.

Farooque, M. & Maru, H.C. 2001. Fuel Cells — The Clean and Efficient Power Generators. *Proceedings of the IEEE*, 89(12): 1819–1829.

Gil, A., Medrano, M., Martorell, I., Lázaro, A., Dolado, P., Zalba, B. & Cabeza, L.F. 2010. State of the art on high temperature thermal energy storage for power generation. Part 1-Concepts, materials and modellization. *Renewable and Sustainable Energy Reviews*, 14(1): 31–55.

Gong, X., Cheng, J.P., Liu, F., Zhang, L. & Zhang, X. 2014. Nickel-Cobalt hydroxide microspheres electrodepositioned on nickel cobaltite nanowires grown on Ni foam for high-performance pseudocapacitors. *Journal of Power Sources*, 267: 610–616. http://dx.doi.org/10.1016/j.jpowsour.2014.05.120.

Guerrero, J.M., Chandorkar, M., Lee, T.-L. & Loh, P.C. 2013. Advanced Control Architectures for Intelligent Microgrids—Part I: Decentralized and Hierarchical Control. *IEEE Transactions on Industrial Electronics*, 60(4): 1254–1262. http://ieeexplore.ieee.org/document/6184305/.

Guerrero, J.M., Vasquez, J.C., Matas, J., De Vicuña, L.G. & Castilla, M. 2011. Hierarchical control of droop-controlled AC and DC microgrids - A general approach toward standardization. *IEEE Transactions on Industrial Electronics*, 58(1): 158–172.

Hadjipaschalis, I., Poullikkas, A. & Efthimiou, V. 2009. Overview of current and future energy storage technologies for electric power applications. *Renewable and Sustainable Energy Reviews*, 13(6–7): 1513–1522.

Hansen, K., Breyer, C. & Lund, H. 2019. Status and Perspectives on 100% Renewable Energy Systems. *Energy*, 175: 471–480. https://www.sciencedirect.com/science/article/pii/S0360544219304967?dgcid=raven_sd_aip_email.

Hemmati, R. & Saboori, H. 2016. Emergence of hybrid energy storage systems in renewable energy and transport applications - A review. *Renewable and Sustainable Energy Reviews*, 65: 11–23. http://dx.doi.org/10.1016/j.rser.2016.06.029.

IEA-PVPS. 2018. *Trends 2018 in Photovoltaics Applications*.

IRENA. 2018. *Power Generation Costs in 2017*. Abu Dhabi: International Renewable Energy Agency.

Jha, A.R. 2012. *Next-Generation Batteries and Fuel cells for Commercial, Military and Space Applications*. CRC Press, Taylor & Francis Group.

Kalaji, M., Murphy, P.J. & Williams, G.O. 1999. Study of conducting polymers for use as redox supercapacitors. *Synthetic Metals*, 102: 1360–1361. https://reader.elsevier.com/reader/sd/pii/S0379677998013344?token=D5CA1791A6763DDD5BE0ADA0438DD9E341487A644A3604217170571182F25C8193197626A5291611F55CF3C902AD9BD9.

Kalinci, Y., Hepbasli, A. & Dincer, I. 2015. Techno-economic analysis of a stand-alone hybrid renewable energy system with hydrogen production and storage options. *International Journal of Hydrogen Energy*, 40: 7652–7664. http://dx.doi.org/10.1016/j.ijhydene.2014.10.147 8 December 2017.

Kanchev, H., Lu, D., Colas, F., Lazarov, V. & Francois, B. 2011. Energy management and operational planning of a microgrid with a PV-based active generator for smart grid applications. *IEEE Transactions on Industrial Electronics*, 58(10): 4583–4592.

Kang, M., Lee, J.E., Shim, H.W., Jeong, M.S., Im, W.B. & Yoon, H. 2014. Intrinsically conductive polymer binders for electrochemical capacitor application. *RSC Advances*, 4:

27939–27945. https://sci-hub.tw/10.1039/c4ra03261f.

Karami, N., Moubayed, N. & Outbib, R. 2017. General review and classification of different MPPT Techniques. *Renewable and Sustainable Energy Reviews*, 68: 1–18.

Katiraei, F., Iravani, R., Hatziargyriou, N. & Dimeas, A. 2008. Microgrids Management. *IEEE Power and Energy Magazin*, 6(3): 54–65.

Khan, M.J. & Iqbal, M.T. 2009. Analysis of a small wind-hydrogen stand-alone hybrid energy system. *Applied Energy*, 86(11): 2429–2442. http://dx.doi.org/10.1016/j.apenergy.2008.10.024.

Kim, H. & Popov, B.N. 2002. Characterization of hydrous ruthenium oxide/carbon nanocomposite supercapacitors prepared by a colloidal method. *power Sources*, 104: 52–61. https://reader.elsevier.com/reader/sd/pii/S037877530100903X?token=8B3FFAE32CDF03F4139DCE8BCFDD25EBC70242EE2906EA9C7D97537D9CF6C3918C3A03E0A28F07655DC5B8BF24BD5B7B.

Kim, Y.T., Tadai, K. & Mitani, T. 2005. Highly dispersed ruthenium oxide nanoparticles on carboxylated carbon nanotubes for supercapacitor electrode materials. *Journal of Materials Chemistry*, 15: 4914–4921. https://sci-hub.tw/10.1039/b511869g.

Kirubakaran, A., Jain, S. & Nema, R.K. 2009. A review on fuel cell technologies and power electronic interface. *Renewable and Sustainable Energy Reviews*, 13(9): 2430–2440.

Kiviluoma, J., Meibom, P., Tuohy, A., Troy, N., Milligan, M., Member, S., Lange, B., Gibescu, M. & Malley, M.O. 2012. Short-Term Energy Balancing with Increasing Levels of Wind Energy. *IEEE Transactions on Sustainable Energy*, 3(4): 769–776. https://ieeexplore-ieee-org.libproxy.cput.ac.za/stamp/stamp.jsp?tp=&arnumber=6298068.

Klessmann, C., Nabe, C. & Burges, K. 2008. Pros and cons of exposing renewables to electricity market risks-A comparison of the market integration approaches in Germany, Spain, and the UK. *Energy Policy*, 36(10): 3646–3661.

Kock, A. De, Ferg, E. & Gummow, R.J. 1996. Electrochemical modification of active carbon fiber electrode and its application to double-layer capacitor. *Science*, 60: 249–253. https://reader.elsevier.com/reader/sd/pii/S0378775396800188?token=D4BD6334D1E5A6966A21146187FDC97C67BEA71D680AF9373BF9749D5E9811EA240D66C2C75746B6FD0A00EBE18B85FB.

Kousksou, T., Bruel, P., Jamil, A., El Rhafiki, T. & Zeraouli, Y. 2014a. Energy storage:

Applications and challenges. *Solar Energy Materials and Solar Cells*, 120: 59–80.

Kousksou, T., Bruel, P., Jamil, A., El Rhafiki, T. & Zeraouli, Y. 2014b. Energy storage: Applications and challenges. *Solar Energy Materials and Solar Cells*, 120: 59–80.

Kumar, D. & Chatterjee, K. 2016. A review of conventional and advanced MPPT algorithms for wind energy systems. *Renewable and Sustainable Energy Reviews*, 55: 957–970. http://dx.doi.org/10.1016/j.rser.2015.11.013.

L.O.Vasquez. 2007. *Fuel cell research trends*. Neww York: Nova Science Pubblisher, Inc.

Lajnef, T., Abid, S. & Ammous, A. 2013. Modeling, control, and simulation of a solar hydrogen/fuel cell hybrid energy system for grid-connected applications. *Advances in Power Electronics*, 2013.

Larminie, J. & Dicks, A. 2003. *Fuel cell systems explained*. 2nd ed. John Wiley & Sons Ltd. http://eu.wiley.com/WileyCDA/WileyTitle/productCd-047084857X.html.

Lee, J.K., Pathan, H.M., Jung, K.D. & Joo, O.S. 2006. Electrochemical capacitance of nanocomposite films formed by loading carbon nanotubes with ruthenium oxide. *Journal of Power Sources*, 159: 1527–1531.

Letcher, T.M. 2016. *Storing Energy: with Special Reference to Renewable Energy Sources*. Elsevier. http://store.elsevier.com/Storing-Energy/Trevor-Letcher/isbn-9780128034408/.

Lewandowski, A., Jakobczyk, P. & Galinski, M. 2012. Capacitance of electrochemical double layer capacitors. *Electrochimica Acta*, 86: 225–231. http://dx.doi.org/10.1016/j.jpowsour.2011.10.083.

Li, P. 2008. Energy storage is the core of renewable technologies. *IEEE Nanotechnology Magazine*, 2(4): 13–18.

Longe, O.M., Rao, N.D., Omowole, F., Oluwalami, A.S. & Oni, O.T. 2017. A Case Study on Off-grid Microgrid for Universal Electricity Access in the Eastern Cape of South Africa. *International Journal or Energy Engineering*, 7(2): 55–63.

López-Peña, A., Pérez-Arriaga, I. & Linares, P. 2012. Renewables vs . energy efficiency : The cost of carbon emissions reduction in Spain. *Energy Policy*, 50(2012): 659–668.

Lucia, U. 2014a. Overview on fuel cells. *Renewable and Sustainable Energy Reviews*, 30: 164–169. http://dx.doi.org/10.1016/j.rser.2013.09.025.

Lucia, U. 2014b. Overview on fuel cells. *Renewable and Sustainable Energy Reviews*, 30:

164–169. http://dx.doi.org/10.1016/j.rser.2013.09.025.

Luo, X., Wang, J., Dooner, M. & Clarke, J. 2015. Overview of current development in electrical energy storage technologies and the application potential in power system operation. *Applied Energy*, 137: 511–536. http://dx.doi.org/10.1016/j.apenergy.2014.09.081.

Luta, Doudou N. & Raji, A.K. 2019a. Comparing fuzzy rule-based MPPT techniques for fuel cell stack applications. *Energy Procedia*, 156(September 2018): 177–182. https://doi.org/10.1016/j.egypro.2018.11.124.

Luta, D.N. & Raji, A.K. 2018. Decision-making between a grid extension and a rural renewable off-grid system with hydrogen generation. *International Journal of Hydrogen Energy*, 43(20): 1–14. https://doi.org/10.1016/j.ijhydene.2018.04.032.

Luta, Doudou N. & Raji, A.K. 2019b. Energy management system for a hybrid hydrogen fuel cell-supercapacitor in an islanded microgrid. *Proceedings - 2019 Southern African Universities Power Engineering Conference/Robotics and Mechatronics/Pattern Recognition Association of South Africa, SAUPEC/RobMech/PRASA 2019*: 611–615.

Luta, D.N. & Raji, A.K. 2016. Energy Management System for a Renewable. *2019 International Conference on the Domestic Use of Energy (DUE)*: 20–24.

Luta, Doudou N. & Raji, A.K. 2019c. Fuzzy rule-based and particle swarm optimisation MPPT techniques for a fuel cell stack. *Energies*, 12(5).

Luta, D.N. & Raji, A.K. 2019. Optimal sizing of hybrid fuel cell-supercapacitor storage system for off-grid renewable applications. *Energy*.

Luta, Doudou Nanitamo & Raji, A.K. 2019. Performance and Cost Analysis of Lithium-Ion Battery for Powering Off-Grid Telecoms Base Stations in Africa. *International Journal of Engineering Research in Africa*, 43: 101–111. https://www.scientific.net/JERA.43.101 18 August 2019.

Luta, D.N. & Raji, A.K. 2017. Potential benefits of renewable fuel cell systems for rural communities' power supply. In *2nd EAI International Conference for Research, Innovation and Development for Africa*. Victorai Falls: European Alliance for Innovation. http://eudl.eu/doi/10.4108/eai.20-6-2017.2270897.

Luta, Doudou N. & Raji, A.K. 2019d. Renewable Hydrogen-Based Energy System for Supplying Power to Telecoms Base Station. *International Journal of Engineering Research in Africa*, 43: 112–126. https://www.scientific.net/JERA.43.112 17 August

2019.

Maletin, Y., Strelko, V., Stryzhakova, N., Zelinsky, S., Rozhenko, A.B., Gromadsky, D., Volkov, V., Tychina, S., Gozhenko, O. & Drobny, D. 2013. Carbon Based Electrochemical Double Layer Capacitors of Low Internal Resistance. *Energy and Environment Research*, 3(2). http://sci-hub.tw/10.1149/1.1825379.

Malysz, P., Sirouspour, S. & Emadi, A. 2014. An optimal energy storage control strategy for grid-connected microgrids. *IEEE Transactions on Smart Grid*, 5(4): 1785–1796.

Mathiesen, B.V., Lund, H. & Karlsson, K. 2011. 100% Renewable energy systems, climate mitigation and economic growth. *Applied Energy*, 88(2): 488–501. http://dx.doi.org/10.1016/j.apenergy.2010.03.001.

Mathworks. 2013. Implement generic supercapacitor model - Simulink. https://www.mathworks.com/help/physmod/sps/powersys/ref/supercapacitor.html 9 November 2019.

Maxwell. 2007. *Introducing the New 3.0-Volt 3000-Farad Cell*. www.maxwell.com/3v 9 November 2019.

Migliavacca, G. 2013. *Advanced Technologies for Future Transmission Grids*. G. Migliavacca, ed. Milano: Springer- Verlag London.

Milligan, M. & Kirby, B. 2010. Utilizing Load Response for Wind and Solar Integration and Power System Reliability. In *Wind Power*. Dallas, Texas. https://www.nrel.gov/docs/fy10osti/48247.pdf.

Moodie, A. 2016. Google, Apple, Facebook race towards 100% renewable energy target. *The Guardian*. https://www.theguardian.com/sustainable-business/2016/dec/06/google-renewable-energy-target-solar-wind-power 28 April 2019.

Mousavi G, S.M., Faraji, F., Majazi, A. & Al-Haddad, K. 2017. A comprehensive review of Flywheel Energy Storage System technology. *Renewable and Sustainable Energy Reviews*, 67: 477–490.

Mutarraf, M.U., Terriche, Y., Niazi, K.A.K., Vasquez, J.C. & Guerrero, J.M. 2018. Energy storage systems for shipboard microgrids—A review. *Energies*, 11(12): 1–32. https://www.mdpi.com/1996-1073/11/12/3492.

Nair, N.K.C. & Garimella, N. 2010. Battery energy storage systems: Assessment for small-scale renewable energy integration. *Energy and Buildings*, 42(11): 2124–2130.

http://dx.doi.org/10.1016/j.enbuild.2010.07.002.

Nehrir, M.H., Caisheng, W. & Shaw, S.R. 2006. Fuel cells: promising devices for distributed generation. *Power and Energy Magazine, IEEE*, 4(1): 47–53. http://ieeexplore.ieee.org/ielx5/8014/33348/01578531.pdf?tp=&arnumber=1578531&isnumber=33348.

Nejabatkhah, F. & Li, Y.W. 2015. Overview of Power Management Strategies of Hybrid AC/DC Microgrid. *IEEE Transactions on Power Electronics*, 30(12): 7072–7089.

Neuhoff, K., Barquin, J., Bialek, J.W., Boyd, R., Dent, C.J., Echavarren, F., Grau, T., von Hirschhausen, C., Hobbs, B.F., Kunz, F., Nabe, C., Papaefthymiou, G., Weber, C. & Weigt, H. 2013. Renewable electric energy integration: Quantifying the value of design of markets for international transmission capacity. *Energy Economics*, 40: 760–772. http://dx.doi.org/10.1016/j.eneco.2013.09.004.

Ogland-Hand, J.D., Bielicki, J.M., Wang, Y., Adams, B.M., Buscheck, T.A. & Saar, M.O. 2019. The value of bulk energy storage for reducing CO2 emissions and water requirements from regional electricity systems. *Energy Conversion and Management*, 181(April 2018): 674–685. https://doi.org/10.1016/j.enconman.2018.12.019.

Ould Amrouche, S., Rekioua, D., Rekioua, T. & Bacha, S. 2016. Overview of energy storage in renewable energy systems. *International Journal of Hydrogen Energy*, 41: 20914–20927. http://dx.doi.org/10.1016/j.ijhydene.2016.06.243.

Palizban, O. & Kauhaniemi, K. 2016. Energy storage systems in modern grids—Matrix of technologies and applications. *Journal of Energy Storage*, 6: 248–259. http://dx.doi.org/10.1016/j.est.2016.02.001.

Papaefthymiou, G. & Dragoon, K. 2016. Towards 100 % renewable energy systems : Uncapping power system fl exibility. *Energy Policy*, 92: 69–82.

Papiewski John, C Victor, Wicks, D., Afework, B., Alberta, M., Hanania, J., Heffernan, B., Jenden, J., Yyelland, B., Donev, J., Stenhouse, K., Dhar, M., US EPA, OW, O., Adhelhamid, A., Woodford, C., Houghtaling, D., Hill, R. & Partain, L.D. 1996. The History of Solar. *Energy efficiency and renewable energy*. http://science.jrank.org/kids/pages/156/Fossil-Fuels-Affect-Environment.html%0Ahttps://www.greenmatch.co.uk/blog/2014/08/5-advantages-and-5-disadvantages-of-solar-energy%0Ahttp://businessfeed.sunpower.com/articles/understanding-solar-panel-efficiency%0Aht.

Pardo, P., Deydier, A., Anxionnaz-Minvielle, Z., Rougé, S., Cabassud, M. & Cognet, P. 2014. A review on high temperature thermochemical heat energy storage. *Renewable and Sustainable Energy Reviews*, 32: 591–610. http://dx.doi.org/10.1016/j.rser.2013.12.014.

Paul, B. & Andrews, J. 2017. PEM unitised reversible / regenerative hydrogen fuel cell systems : State of the art and technical challenges. *Renewable and Sustainable Energy Reviews*, 79(May): 585–599. http://dx.doi.org/10.1016/j.rser.2017.05.112.

Peppley, B.A. 2013. Fuel Cell Power Systems. : 2013.

Per.gov.ie. Real Discount Rate. https://www.homerenergy.com/products/pro/docs/3.11/real_discount_rate.html 29 August 2018.

Perlstein, B., Gilbert, E., Stern, F., Corfee, K., Battenberg, L., Maslowski, R., Schare, S. & Firestone, R. 2012. *Potential Role of Demand Response Resources in Maintaining Grid Stability and Integrating Variable Renewable Energy under California's 33 Percent Renewable Portfolio Standard*. www.navigant.com 25 April 2019.

Ponce de Leon, C., Friıas-Ferrer, A., Gonzalez-Garcıa, J., Szanto, D.. & Walsh, F.C. 2006. Redox flow cells for energy conversion. *Journal of Power Sources*, 160: 716–732.

Prasad, K.R., Koga, K. & Miura, N. 2004. Electrochemical deposition of nanostructured indium oxide: High-performance electrode material for redox supercapacitors. *Chemistry of Materials*, 16(10): 1845–1847. https://pubs.acs.org/doi/pdf/10.1021/cm0497576.

Pursiheimo, E., Holttinen, H. & Koljonen, T. 2017. Path toward 100% renewable energy future and feasibility of power-to-gas technology in Nordic countries. *IET Renewable Power Generation*, 11(13): 1695–1706.

Raccichini, R., Varzi, A., Passerini, S. & Scrosati, B. 2015. The role of graphene for electrochemical energy storage. *Nature Materials*, 14: 271–279. https://sci-hub.tw/10.1038/nmat4170.

Raj, A. & Sreekumar, M. 2016. A Comparison of MPPT Control of Photovoltaic System using Conventional and Artificial Intelligence Techniques. *IJET*, 38(1): 16–19.

Raza, W., Ali, F., Raza, N., Luo, Y., Kim, K.H., Yang, J., Kumar, S., Mehmood, A. & Kwon, E.E. 2018. Recent advancements in supercapacitor technology. *Nano Energy*, 52: 441–473. https://doi.org/10.1016/j.nanoen.2018.08.013.

RE100. 2019. RE100: The world's most influential companies, committed to 100% renewable

power. http://there100.org/re100 28 April 2019.

REN21. 2018. *Renewables 2018 Global Status Report*. Paris. www.ren21.net 28 April 2019.

Ryu, I., Yang, M., Kwon, H., Park, H.K., Do, Y.R., Lee, S.B. & Yim, S. 2014. Coaxial RuO2-ITO nanopillars for transparent supercapacitor application. *Langmuir*, 30: 1704–1709. https://sci-hub.tw/10.1021/la4044599.

Sakulin, M., Friedrich, K., Bachhiesl, U. & Braunstein, R. 2009. Policies for reasonable system integration of renewable energy sources in Austria. *International Conference on Clean Electrical Power, ICCEP*: 540–544. https://ieeexplore-ieee-org.libproxy.cput.ac.za/stamp/stamp.jsp?tp=&arnumber=5211997.

Samantara, A.K. & Ratha, S. 2018. *Materials development for Active/Passive components of a supercapacitor : background, present status and future perspective*. Springer. https://books.google.co.uk/books?hl=en&lr=&id=dfVADwAAQBAJ&oi=fnd&pg=PR5&dq=Aneeya+K.+Samantara+Satyajit+Ratha+materials+development&ots=v5UOewLdnC&sig=n8TXALS8quiE6cLC7v7g-xO5WpQ#v=onepage&q=Aneeya K. Samantara Satyajit Ratha materials development&f=fals.

Sharma, A., Tyagi, V. V., Chen, C.R. & Buddhi, D. 2009. Review on thermal energy storage with phase change materials and applications. *Renewable and Sustainable Energy Reviews*, 13(2): 318–345. https://pdf.sciencedirectassets.com/271969/1-s2.0-S1364032108X00103/1-s2.0-S1364032107001402/main.pdf?x-amz-security-token=AgoJb3JpZ2luX2VjEGQaCXVzLWVhc3QtMSJIMEYCIQCb0QVO0cZpGi6stSFqBAZi2PkvXnZxrIRNjh%2F5Gp08mQIhAO5STz1FQxlsqUumGC5xVTuQYSbgIzMEzyYde35bca.

Shulga, Y.M., Baskakov, S.A., Smirnov, V.A., Shulga, N.Y., Belay, K.G. & Gutsev, G.L. 2014. Graphene oxide films as separators of polyaniline-based supercapacitors. *Journal of Power Sources*, 245: 33–36. http://dx.doi.org/10.1016/j.jpowsour.2013.06.094.

Singh, G., Baredar, P., Singh, A. & Kurup, D. 2017. Optimal sizing and location of PV, wind and battery storage for electrification to an island: A case study of Kavaratti, Lakshadweep. *Journal of Energy Storage*, 12: 78–86. http://dx.doi.org/10.1016/j.est.2017.04.003.

Souleman, N.M., Tremblay, O. & Dessaint, L.-A. 2009. A Generic Fuel Cell Model for the Simulation of Fuel Cell Vehicles. *2009 IEEE Vehicle Power and Propulsion Conference*: 1722–1729.

Stankovich, S., Dikin, D.A., Dommett, G.H.B., Kohlhaas, K.M., Zimney, E.J., Stach, E.A.,

Piner, R.D., Nguyen, S.B.T. & Ruoff, R.S. 2006. Graphene-based composite materials. *Nature*, 442: 282–286. https://sci-hub.tw/10.1038/nature04969.

Swider-Lyons, K.E., Carlin, R.T., Rosenfeld, R.L. & Nowak, R.J. 2003. Technical issues and opportunities for fuel cell development for autonomous underwater vehicles. : 61–64.

Teodorescu, R., Liserre, M. & Rodriguez, P. 2011. *Grid Converters for Photovoltaic and Wind Power Systems Chapter 10 Control of Grid Converters under Grid F lt Faults*. John Wiley & Sons Ltd.

Tõnurist, K., Thomberg, T., Jänes, A., Kink, I. & Lust, E. 2012. Specific performance of electrical double layer capacitors based on different separator materials in room temperature ionic liquid. *Electrochemistry Communications*, 22: 77–80. http://dx.doi.org/10.1016/j.elecom.2012.05.029.

Torres, F.G. 2015. *Advanced Control of Renewable Energy Microgrids with Hybrid Energy Storage System*. University of Sevilla. https://idus.us.es/xmlui/bitstream/handle/11441/32946/thesis.pdf?sequence=1&isAllowed=y 22 October 2017.

Trancik, J.E. & Cross-Call, D. 2013. Energy technologies evaluated against climate targets using a cost and carbon trade-off curve. *Environmental Science and Technology*, 47(12): 6673–6680.

Vagus, S. 2012. Researchers experiment with phosphoric acid to make more efficient fuel cells - Hydrogen Fuel News. http://www.hydrogenfuelnews.com/researchers-experiment-with-phosphoric-acid-to-make-more-efficient-fuel-cells/853259/ 10 November 2019.

Vandoorn, T.L., Vasquez, J.C., De Kooning, J., Guerrero, J.M. & Vandevelde, L. 2013. Microgrids: Hierarchical control and an overview of the control and reserve management strategies. *IEEE Industrial Electronics Magazine*, 7(4): 42–55.

Varzi, A., Balducci, A. & Passerini, S. 2014. Natural Cellulose: A Green Alternative Binder for High Voltage Electrochemical Double Layer Capacitors Containing Ionic Liquid-Based Electrolytes. *Journal of The Electrochemical Society*, 161(3): A368–A375. https://sci-hub.tw/10.1149/2.063403jes.

Venkateshkumar, M., Ieee, M. & Description, A. 2013. Intelligent Control Based MPPT Method for Fuel Cell Power System. : 253–257.

Villers, D., Jobin, D., Soucy, C., Cossement, D., Chahine, R., Breau, L. & Bélanger, D. 2003.

The Influence of the Range of Electroactivity and Capacitance of Conducting Polymers on the Performance of Carbon Conducting Polymer Hybrid Supercapacitor. *Journal of The Electrochemical Society*, 150(6): A747–A752. http://sci-hub.tw/10.1149/1.1571530.

Wen, Z., Cao, J., Gu, Z., Xu, X., Zhang, F. & Lin, Z. 2008. Research on sodium sulfur battery for energy storage. *Solid State Ionics*, 179: 1697–1701.

Yu, H., Tang, Q., Wu, J., Lin, Y., Fan, L., Huang, M., Lin, J., Li, Y. & Yu, F. 2012. Using eggshell membrane as a separator in supercapacitor. *Journal of Power Sources*, 206: 463–468. http://dx.doi.org/10.1016/j.jpowsour.2012.01.116.

Zhang, C., Wei, Y.L., Cao, P.F. & Lin, M.C. 2018. Energy storage system: Current studies on batteries and power condition system. *Renewable and Sustainable Energy Reviews*, 82(November 2017): 3091–3106. https://doi.org/10.1016/j.rser.2017.10.030.

Zhang, Y., Feng, H., Wu, X., Wang, L., Zhang, A., Xia, T., Dong, H., Li, X. & Zhang, L. 2009. Progress of electrochemical capacitor electrode materials: A review. *International Journal of Hydrogen Energy*, 34(11): 4889–4899. http://dx.doi.org/10.1016/j.ijhydene.2009.04.005.

Zhong, C., Deng, Y., Hu, W., Qiao, J., Zhang, L. & Zhang, J. 2015. A review of electrolyte materials and compositions for electrochemical supercapacitors. *Chemical Society Reviews*, 44(21): 7431–7920. https://sci-hub.tw/10.1039/C5CS00303B.